INVESTIGATING THE MOLECULAR MECHANISMS BEHIND ON-DOWN DIRECTION-SELECTIVE GANGLION CELL CIRCUIT DEVELOPMENT

by

Andrew Scasny

A dissertation submitted to Johns Hopkins University in conformity with the requirements for the degree of Doctor of Philosophy

Baltimore, Maryland

August 2022

Abstract

Each of the dozens of cells within the mouse retina is tuned for detecting a specific element within the visual scene. One class of retinal cell is the direction-selective ganglion cell (DSGC), which preferentially fires in response to motion in a specific direction. The molecular mechanisms that dictate DSGC directional preference remain unknown. A single-cell RNA-Seq (scRNA-Seq) experiment performed by the Kolodkin Lab compared transcriptomes of ON DSGCs that prefer upward and downward motion. Two genes enriched in upward-preferring DSGCs, *Ptprk* and *Tbx5*, are required for their normal development and function; however, the effects of genes enriched in downward-preferring DSGCs remain unexplored.

The first aim of my thesis was to generate the reagents necessary for investigating ON-Down DSGCs. The lack of progress in understanding ON-Down DSGCs is due in part to a lack of mouse lines that provide genetic access to them. I achieved this by creating the *Fibcd1*^{Cre} mouse line, where Cre is knocked into the locus of *Fibcd1*, the gene most significantly enriched in ON-Down DSGCs. These results enable the visualization and manipulation of downward-preferring DSGCs necessary for their study.

The second aim of my thesis was to examine two genes enriched in ON-Down DSGCs. The first, *Ptprm*, encodes a receptor tyrosine phosphatase in the same subfamily as *Ptprk*. Loss of *Ptprm*, both globally and conditionally in ON-Down DSGCs, impaired the detection of upward motion. In contrast, loss of *Fibcd1*, which encodes a transmembrane protein that binds to acetylated compounds, had no impact on detecting

visual motion; it is necessary, however, for proper ON-Down DSGC dendritic development. These results provide the first insight into the molecular mechanisms responsible for ON-Down DSGC development and function.

Taken together, this work provides a foundation for the study of ON-Down DSGCs and how they acquire their specific directional preference. The *Fibcd1*^{Cre} line allows for visualizing these cells and performing subtype-specific manipulations. *Ptprm* and *Fibcd1* represent the first genes identified as tied to ON-Down DSGC development and function. These results will allow for more extensive study into the molecules that control wiring of DS circuitry.

Advisor: Alex Kolodkin, PhD

Charles J. Homcy and Simeon G. Margolis Professor

The Solomon H. Snyder Department of Neuroscience

The Johns Hopkins University School of Medicine

Readers: Robert Johnston, PhD

Assistant Professor

The Solomon H. Snyder Department of Neuroscience

The Johns Hopkins University

Don Zack, MD, PhD

Guerrieri Professor of Genetic Engineering and Molecular Ophthalmology

Department of Ophthalmology

The Johns Hopkins University School of Medicine

Acknowledgments

Any one researcher can only be as good as those who nurture and support their work. My thesis work would not have been possible without the people, both inside the lab and outside of it, who guided me through the last 6 years. I would like to thank my advisor, Alex Kolodkin, for providing the mentorship and opportunity needed to undertake this research. I admire his ability to tackle challenging questions undaunted, to bring out the best in people, both in celebrating when things go well and giving support when they are not, and to cultivate an environment where everyone knows they're on the same team. I would be fortunate if I could be half as effective a leader as him in my future career.

I would also like to thank the members of my thesis committee: Bob Johnston, Shan Sockanathan, Don Zack, and, though he is no longer serving on it, King-Wai Yau. Their distinct scientific perspectives and shared dedication to supporting my work allowed me to hone in on what was most needed for a successful project. I'd also like to thank Chip Hawkins and the entire staff of the Johns Hopkins Transgenic Core for making the novel mouse lines I sought a reality.

I would like to thank all members of the Kolodkin Lab, current and former, who made me look forward to coming into lab each day and helped me navigate a life in science: Maame Amoah-Dankwah, Yati Awasthi, Matt Brown, Karina Chaudhari, Joelle Dorskind, Sierra Foshe, Preethi Gopal, Katherine Gribble, Natalie Hamilton, Randal Hand, John Hunyara, Rebecca James, Dontais Johnson, James Kiraly, Nicole

Kropkowski, Brendan Lilley, Tzu-Huai (Leo) Lin, Anna Luo, Zhiwei Pan, Michael Sherman, Sriram Sudarsanam, Brian Trigg, Qiang Wang, Yvonne Yen, and Jakub Ziak. I'd especially like to thank Timour Al-Khindi, whose bold and painstaking RNA-Seq experiment made all of this work (and the work of many others in the lab) possible.

I would like to thank my fiancée, Casey Haughin, for being a better partner through this degree and this life than I could have dreamed of. I hope that I can provide you with as much during your path to your PhD as you have provided me during mine, especially now that we will no longer be a continent or ocean apart.

I would like to thank my mom, Paula Scasny, and my dad, Mark Scasny, as well as my future in-laws Jody Haughin and Bert Haughin; your love and support meant that no obstacle in my path was too much to overcome. I'd also like to thank my "pets-in-law," Dusty, Sugar, and Spice, for being essential parts of the love I received on my trips to Hilltown, PA.

I would like to thank the workers who make the Johns Hopkins School of Medicine a space in which we can do our best work – the construction and maintenance staff who provide us with our buildings, the custodial staff who keep them clean, the security staff who keep them safe, the IT staff who keep our machines running (no matter how many times they break), the culinary staff who provide us food, and the veterinary staff who allow us to perform animal research humanely and effectively.

Finally, I would like to thank the model organisms whose lives have been sacrificed to make biomedical research possible. None of this work could have been done without them.

Table of Contents

List of Figures

Chapter 1: Introduction

Portions of this chapter were previously published in: Hamilton, N.R., Scasny, A.J., and Kolodkin, A.L. (2021). Development of the vertebrate retinal direction-selective circuit. Dev Biol 477, 273-283. 10.1016/j.ydbio.2021.06.004. The section from "The retina provides an ideal model system…" on page 1 to "…genetic tools available in mouse models" on page 4 was written by Natalie Hamilton; the section from "Synapse formation and refinement…" on page 4 to "…a specific DSGC subtype" on page 7 was written by Andrew Scasny.

A central question in developmental neuroscience is how individual neurons form the correct connections with their presynaptic inputs and postsynaptic targets. Along with its intrinsic electrophysiological properties, the ability of a neuron to process information and provide an appropriate readout is chiefly dictated by the inputs it receives and where those inputs are placed onto it. Proper nervous system function also requires neurons to send their axonal projections to the correct target region(s), sometimes meters away, and form connections with the appropriate neurons therein (Sanes and Masland, 2015). Although the last several decades have brought numerous advances to our understanding of how neuronal circuits are wired together, our knowledge of the genetic and molecular programs that guide this wiring still remains quite limited.

The retina provides an ideal model system for identifying broader mechanisms that drive neuronal circuit assembly. The retina includes a remarkable array of neural circuits that detect, extract, and process key features in the visual world. Like many other CNS structures, the retina has a laminar architecture, separating the cell bodies and synapses of the six main neuronal types into distinct layers. Vision begins in rod and cone photoreceptors, which detect photons of light and reside at the back of the retina in the outer nuclear layer (ONL). Bipolar cells (BCs), located in the inner nuclear layer (INL), transduce signals from photoreceptors to the projection neurons of the retina, the retinal ganglion cells (RGCs), which reside in the ganglion cell layer (GCL) and target visual brain areas. Horizontal and amacrine cell (AC) interneurons, which also reside in the INL, filter the synaptic inputs received by BCs and RGCs, respectively. There are two synaptic layers: the outer plexiform layer (OPL) that separates the ONL from the INL, and the inner plexiform layer (IPL) that separates the INL from the GCL. The processing power of the retina follows from this precise organization of cell bodies and synapses, allowing for interpretation of color, contrast, and motion even before visual information reaches the brain (Masland, 2012).

One of the best-characterized retinal circuits, the direction-selective (DS) circuit, specializes in motion detection. The DS circuit motif is evolutionarily conserved in flies, zebrafish, rodents, rabbits, and primates (Giolli et al., 2006; Simpson, 1984; Masseck & Hoffmann, 2009, Fredericks et al., 1988). In many vertebrates it consists of two separate components – one for fast and one for slow motion – that contribute to visual behavior. DS circuits include three specialized types of neurons: direction-selective

ganglion cells (DSGCs), BC subtypes, and starburst amacrine cells (SACs) that together respond to increases (ON) or decreases (OFF) in illumination. SACs are GABAergic and cholinergic ACs whose dendrites selectively release neurotransmitter in response to centrifugal, but not centripetal, motion along a given dendrite (Wei and Feller, 2011). BCs and SACs wire precisely onto DSGCs such that a given DSGC fires robust action potentials in response to a single preferred direction (PD) but does not fire in response to motion in the opposite, or null, direction (ND).

DSGCs were first discovered by Barlow and Hill in the rabbit retina (Barlow & Hill, 1963). Subsequent studies established that DSGCs fall into two broad classes, ON-OFF and ON, based on whether or not they respond to light decrements in addition to light increments. ON-OFF DSGCs detect motion in four PDs spaced 90 degrees apart – dorsal, ventral, nasal, and temporal – and are tuned to fast motion; they project to brain areas involved in pattern vision, such as the dorsolateral geniculate nucleus (dLGN) and superior colliculus (SC). Within these targets, they preferentially target the dLGN shell and upper SC, respectively (Zhang et al, 2017). ON DSGCs were originally described as having three PDs spaced about 120 degrees apart – upward (ON-Up DSGCs), downward (ON-Down DSGCs), and forward (ON-Forward DSGCs). ON DSGCs respond to slower motion. They project to central targets that belong to the accessory optic system (AOS), comprising the medial terminal nucleus (MTN) for vertical motion and the nucleus of the optic tract (NOT) & dorsal terminal nucleus (DTN) for horizontal motion, and they generate the optokinetic reflex (OKR) that compensates for retinal slip during image motion (Simpson, 1984; Dhande and Huberman, 2014). The three

canonical PDs of ON DSGCs have classically been aligned with the axes of the vestibular system; however, a recent study has identified a fourth nasal-preferring ON DSGC and describes ON DSGC PDs spread 90 degrees apart and aligned with those of ON-OFF DSGCs but not vestibular coordinates (Sabbah et al., 2017). Nevertheless, this newer view of ON DSGC tuning only adds to our understanding of AOS-projecting ON DSGCs accrued over the last several decades. In the early 2000s, the study of DSGCs expanded into the mouse retina (Yoshida et al., 2001), enabling the use of the vast set of genetic tools available in mouse models.

Synapse formation and refinement among BCs, SACs, and DSGCs leads to the mature connectivity patterns that underlie DS tuning properties. The Barlow-Levick model (reviewed in Borst & Euler, 2011) proposes that inhibitory SAC input is shifted laterally and either delayed or sustained; in this model, ND stimuli activate SACs that block activity in the DSGCs next in line to receive excitation, while PD stimuli only elicit inhibition long after the DSGC has fired. Seminal work in the rabbit retina demonstrated that DSGCs receive asymmetric inhibition, that SACs are required for retinal DS, that SACs themselves are DS, and that null-side SACs ultimately drive greater inhibition than those on the preferred side of DSGC dendritic arbors through larger releases of GABA (Fried et al., 2002). Thus, the asymmetric inhibitory wiring of SACs onto DSGCs is essential for motion preference tuning, supporting the Barlow-Levick model.

When, and how, is asymmetric SAC input onto DSGCs formed during development? Two landmark studies established that for both ON-OFF DSGCs and ON DSGCs, asymmetric inhibition from SACs arises during the second postnatal week

during a relatively narrow window between ~P6 and P8 (Wei et al., 2011; Yonehara et al., 2011). This asymmetry is independent of both spontaneous activity and visual experience, since direction selectivity arises prior to eye opening (at P13) and pharmacological blockade of activity from P6-P12 does not alter the direction-selectivity of DSGCs. During the first postnatal week, the somas of SACs synaptically connected to DSGCs are equally distributed between the null and preferred side of DSGC dendritic arbors. Further, at P6 the spatial distribution and strength of inhibitory synapses onto both ON-OFF DSGCs and ON DSGCs is also symmetric. However, at P8, SACs located on the null side of these DSGCs elicit greater inhibitory currents than those on the preferred side, and at P14, GABAergic conductances are higher when elicited from depolarization of null side SACs than from the preferred (Wei et al., 2011; Yonehara et al., 2011). Direct support for the conclusions drawn from these observations comes from experiments combining two-photon calcium imaging with serial block-face EM, revealing that SACs on the null side of DSGC dendrites form a greater number of inhibitory synapses onto DSGCs than those on the preferred side (Briggman et al., 2011).

Furthermore, these experiments (Briggman et al., 2011) revealed that asymmetric connectivity is driven by the relationship between SAC dendritic orientation and DSGC PD, rather than by SAC soma location alone. Maximal connectivity occurs when SAC dendrites and the PD of a postsynaptic DSGC are antiparallel; since SAC dendrites extend radially, this gives null-side SACs the greatest level of connectivity and preferred-side SACs the least. When SAC somas are at more intermediate locations

along the preferred-null axis, however, these SAC dendrites overlap with the DSGC arbor at a variety of orientations. Though a model driven by soma location predicts that all SAC dendrites form synapses equally, synapse formation is biased towards those in an antiparallel orientation, indicating that this is a key determinant of asymmetric connectivity. Since this analysis defines SAC dendritic orientation as the vector connecting the SAC soma to the synapse, the orientation used does not represent the distal dendrite immediately surrounding the synapse, but rather the proximal dendrite to which it belongs. Experiments performed in *Sema6A*$^{-/-}$ SACs underscore the importance of the orientation of the proximal, rather than distal, SAC dendrite in asymmetric SAC-DSGC connectivity (Morrie & Feller, 2018). In these mutants, distal SAC dendrites take on disorganized orientations, while proximal dendrites mostly retain their normal orientations. Although DS responses are weakened in *Sema6A* mutants, asymmetric SAC-DSGC wiring remains intact, indicating that the correct orientation of proximal SAC dendrites is sufficient to preserve this asymmetric connectivity.

The importance of proximal dendritic orientation supports the idea that asymmetric connectivity between SACs and DSGCs is driven by synaptogenic cues that are selectively trafficked to a specific quadrant of the SAC arbor and that recognize a subtype-specific partner in the DSGC arbor, with these cues being distributed such that antiparallel orientations of SAC proximal dendrites and DSGC PDs are preferred. Rather than requiring detection of the local orientation of each distal dendritic segment and sending out the appropriate molecule, correct distribution of such cues could be achieved by sorting at the soma-dendrite border. The search for the molecular

determinants of asymmetric connectivity, therefore, should benefit from focusing on identifying sets of proteins localized to specific quadrants of the SAC arbor and complementary cues, perhaps CAMs, with expression limited to a specific DSGC subtype.

Identifying genes specific to ON-Down DSGCs

Identifying genes whose expression is limited to specific cell types has been greatly aided by the advent of single-cell RNA sequencing (scRNA-Seq) technology (Picelli et al, 2014; Macosko et al, 2015). scRNA-Seq profiles the transcriptome of individual cells within a tissue, providing insight into which genes are expressed differentially across cell types. These approaches have already facilitated discovery of mechanisms regulating DS circuitry; a scRNA-Seq study of SACs identified the transcription factor *Fezf1* as a regulator of ON vs OFF cell fate, promoting ON-specific molecular programs and inhibiting OFF-specific ones (Peng et al, 2020). While some scRNA-Seq technologies are optimized for processing thousands of cells for division into numerous clusters, a technique suited for experiments such as creating atlases of subtypes of RGCs (Rheaume et al, 2018; Tran et al, 2019), ACs (Yan et al, 2020), and BCs (Shekhar et al, 2016), the breadth of the survey comes with a tradeoff in depth; genes with low levels of transcription, even if highly specific to one cell type, and rarer cell types are less likely to be captured. Analysis of cells as rare as ON DSGCs is more

suited for technologies such as Smart-Seq2 (Picelli et al, 2014), capable of examining a small pool of cells at greater depth and thus able to identify lowly-expressed genes.

The study of molecular factors determining ON-DSGC directional preference has been greatly aided by a scRNA-Seq experiment performed by Timour Al-Khindi, a graduate student in the Kolodkin Laboratory. In this experiment, ON-Up and ON-Down DSGCs were labeled with P3 injections of CTB-647 into the MTN of *Spig1-GFP* mice, which selectively express GFP in ON-Up DSGCs within the pan-ventronasal retina (Yonehara et al, 2008). Thus, ON-Up DSGCs are co-labeled with GFP and CTB-647, whereas ON-Down DSGCs are labeled solely with CTB-647. Retinas were collected at time points before (P4, P5), during (P7, P8), and after (P10, P12) the onset of DS responses (Yonehara et al, 2011), sorted by fluorescence activated cell sorting (FACS) to isolate the desired ON-DSGCs, and subjected to Smart-Seq2 at a read depth of $1.5*10^6 \pm 0.4*10^6$ reads per cell, with 89% $\pm$ 4% alignment with the reference genome. Clustering the transcriptomic data based on *Spig1* expression revealed numerous genes that were enriched in one of the two profiled subtypes of ON-DSGC (Figure 1).

Initial studies by the Kolodkin Laboratory of two genes identified as enriched in ON-Up DSGCs revealed roles for them in developing the circuitry containing these DSGCs. The first gene, *Tbx5*, encodes a transcription factor that is expressed in a spatially graded fashion across the retina (Barbieri et al, 2002). Embryonic ablation of *Tbx5* leads to a complete loss of the OKR response to continuous vertical stimuli, with no impact on responses to continuous horizontal stimuli, as well as a complete and selective loss of ON-Up DSGCs, suggesting roles for ON-Up DSGC fate determination

and/or survival (Al-Khindi et al., s*ubmitted*). The second, *Ptprk*, encodes a receptor tyrosine phosphatase (RTP) whose extracellular region contains numerous domains related to cell adhesion (Aricescu et al, 2007). Loss of *Ptprk* causes a significant reduction in the OKR response to upward continuous stimuli and a strong trend towards reduction of the response to downward stimuli, with no effects on the response to horizontal stimuli. While ON-Up DSGCs are still present in *Ptprk-KO* mice, they exhibit an altered dendritic arbor with a greater dendritic area and fewer branch points, with no effect on dendritic length or asymmetry (TAK, unpublished work; Figure 2). These results indicate that scRNA-Seq identifies genes that play roles in DS circuit development, validating the exploration of additional genes with differential expression.

While the catalog of genes expressed specifically in ON-Down DSGCs encode numerous classes of proteins, I focused on genes that encode cell surface molecules. The particular importance of these proteins for proper circuit formation is exemplified by molecular programs found in the retina. Interactions between transmembrane members of the semaphorin family and the plexin family of receptors are critical for laminar organization throughout the retina. *Sema6A* and *PlexA4* are required for laminar targeting and ribbon synapse formation in horizontal cells of the outer retina (Matsuoka et al, 2012), while recognition of Sema5A and Sema5B by PlexA1 and PlexA3 is essential for preventing IPL-targeted neurites from inappropriately expanding into the INL (Matsuoka et al, 2011). Within the DS circuit, the study of type II cadherins revealed axis-dependent requirements for distinct cadherins in the wiring of ON-OFF DSGCs with SACs. Cdh6 and Cdh10 in vertically-tuned ON-OFF DSGCs bind to Cdh6 in SACs to

promote attachment to the SAC dendritic scaffold, whereas Cdh7 plays an analogous role in nasal ON-OFF DSGCS by binding to SAC-expressed Cdh18 (Duan et al, 2018). Although this model does not distinguish upward- and downward-tuned ON-OFF DSGCs, it nevertheless illustrates how cell-surface molecules whose expression is limited to distinct DSGC subtypes can be required for subtype-specific circuit development. The role for *Tbx5* in ON-Up DSGCs does support the study of transcription factors as well. However, a single transcription factor is capable of regulating numerous genes involved in neuronal wiring, rendering it difficult to determine which downstream effector is responsible for the ultimate phenotype (Xie et al, 2022). This is true for *Tbx5*, as the abundance of genes whose expression appears to be controlled by *Tbx5* in cardiac tissue (Waldron et al, 2016) leaves open numerous possibilities for which targets are required for its DSGC-specific role. In contrast, the known molecular functions of a given cell-surface protein and its narrower interactome provide a more well-defined roadmap for investigating how it regulates DSGC circuit formation, though also with lower odds of observing a phenotype.

The primary focus of my investigation of genes identified by scRNA-Seq as enriched in ON-Down DSGCs was *Ptprm*. This gene encodes an RTP in the same subfamily as *Ptprk*, with a similar extracellular region rich in cell-adhesion domains (Aricescu et al, 2006). The effects of *Ptprk* on the development of the circuitry containing ON-Up DSGCs raise the intriguing possibility that *Ptprm* has a similar impact on the circuitry containing ON-Down DSGCs. The second gene was *Fibcd1*, which encodes a type II single-pass transmembrane protein (Schlosser et al, 2009). Although

this gene has been primarily studied in the context of recognition of fungal pathogens by endothelial cells (Jepsen et al, 2018; Moeller et al, 2019), its strong expression in ON-Down DSGCs motivates the study of this gene in the retina.

These genes could affect numerous components of the DS circuit. Given the overwhelming importance of asymmetric inhibition in DS circuit function, the proper formation of inhibitory connections with SACs is a promising site at which these genes could play a role. This role could take the form of controlling (1) inhibitory synapse localization, ensuring that inhibitory input is positioned to provide the local control over excitation observed in calcium imaging studies (Jain et al, 2020); (2) synapse number, as the increase in null-side inhibition during the second postnatal week is driven by increased synapse number (Morrie and Feller, 2015); (3) synaptic efficacy, as the asymmetry of inhibitory circuitry will not lead to an asymmetry in DSGC firing if the synapses cannot provide sufficient inhibitory drive; or (4) a combination of these. Other PTPs, such as PTPRS and LAR, are critical for regulating excitatory synapses (Fukai and Yoshida, 2020), suggesting that *Ptprm* could act as a synaptic regulator. As the association of a2 subunits of $GABA_A$Rs with gephyrin, the postsynaptic scaffolding protein at inhibitory synapses, is downregulated by phosphorylation (Nakamura et al, 2020), *Ptprm* may promote GABRA2 dephosphorylation and thus the efficacy of inhibitory synapses. These genes could also regulate excitatory synapses. Though DS responses in DSGCs have largely been attributed to asymmetric inhibitory circuitry, particularly given earlier studies that suggested excitatory input onto DSGCs is symmetrical (Poleg-Polsky and Diamond, 2011; Yonehara et al, 2013), a recent

analysis found that BC subtypes with different response kinetics are arranged across the DSGC dendritic arbor such that they will provide a synchronized burst of excitatory input when a stimulus travels along the PD, but not the ND (Matsumoto et al, 2019). *Ptprm* could regulate such an arrangement, since *Ptprm* is expressed in at least some subtypes of ON-BCs (Kay et al, 2011b). Postsynaptically, these genes could act as axon guidance cues, preventing the premature exit of axons from the optic tract and/or promoting their correct targeting to the MTN. Within the target region, they could control the preferential, though not exclusive, targeting of ON-Down inputs to the ventral portion of the MTN (vMTN; Yonehara et al, 2009). Given the hypothesized role for *Ptprm* in the chick visual system as an arrestive retinotopic cue restricting RGCs from the temporal retina to the anterior tectum (Burden-Gulley et al, 2002), it is plausible that *Ptprm*+ ON-Down DSGC axons recognize a cue in the vMTN that largely prevents their progression into the dorsal MTN. Additionally, these genes could be important for the formation of functional synapses with target neurons in the MTN, a possibility further in line with the known roles for PTPs in synaptogenesis being presynaptic in nature (Fukai and Yoshida, 2020).

To examine these genes in ON-Down DSGC development, I first worked to generate the reagents required to gain genetic access to these cells. Unlike with ON-Up DSGCs, no Cre lines were known to drive recombinase expression specifically in ON-Down DSGCs. Thus, the aims of my thesis were twofold: first, to generate the reagents required for the general study of ON-Down DSGCs; and second, to examine the roles of *Ptprm* and *Fibcd1* in the development of ON-Down DSGCs.

Figure 1

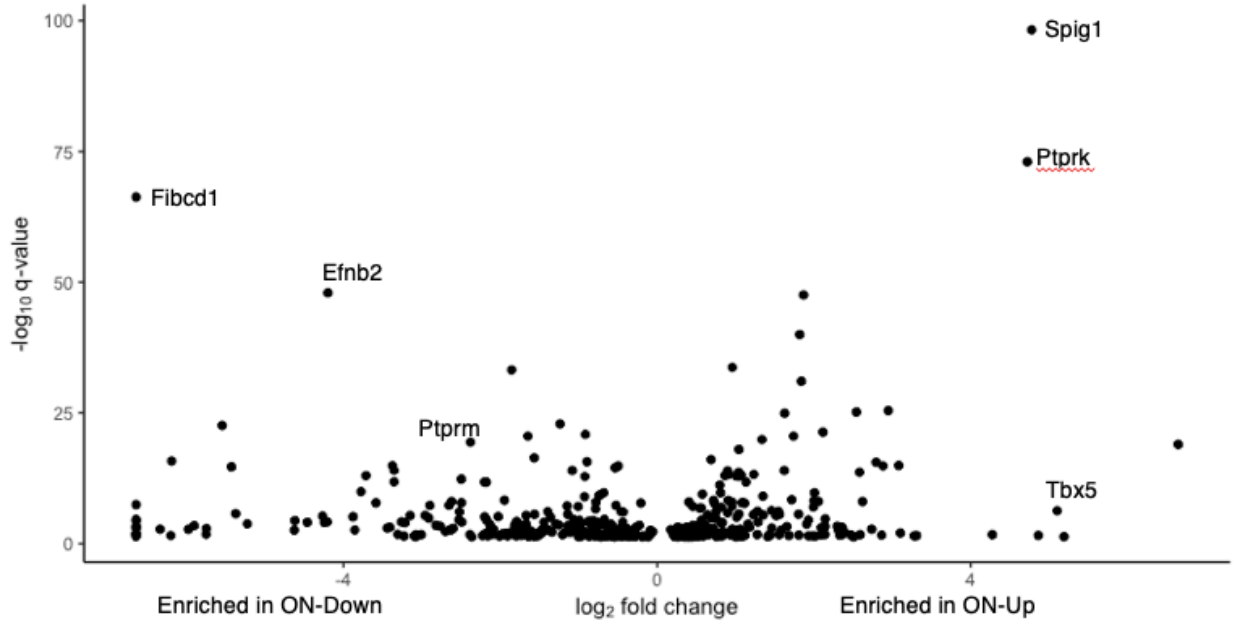
100
75
50
25
0
-log10 q-value
Spig1
Ptprk
Fibcd1
Efnb2
Ptprm
Tbx5
-4
0
4
Enriched in ON-Down
log2 fold change
Enriched in ON-Up

Figure 1. Differentially expressed genes identified by scRNA-Seq. Genes were considered significantly differentially expressed based on a q-value threshold of 0.05. Positive values on the x-axis denote genes enriched in ON-Up DSGCs, while negative values denote enrichment in ON-Down DSGCs. As expected, the most significantly enriched gene is *Fstl4*, which encodes Spig1. Other genes enriched in ON-Up DSGCs include *Ptprk* and *Tbx5*, while genes enriched in ON-Down DSGCs include *Fibcd1*, *Efnb2*, and *Ptprm*. Figure courtesy of Timour Al-Khindi, Kolodkin Lab, unpublished work.

Figure 2

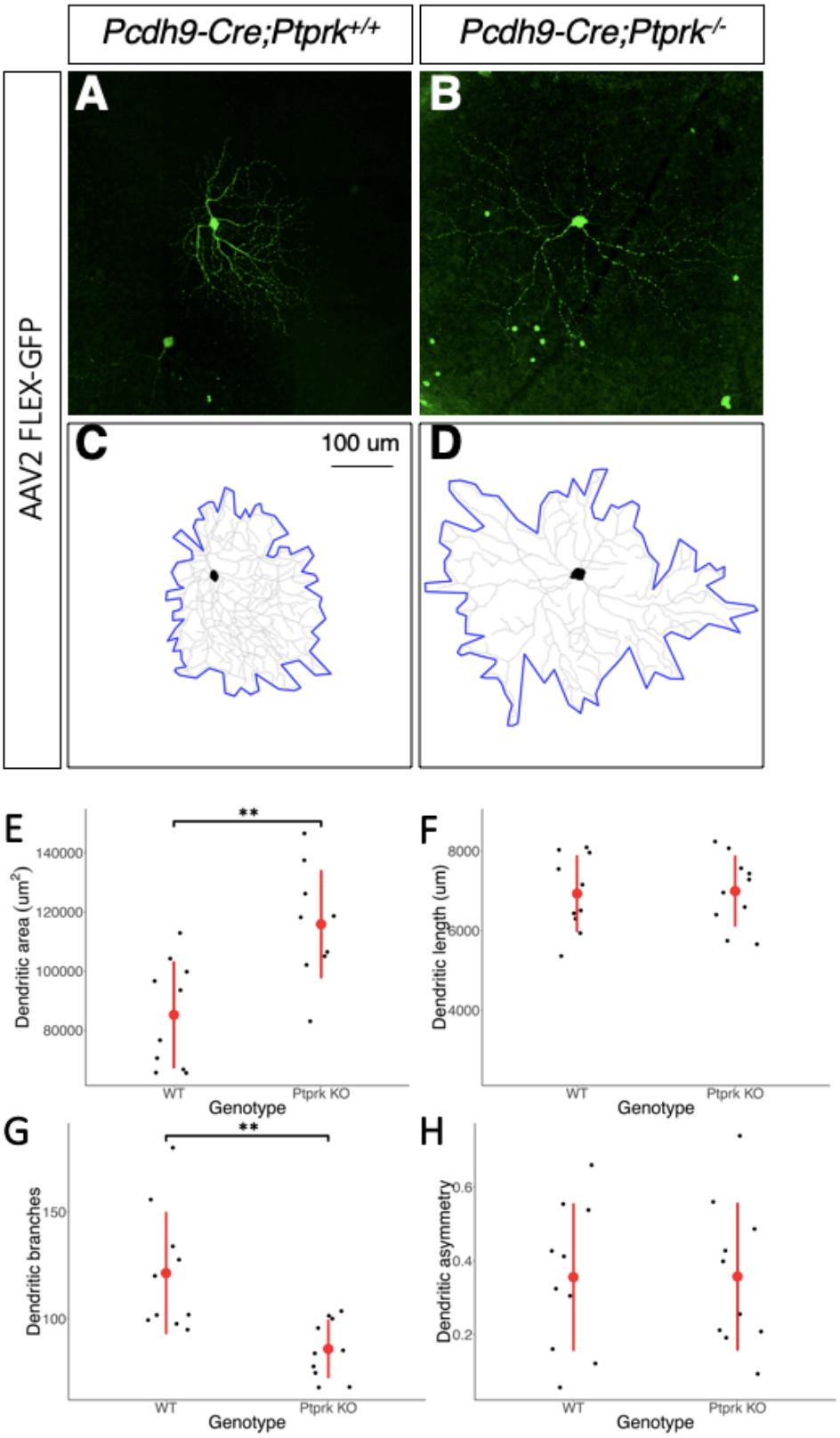
Pcdh9-Cre;Ptprk+/+
Pcdh9-Cre;Ptprk-/-
AAV2 FLEX-GFP
A
B
C
D
100 um
E
Dendritic area (um2)
140000
120000
100000
80000
**
WT
Ptprk KO
Genotype
F
Dendritic length (um)
8000
6000
4000
WT
Ptprk KO
Genotype
G
Dendritic branches
150
100
**
WT
Ptprk KO
Genotype
H
Dendritic asymmetry
0.6
0.4
0.2
WT
Ptprk KO
Genotype

Figure 2. Loss of *Ptprk* induces an expansion of the ON-Up DSGC dendritic arbor and reduction in geometric complexity. (A-B) Labeling of adult *Ptprk +/+* (A) and *Ptprk -/-* (B) ON-Up DSGCs on a *Pcdh9-Cre* background using IO injections of AAV2-FLEX-GFP. (C-D) Measuring the dendritic area of *Ptprk +/+* (C) and *Ptprk -/-* (D) ON-Up DSGCs. (E-H) Loss of *Ptprk* leads to a significant increase in dendritic arbor area (E) and significant decrease in dendritic branching (G), but no changes in dendritic length (F) or asymmetry (H). Figure courtesy of Timour Al-Khindi, Kolodkin Lab, unpublished work.

Chapter 2: Generating *Fibcd1*^{Cre} and pAAV-fNPY-FLEX-GFP

Introduction

Our understanding of the mechanisms behind ON-Up DSGC development was advanced by the Kolodkin Lab's study of genes identified by scRNA-Seq. I sought to further advance our understanding of the molecular mechanisms driving ON-Down DSGC development. The primary obstacle to studying ON-Down DSGCs was a lack of reagents enabling the examination and manipulation of these cells. *Spig1-GFP* was identified more than a decade ago as a line marking ON-Up DSGCs through P12 (Yonehara et al, 2008), while a recent study of the *Pcdh9-Cre* line (Lilley et al, 2019) found it provided genetic access to these DSGCs. In contrast, the primary methods for identifying ON-Down DSGCs have been by exclusion, such as backfills of CTB in *Spig1-GFP* mice (Yonehara et al, 2009). These methods do not provide adequate dendritic labeling for tracing experiments. Furthermore, a lack of genetic access precludes the performance of cell-type-specific manipulations of ON-Down DSGCs. Therefore, the study of ON-Down DSGC development required the generation of a mouse line capable of providing genetic access to these cells. Moreover, while Cre lines such as *Pcdh9-Cre* provide access to ON-DSGCs, these lines often exhibit Cre expression in other retinal cells. For example, *Pcdh9-Cre* labels ON SACs (Lilley et al, 2019), requiring viral labeling experiments using intraocular injections to pay careful attention to viral titer to get labeling sparse enough for dendritic tracing of the occasional

well-isolated cell. This undesired labeling of non-DSGC cells is also problematic for performing electrophysiological analyses, as it forces the experimenter to determine whether a particular cell is the type they want to record. For 2-photon calcium imaging experiments, this could prove impossible if soma size does not distinguish cell types. Thus, a viral tool was needed to study ON DSGCs.

Results

Generating Fibcd1^{Cre} *mice*

To address the need for genetic access to ON-Down DSGCs, I used CRISPR-Cas9 technology to insert a Cre cassette immediately following the start codon of the *Fibcd1* locus, creating the *Fibcd1^{Cre}* line (Figure 3). *Fibcd1* was chosen as the knock-in locus due to its expression in ON-Down DSGCs (see Chapter 4 below for a detailed discussion of the Fibcd1 protein and function). Moreover, a previously published transcriptomic atlas of P5 RGCs (Rheaume et al, 2018) found *Fibcd1* expression limited to a single cluster of RGCs (Figure 4A). Based on expression of ON-Up markers such as *Fstl4* (encoding Spig1) in cells distinct from *Fibcd1*-expressing cells in this same cluster (Figure 4B), we hypothesized that this cluster contains vertically tuned ON-DSGCs that respond to upward or downward motion. Thus, I predicted that *Fibcd1^{Cre}* would provide genetic access to a population of retinal cells that, with respect to RGCs, would be nearly or totally comprised of ON-Down DSGCs.

Out of ~75 mice produced by the CRISPR experiment, 8 mice demonstrated successful integration of the full Cre cassette at the desired site (Figure 5). Integration was verified using 2 pairs of primers, each comprised of a primer binding to genomic DNA distal to the homology arms of the insert and a primer binding to the Cre cassette. PCR therefore only generates a band if the insert was placed at the correct locus in the correct orientation. Sequencing of the resulting bands confirmed successful integration of the desired sequence with no undesired changes to the genomic DNA immediately flanking the insert.

I crossed the potential founder mice to *Ai14* (loxP-STOP-loxP-tdTomato) to assess Cre expression. One founder, #1368, produced progeny with a rare subset of RGCs labeled by Cre as determined by tdTomato and RBPMS staining (Figure 6). However, numerous displaced ACs, determined as such by a lack of RBPMS staining, were also labeled. Staining for ChAT, a SAC marker, revealed that these ACs are not SACs, as tdTomato+ RBPMS- cells were also ChAT- (Figure 6D). This agrees with transcriptomic data from a recent scRNA-Seq atlas of ACs (Yan et al, 2020), in which the clusters with *Fibcd1* expression did not include the sole cluster expressing *Chat*, which corresponds to SACs. Lack of *Cre* expression in SACs indicates that any conditional manipulations using *Fibcd1*^{Cre} will not directly impact this component of the DS circuitry. This atlas, however, could not map *Fibcd1*+ ACs onto known AC subtypes, leaving unclear which AC subtypes are labeled by *Fibcd1*^{Cre}.

Examining retinorecipient regions in *Fibcd1*^{Cre}*;Ai14* mice, I found robust innervation of the MTN by Cre+ axons, indicating that Cre+ RGCs project axons to the

region targeted by vertical ON-DSGCs (Figure 7). While the bulk of mCherry signal was within the ventral MTN (vMTN), a portion of labeled axons extended into the dorsal MTN (dMTN; Figure 7B); although signaling to the dMTN is dominated by ON-Up DSGCs, previous studies have found that many dMTN neurons can be activated by downward stimuli as well, indicating that ON-Down DSGCs also form connections with this portion of the MTN (Yonehara et al, 2009). Other retinorecipient regions such as the SC (Figure 7C) and dLGN (Figure 7D) did not appear to receive retinorecipient targeting by Cre+ axons; this analysis did not check the NOT or DTN, centers of the AOS receiving horizontal motion information.

In addition to retinorecipient axons targeting the MTN, robust Cre expression was observed in the hippocampus (Figure 7A). This intense expression of *Fibcd1*^{Cre} in the hippocampus agreed with published *in situ* hybridization data (Allen Brain Atlas) and a recent preprint identifying a role for *Fibcd1* in hippocampal short-term plasticity and hippocampus-dependent fear conditioning (Fell et al, 2021).

These data still left open the possibility that ON-Up DSGCs were also labeled by *Fibcd1*^{Cre}, as they are also rare RGCs that project to the MTN. To test for this, I crossed *Fibcd1*^{Cre}*;Ai14* mice to the *Spig1-GFP* line, which selectively labels ON-Up DSGCs through P12 (Yonehara et al, 2008), and stained P11 *Fibcd1*^{Cre}*;Ai14;Spig1-GFP* whole-mount retinas for RBPMS, tdTomato, and GFP (Figure 8). I found that nearly all tdTomato+ RGCs were GFP- (78/79 cells, 4 retinas from 2 mice), indicating a lack of overlap between the two populations. This demonstrates that RGCs labeled by *Fibcd1*^{Cre} are not ON-Up DSGCs. Moreover, the spatial density of tdTomato+ RGCs

(44.0 cells/mm^2) was comparable to the density of GFP+ ON-Up DSGCs (52.7 cells/mm^2, n=93 cells), suggesting that the tdTomato+ RGCs did not include RGCs beyond the presumptive ON-Down DSGCs. A portion of ON-Up DSGCs and Cre+ RGCs formed "doublets," such as the pairs at the top-right and bottom-left of Figure 8. These matched the "doublets" of ON-Up and ON-Down DSGCs described in Yonehara et al, 2008. As the frequency with which these DSGCs form "doublets" has not been previously quantified, I could not determine whether the frequency with which Cre+ RGCs formed "doublets" with ON-Up DSGCs agreed with how frequently ON-Down DSGCs do so.

A technical consideration for use of the *Fibcd1^{Cre}* line became apparent as I attempted to generate mice that were homozygous for Cre-dependent reporter alleles. The first generation of crosses yielded reporter expression similar to my original findings. However, a substantial fraction of mice in subsequent generations showed ubiquitous expression of the reporter, indicating that the reporter allele had undergone germline recombination. Given that this pattern of ubiquitous expression would only begin appearing in the second generation of crosses, this indicated that *Fibcd1^{Cre}* mice with floxed alleles recombine these alleles in their gametes. This effect was observed in *Fibcd1^{Cre}* parents of both sexes. Therefore, breeding strategies involving *Fibcd1^{Cre}* and floxed alleles must be designed such that the Cre allele and floxed alleles are sourced from separate parents in the final cross to yield experimental progeny. Moreover, it is not possible to generate mice that are homozygous for a given floxed allele and have the *Fibcd1^{Cre}* allele.

Generating pAAV-fNPY-FLEX-GFP

Existing labeling methods present issues for using *Fibcd1*^{Cre} to label ON-Down DSGCs in a variety of experimental contexts. While intraocular injection of a Cre-dependent virus encoding a fluorophore, such as AAV2-pCAG-FLEX-GFP, would restrict fluorophore expression to Cre+ cells, the ON-Down DSGCs would be vastly outnumbered by Cre+ ACs, rendering definitive assessment of a labeled cell as an RGC problematic for 2-photon calcium imaging. Furthermore, the abundance of non-DSGC labeling renders using this approach for dendritic tracing experiments problematic. Even with RBPMS staining to identify cell bodies as ON-Down DSGCs, definitively assigning dendritic segments to these cells is challenging. Labeling can be restricted to ON-Down DSGCs through injection of a Cre-dependent retro-AAV, such as rAAV2-FLEX-GFP, into the MTN. However, these injections are low-throughput due to the time required for each surgery.

In order to combine the efficiency of intraocular injections with the specificity of MTN injections, I designed a Cre-dependent AAV that places expression of the fluorophore under control of the *Npy* promoter, in collaboration with Natalie Hamilton (Figure 9). *Npy* is expressed in all AOS-projecting DSGCs, according to our scRNA-Seq data (Figure 10A) and a previously published atlas of P5 RGCs (Figure 10B; Rheaume et al, 2018), but not in *Fibcd1*+ ACs according to a recently published AC atlas (Yan et al, 2020). Thus, in *Fibcd1*^{Cre} mice, the ON-Down DSGCs will be the only retinal cells

capable of both inverting the fluorophore coding sequence into the correct orientation and driving expression of the fluorophore from the *Npy* promoter. This design also prevented undesired fluorophore expression in extraneous cells when labeling ON-Up DSGCs using *Pcdh9-Cre* (Lilley et al, 2019). Thus, this viral construct will be useful for the study of all vertically-tuned ON DSGCs.

We took advantage of an existing AAV plasmid, fugu *Npy* promoter> GFP, that drives expression of *GFP* in Npy+ interneurons when injected into mouse cortex (Nathanson et al, 2009). We inverted the GFP coding sequence and polyA tail of this plasmid and cloned in loxP and lox2272 sites such that the CDS and polyA tail enter the correct orientation following recombination by Cre. The novel pAAV-fNPY-FLEX-GFP construct, as well as the original pAAV-fNPY-GFP construct, have been sent to the UNC BRAIN Initiative Viral Vector Core for packaging into AAV9. Once received, we will first test AAV9-fNPY-GFP to check for proper infection of *Npy+* retinal cells. Should this succeed, we will then test AAV9-fNPY-FLEX-GFP in *Fibcd1*^{Cre};*Ai14* to see whether it provides the intended labeling of ON-Down DSGCs without labeling of Cre+ ACs. If we observe the desired labeling, this would position AAV9-fNPY-FLEX-GFP as usable for labeling any subset of AOS-projecting RGCs using the appropriate Cre line. The ability to specifically label these DSGCs without the use of stereotaxic injections into their target regions would be highly useful for performing dendritic morphology assessments as well as electrophysiological recordings of these RGCs.

Discussion

Gaining genetic access to ON-Down DSGCs vastly expands our ability to study this RGC population. Previous studies aiming to examine ON-Down DSGCs in isolation could use mice no older than P12, as this is the limit for when GFP expression in *Spig1-GFP* is linked to ON-Up DSGCs (Yonehara et al, 2008) and thus can be used to distinguish ON-Up DSGCs from ON-Down DSGCs among cells labeled with stereotaxic MTN injections. *Pcdh9-Cre* cannot be crossed to a Cre-dependent genetic reporter for this purpose, as its widespread expression in the early embryonic retina leads to undesired labeling (Lilley et al, 2019); postnatal viral labeling approaches also cannot be used, as the inability for a viral reporter to label every Cre+ cell means that a CTB+ cell lacking the viral label cannot be identified definitively as an ON-Down DSGC. Thus, gaining direct access to ON-Down DSGCs with *Fibcd1*^{Cre} allows for experiments in mice older than P12. Being able to access these cells directly also enables use of the suite of Cre-dependent approaches that have been developed in the last two decades. Conditional mutants for genes of interest can be generated, enabling research into whether genes are specifically required in ON-Down DSGCs as well as research into genes whose global loss is lethal.

This represents the first time that a line for labeling a specific DSGC subtype, preferring only one direction, has been intentionally generated for that purpose. For *Pcdh9-Cre*, for example, its utility for labeling ON-Up DSGCs was identified through a screen of various Cre drivers for RGC labeling that revealed labeling of a cell type

appearing to correspond with ON DSGCs (Martersteck et al, 2017) followed by an in-depth characterization that confirmed the identity of labeled cells as ON-Up DSGCs (Lilley et al, 2019). The majority of lines used to label particular DSGC subtypes were identified using similar screens (Yonehara et al, 2008; Trenholm et al, 2011; Dhande et al, 2013). Directed generation of mouse lines suitable for this purpose bypasses the need to perform a screen of numerous marker lines, which has no guarantee that a successful line will be found. Furthermore, even if an existing reporter line labels the desired subtype, this does not necessarily mean that the gene whose expression is ostensibly reported by the line can be successfully used as a locus for knocking in Cre to gain genetic access to that subtype. For example, although *Hb9-GFP* labels ON-OFF DSGCs that prefer ventral motion across the retina (Trenholm et al, 2011), *Hb9* is not endogenously expressed in these cells; instead, GFP expression is due to the random insertion of the *Hb9-GFP* BAC placing it close enough to the *Cdh6* locus for its expression to be partially influenced by *Cdh6* expression (Laboulaye et al, 2018). Thus, an $Hb9^{Cre}$ allele would not provide genetic access to these ON-OFF DSGCs. The generation of the *Cdh6-CreER* line to label vertically-tuned ON-OFF DSGCs was motivated by transcriptomic data indicating *Cdh6* is selectively expressed in these DSGCs (Kay et al, 2011a); however, this line labels two ON-OFF DSGC subtypes (Up and Down), whereas $Fibcd1^{Cre}$ exclusively labels ON-Down DSGCs.

The above studies provide a compelling argument that ON-Down DSGCs are the sole RGCs labeled in $Fibcd1^{Cre}$. *Cre+* RGCs are nearly identical in number to ON-Up DSGCs; *Cre+* RGCs and ON-Up DSGCs are mutually exclusive; and *Cre+* RGCs

project to the MTN, the target region for ON-Down DSGCs. However, direct electrophysiological recordings from labeled RGCs are needed to further support this claim. To this end, we are collaborating with the Lab of M. Feller at UC Berkeley to record labeled RGCs responding to various directional stimuli.

That study, along with many others of ON DSGCs, will be greatly aided by the creation of the pAAV-fNPY-FLEX-GFP viral construct. With fluorophore expression restricted to ON-Down DSGCs, there is no possibility for recording from a Cre+ AC instead of a DSGC. In addition to the convenience afforded by use of intraocular injections instead of stereotaxic MTN injections, this approach allows for studying ON-Down DSGCs at juvenile timepoints inaccessible by MTN injections. The only ages for which MTN stereotaxic coordinates exist are P3 and P42; the 14-day window needed for full expression of a retro-AAV thus represents a barrier to examination of the retina prior to P17, and the toxicity of other viruses taken up in a retrograde fashion such as Rabies-ΔG-mCherry prevents studies from being done with this approach beyond P10. The more rapid onset of expression driven by AAV9 enables AAV9-fNPY-FLEX-GFP to bridge this gap, enabling the labeling of ON-Down DSGCs at all desired timepoints.

The need for combinatorial approaches for restricting labeling to an RGC subtype of choice is not limited to ON DSGCs. For the majority of RGC subtypes, molecular classification cannot be achieved on the basis of singular marker genes, but rather the expression of specific combinations (Sanes and Masland, 2015). In this sense, we are fortunate that the two classes of vertical ON DSGCs have marker genes (*Fstl4* and *Fibcd1*) whose expression is specific enough among RGCs that their loci could be used

to generate subtype-specific marker alleles. Placing the expression of a Cre-dependent fluorophore under the control of a particular promoter could enable the specific study of subtypes defined by the expression of a pair of markers, vastly expanding our capacity to explore subtype-specific molecular mechanisms. Such an expansion would render the mouse retina an even greater model system for studying the wiring of neural circuits.

Figure 3

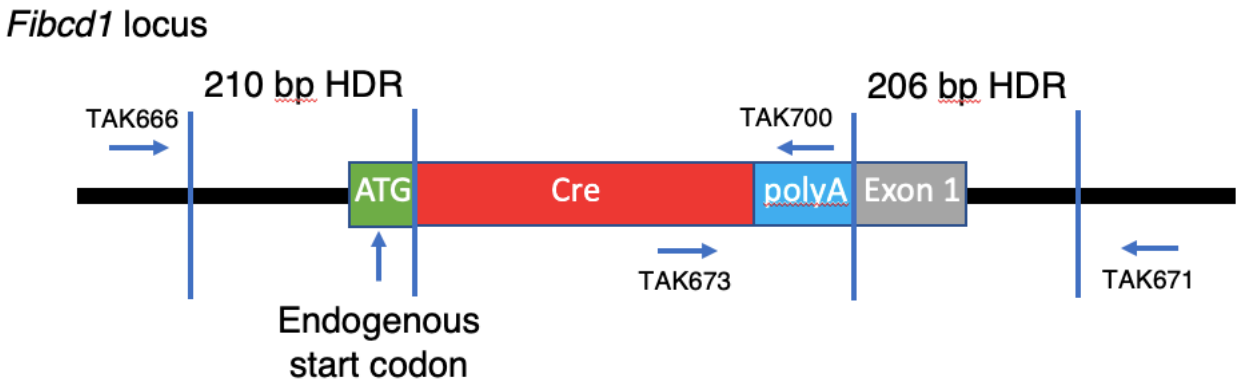
Fibcd1 locus
210 bp HDR
206 bp HDR
TAK666
TAK700
ATG
Cre
polyA
Exon 1
TAK673
TAK671
Endogenous
start codon

Figure 3. Design of the *Fibcd1*^{Cre} allele. CRISPR-mediated mutagenesis was used to insert the full-length Cre CDS, followed by the rabbit globulin polyA tail, immediately following the endogenous start codon of *Fibcd1*. Screening of founder mice from the CRISPR mutagenesis experiment was performed with PCR reactions using TAK666 & TAK700 and TAK673 & TAK671; bands could only appear for each reaction due to placement at the correct genetic locus due to TAK666 and TAK671, respectively, being placed distal to each homology arm. Sites for TAK700 and TAK673 were chosen to allow full-length sequencing of the insert to ensure the desired sequence was inserted without undesired mutations. Distances not drawn to scale.

Figure 4

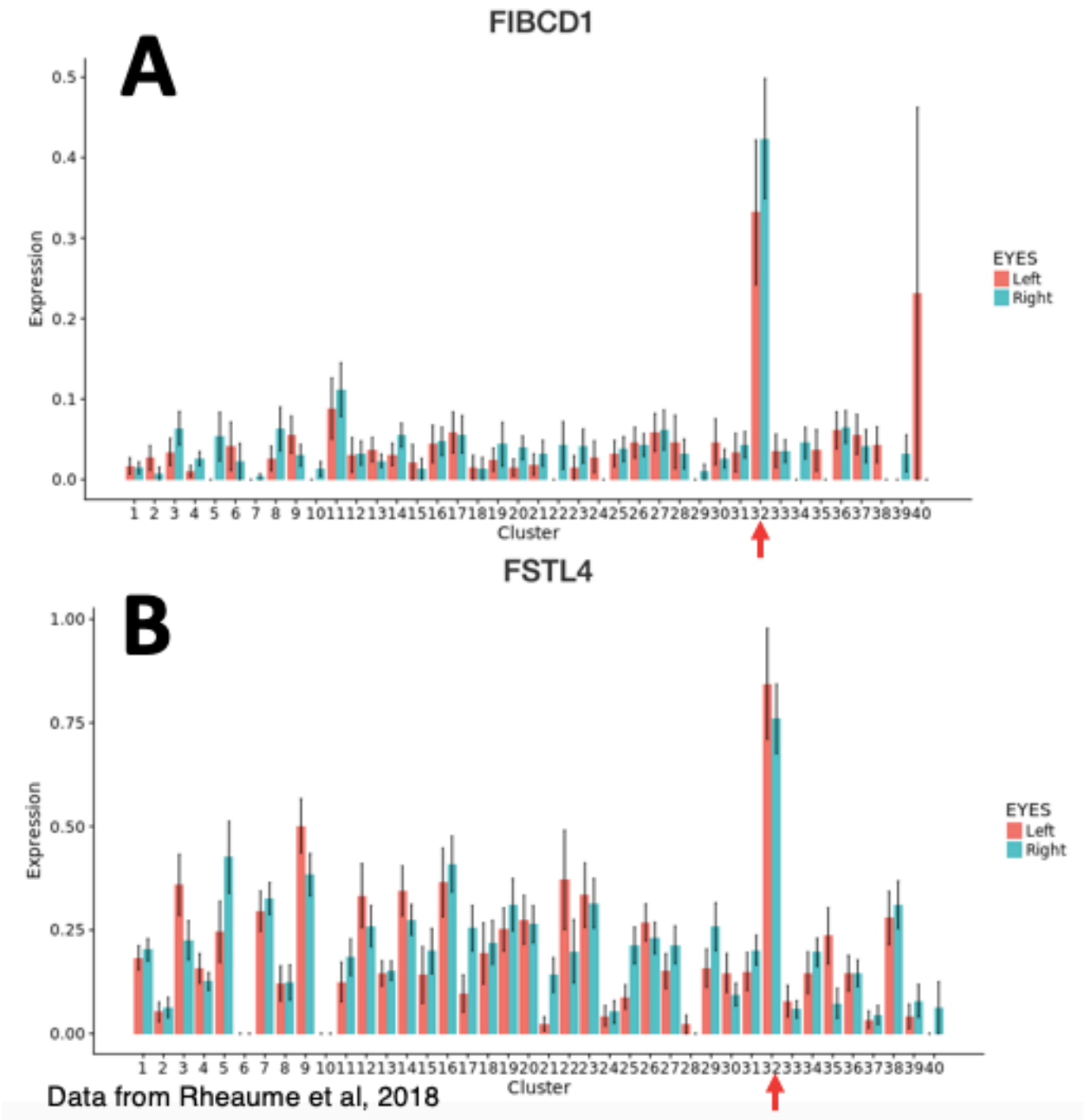
FIBCD1
A
Expression
0.0
0.1
0.2
0.3
0.4
0.5
1 2 3 4 5 6 7 8 9 10 11 12 13 14 15 16 17 18 19 20 21 22 23 24 25 26 27 28 29 30 31 32 33 34 35 36 37 38 39 40
Cluster
EYES
Left
Right
FSTL4
B
Expression
0.00
0.25
0.50
0.75
1.00
1 2 3 4 5 6 7 8 9 10 11 12 13 14 15 16 17 18 19 20 21 22 23 24 25 26 27 28 29 30 31 32 33 34 35 36 37 38 39 40
Cluster
EYES
Left
Right
Data from Rheaume et al, 2018

Figure 4. *Fibcd1* expression limited to a subset of RGCs containing ON-Up DSGCs. (A) Expression of *Fibcd1* is largely restricted to a single cluster, #32, in a P5 RGC atlas, suggesting that few other RGCs express *Fibcd1*. (B) Expression of *Fstl4*, which encodes the ON-Up DSGC marker Spig1, is also limited to cluster #32, further suggesting that this cluster contains the ON DSGCs.

Figure 5

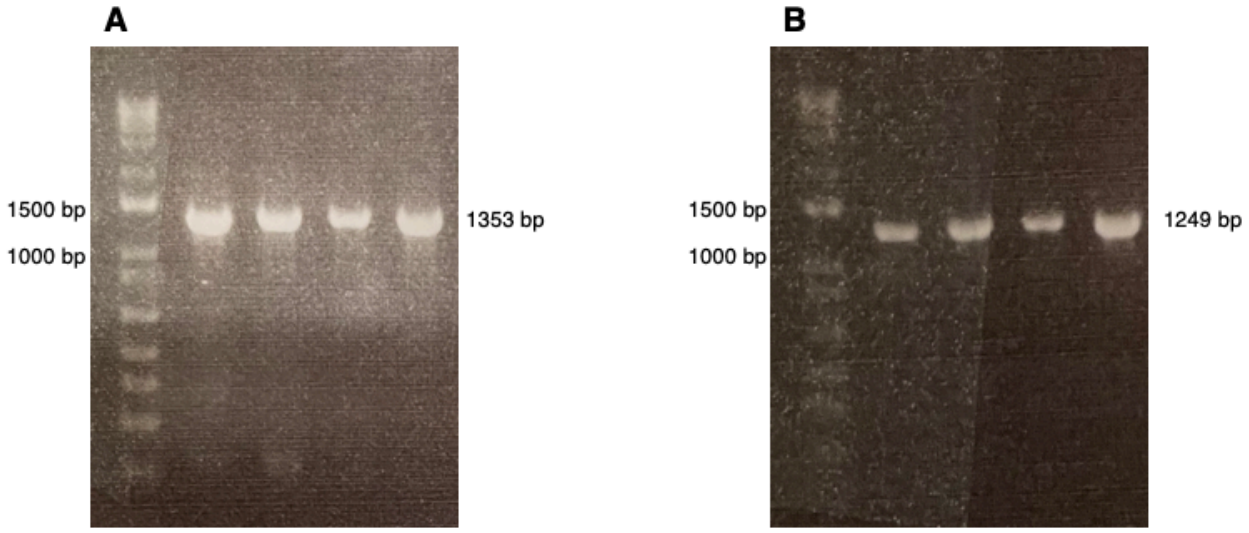

Figure 5. Successful integration of the Cre cassette at the *Fibcd1* locus. Bands indicating successful knock-in from 4 founders using TAK666 & TAK700 (A) and TAK673 & TAK671 (B).

Figure 6

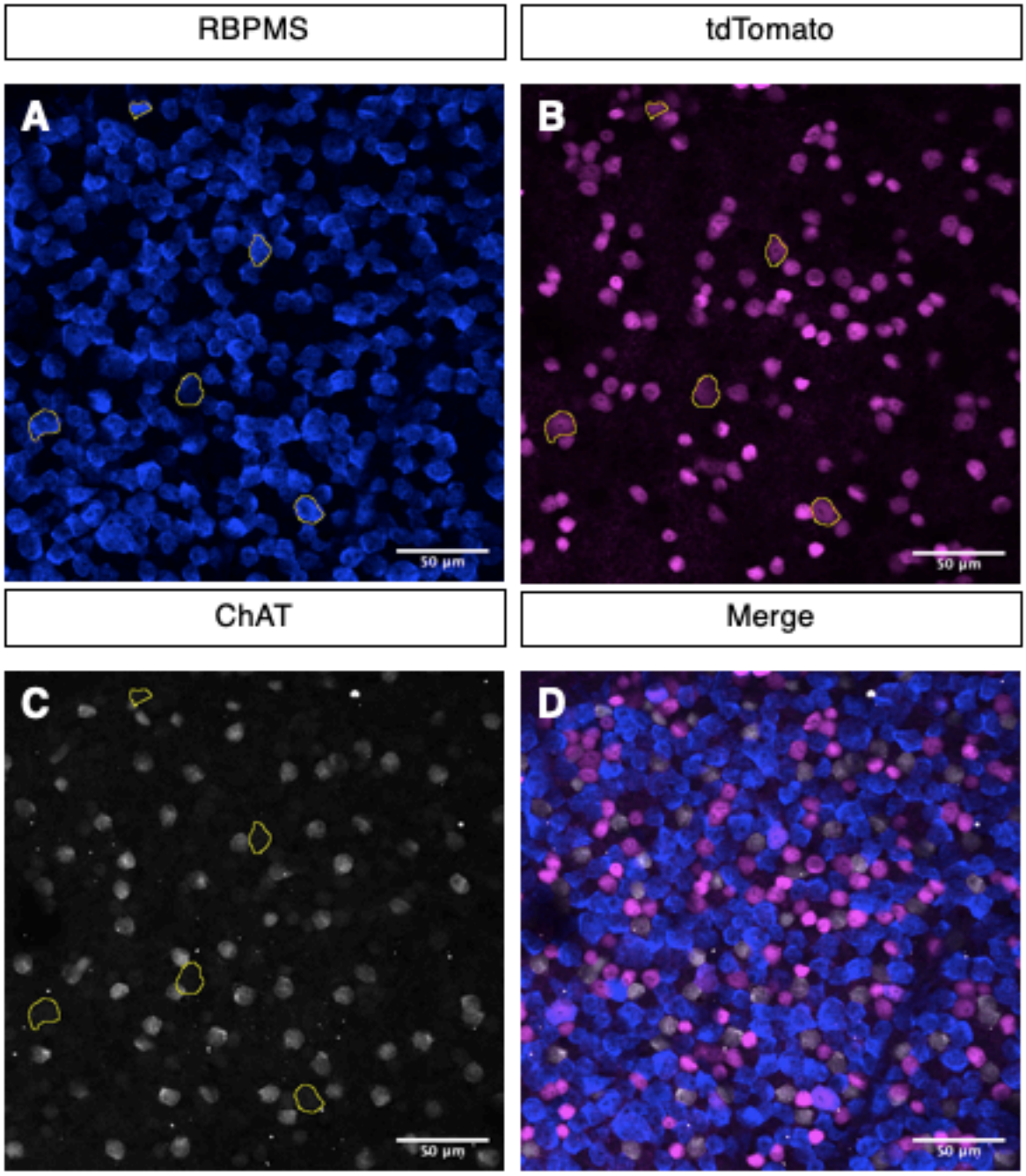

Figure 6. *Fibcd1*^{Cre} labels a rare RGC subtype and numerous ACs that are not SACs. (A-C) Staining of a whole-mount *Fibcd1*^{Cre}*;Ai14* retina for the RGC marker RBPMS (A), tdTomato to label Cre+ cells (B), and the SAC marker ChAT (C). (D) Merge of the channels. Arrow in the bottom-right corner marks an example of a cell that is a Cre+ (by tdTomato staining) AC (by lack of RBPMS staining) that is not a SAC (by lack of ChAT staining).

Figure 7

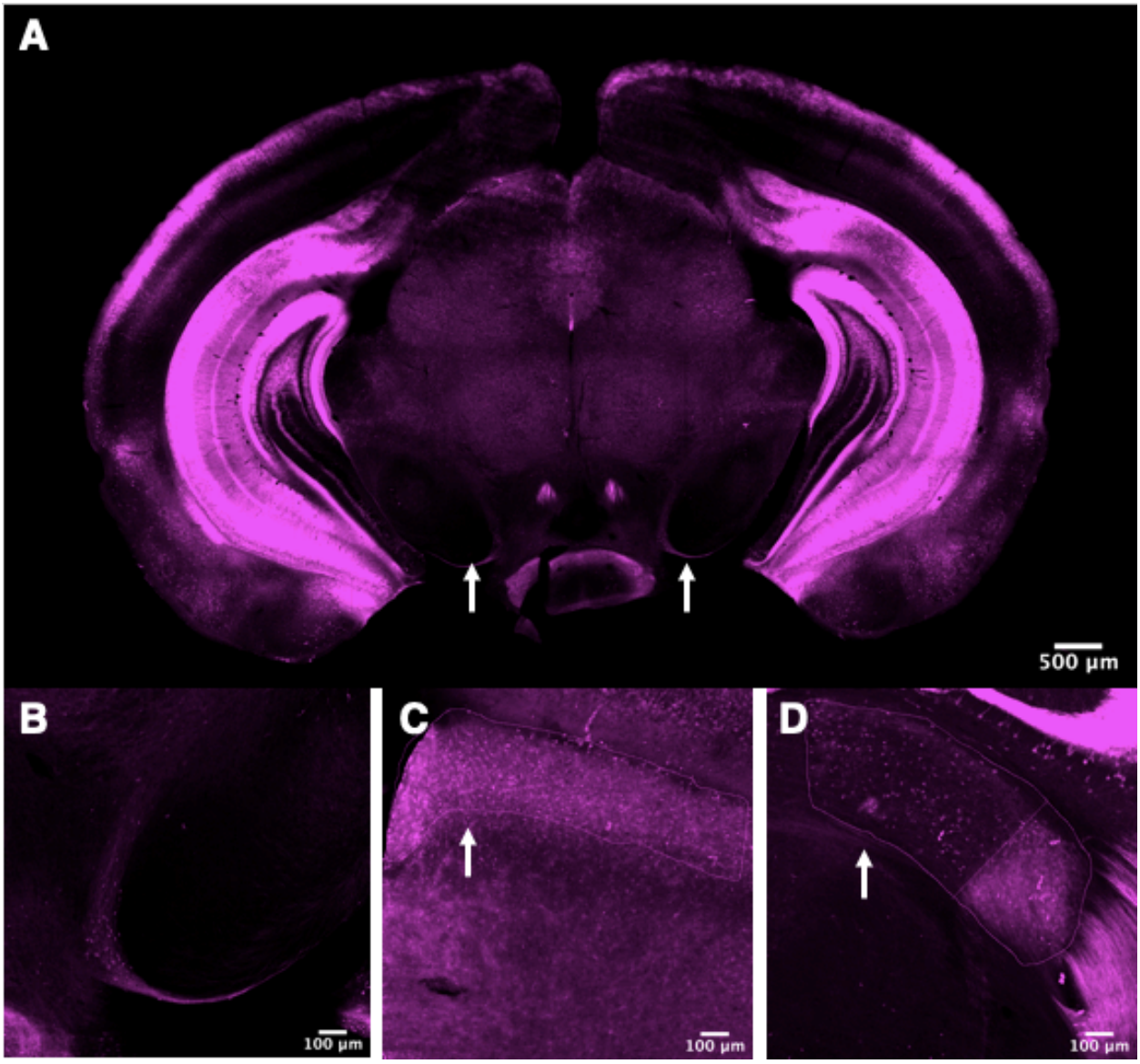

Figure 7. Expression of *Fibcd1^{Cre}* in retinorecipient regions. (A) Coronal section of a *Fibcd1^{Cre};Ai14* mouse stained for mCherry. White arrowheads point to the MTN, innervated by Cre+ axons. Note the abundant signal in the hippocampus. (B) Detail view of the right MTN in A. (C-D) Staining of the SC (C, white arrowhead) and dLGN (D, white arrowhead) do not reveal innervation by Cre+ axons, though the SC shows Cre+ cell bodies.

Figure 8

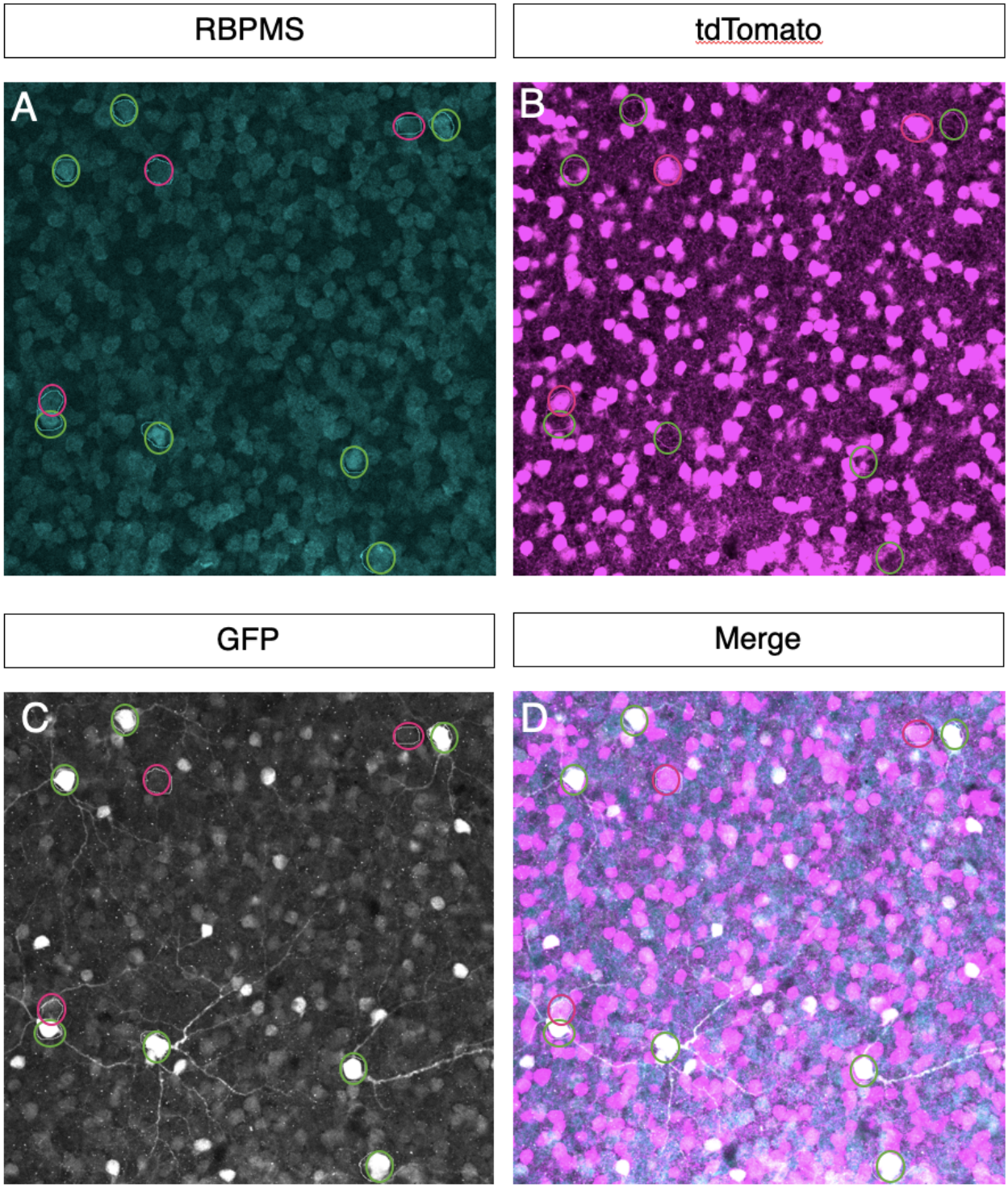

Figure 8. *Fibcd1*^{Cre} RGCs are not ON-Up DSGCs. (A-C) P11 whole-mount *Fibcd1*^{Cre}*;Ai14;Spig1-GFP* retinas stained for RBPMS (A, to label RGCs), tdTomato (B, to label Cre+ cells), and GFP (C, to label ON-Up DSGCs). (D) Merge of the channels. ON-Up DSGCs are circled in green; Cre+ RGCs are circled in magenta. Note the lack of overlap between the two groups, as well as the "doublets" of GFP+ ON-Up and tdTomato+ ON-Down DSGCs.

Figure 9


AAV2 ITR
fNPY promoter
loxP
lox2272
BGH polyA
EGFP
loxP
lox2272
AAV2 ITR

Figure 9. Design of pAAV-fNPY-FLEX-GFP. This plasmid is a modification of the pAAV-fNPY-GFP construct generated by the Lab of Dr. E. Callaway, Salk Institute, described in Nathanson et al, 2009. The original EGFP-BGH polyA cassette was excised using NotI/PstI sites and replaced with a FLEX version of the same sequence using NotI/PstI sites. In Cre lines that label a particular AOS-projecting DSGC subtype, the desired DSGC will be the only retinal cell capable of both recombining the FLEX cassette and driving EGFP expression from the fNPY promoter.

Figure 10

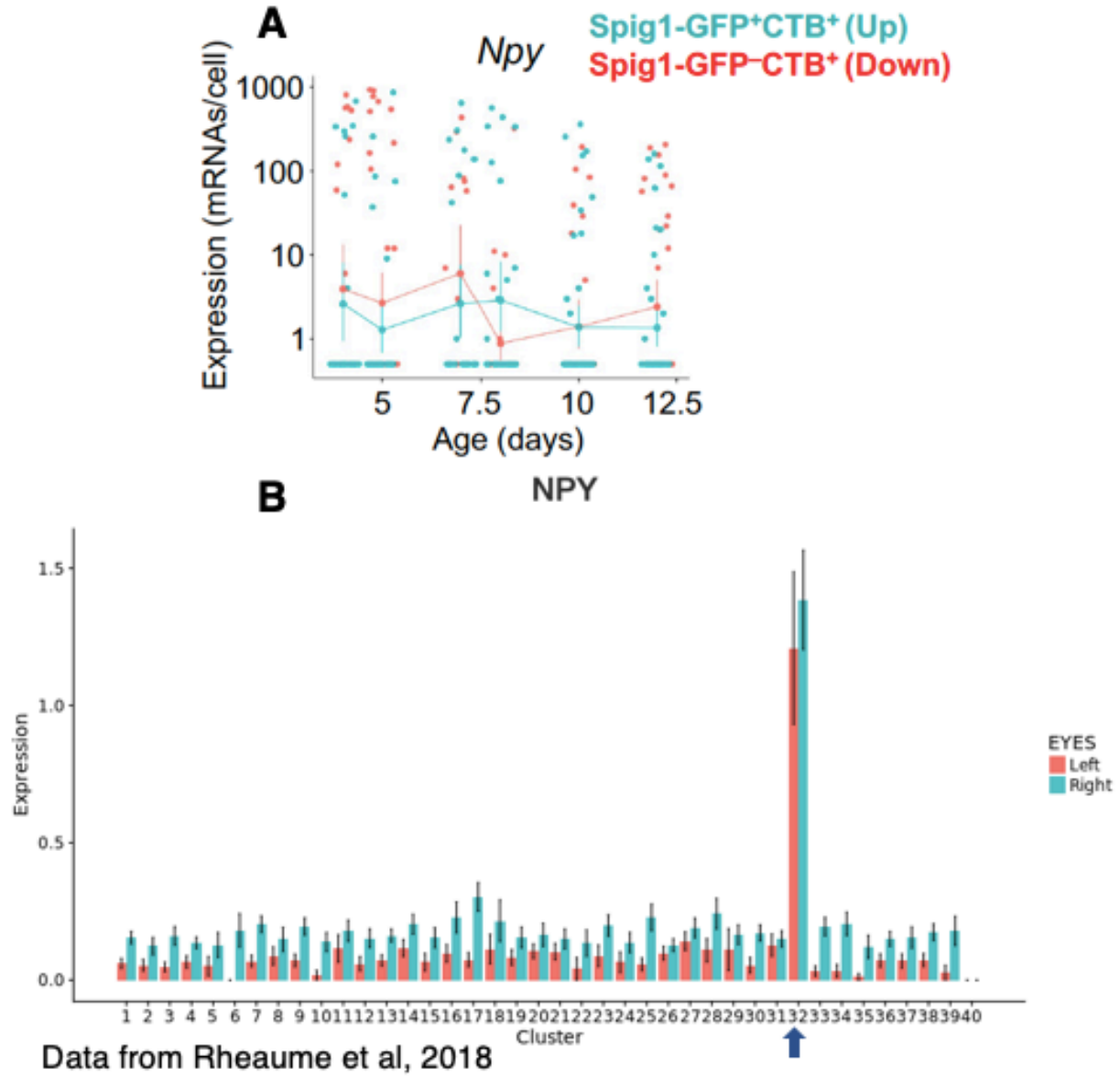
A
Npy
Spig1-GFP+CTB+ (Up)
Spig1-GFP−CTB+ (Down)
Expression (mRNAs/cell)
1000
100
10
1
5
7.5
10
12.5
Age (days)
B
NPY
Expression
1.5
1.0
0.5
0.0
EYES
Left
Right
Cluster
Data from Rheaume et al, 2018

Figure 10. *Npy* expression in RGCs tied to vertically-tuned ON DSGCs. (A) Jitter plot from our scRNA-Seq experiment for *Npy*, revealing expression in both ON-Up and ON-Down DSGCs. (B) Data from a P5 RGC atlas (Rheaume et al, 2018) further corroborating the expression of *Npy* in vertically-tuned ON DSGCs; expression is limited to cluster #32, the cluster containing *Fibcd1* and *Fstl4* expression.

Chapter 3: Examining the role of *Ptprm* in ON-Down DSGCs

Introduction

Ptprm encodes PTPRM, a receptor tyrosine phosphatase (RTP) comprised of an extracellular portion containing 1 MAM domain, 1 immunoglobulin-like domain, and 4 fibronectin type III domains; a single-pass transmembrane domain; and an intracellular portion with 2 phosphatase domains, only 1 of which is catalytically active (Aricescu et al, 2006). *Ptprm* belongs to the R2B subfamily of RTPs, the other members of which are *Ptprk*, *Ptprt*, and *Ptpru* (Tonks, 2006). Each member of this subfamily exhibits homophilic binding, but does not bind other members of the subfamily heterophilically (Zondag et al, 1995). As the phosphorylation of cadherins and catenins is negatively associated with cell-cell contact interactions at adherens junctions (Behrens et al, 1993), it is notable that PTPRM also binds the type I classical cadherins E-cadherin (in a mink lung cell line *in vitro*; Brady-Kalnay et al, 1995) and VE-cadherin (in human lung microvascular endothelial cells *in vitro;* Sui et al, 2005), as well as the catenins β-catenin (in rat brain lysate; Brady-Kalnay et al, 1995) and $p120^{ctn}$ (in COS-7 cells; Zondag et al, 2000). The interaction of these proteins with PTPRM promotes their dephosphorylation in order to stabilize cadherin-catenin interactions and thereby stabilizing adherens junctions (Sallee et al, 2006). This positions *Ptprm* to be a potential regulator of synaptic connectivity, a process critical for the establishment of neuronal circuits such as the DS circuitry.

Studies of the chick visual system suggest that *Ptprm* has a role in proper retinotopic mapping within the optic tectum. At E8, when innervation of the anterior optic tectum by RGCs is underway (Crossland et al, 1975), *Ptprm* expression in the chick is high in the temporal retina and low in the nasal retina; within the optic tectum, *Ptprm* expression varies in a smooth gradient with maximal expression in the anterior tectum and minimal in the posterior tectum. Thus, these regions of the retina innervate portions of the optic tectum with similar *Ptprm* expression levels; this raises the possibility that *Ptprm* serves as a retinotopic cue, with *Ptprm*+ temporal RGCs halting their axons in the *Ptprm*+ anterior tectum and *Ptprm*- nasal RGCs routing their axons through to the posterior tectum. Importantly, the timing of this experiment indicates that *Ptprm* is present in the anterior optic tectum when RGC axons from the temporal retina have reached it and must choose whether to proceed into the posterior tectum or halt their growth. The possibility of *Ptprm* serving as a retinotopic cue is further supported by stripe assays that indicate PTPRM is an inhibitory substrate for retinal explants taken from the temporal retina, whereas it is a permissive substrate for explants from the nasal retina (Burden-Gulley et al, 2002). These findings in the chick visual system raise the possibility that *Ptprm* may function in retinorecipient targeting within the mouse visual system, though a role for *Ptprm* in RGC dendritic development has not yet been identified.

Remarkably, our scRNA-Seq data indicate that two other members of the R2B subfamily show selective expression in two other subtypes of ON DSGCs. In the transcriptomic dataset that revealed selective expression of *Ptprm* in ON-Down DSGCs,

Ptprk is the second-most significantly enriched gene in ON-Up DSGCs, behind only *Fstl4* (which encodes *Spig1*). Moreover, an analysis of cells labeled by *Hoxd10-GFP*, which labels ON-Forward DSGCs as well as ON-Up and ON-Down DSGCs (Dhande et al, 2013), indicates that *Ptprt* is selectively enriched in a population that we speculate to contain or comprise the ON-Forwards (Natalie Hamilton, unpublished observations). This positions the R2B subfamily of RTPs as a potential molecular code for the different subtypes of ON-DSGCs. Most importantly, *Ptprk-KO* mice have a selective impairment in the circuitry mediating responses to slow vertical, but not horizontal, motion. Responses to stimuli traveling upward are significantly reduced, whereas responses to horizontal motion remain undisturbed. Following loss of *Ptprk*, the dendritic arbors of ON-Up DSGCs expand in area and decrease in branch point number, with no change in total dendritic length or asymmetry (TAK, unpublished work). These changes in behavior and ON-Up DSGC morphology following loss of *Ptprk* suggest that similar changes may be observed in ON-Down DSGCs following loss of *Ptprm*.

Results

Generating Ptprm-flox *and* Ptprm-null *alleles*

The only *Ptprm* loss-of-function (LOF) allele in the literature is a *LacZ* knock-in allele, providing a *Ptprm-null* allele. Acquiring this mouse would be problematic, as its only known source is a laboratory in the Netherlands, where it is kept on an FVB

background (Koop et al, 2003); since mice on this background go blind at weaning (Wong et al, 2012), they would need to be bred onto a B6 background prior to testing visual function. Moreover, the lack of a *Ptprm-flox* allele would preclude conditional ablation experiments, preventing assessment of requirements for *Ptprm* in specific cell types.

To address this, I first used CRISPR-Cas9 technology to insert loxP sites flanking exon 3 of *Ptprm*, creating a *Ptprm-flox* allele (Figure 11A). Recombination of this allele by Cre will cause a frameshift that introduces a premature stop codon into exon 4. In addition to being the 5'-most exon, aside from exon 1, whose loss would cause the desired frameshift, I chose exon 3 because it is also the exon deleted in the existing *Ptprk-KO* allele (The Jackson Laboratory, 2012) and the intron-exon structure of the two genes is similar.

Out of 45 mice produced by the CRISPR experiment, 3 mice demonstrated successful integration of both loxP sites. Integration was verified using 2 pairs of PCR primers, each flanking the integration locus of one loxP site; one primer in each pair was placed distal to the homology arms of the insert, such that bands would only be generated if the insert were integrated at the intended locus (Figure 11A). In these 3 mice, these reactions yielded a WT band and a knock-in band ~34 bp larger; sequencing of the larger bands confirmed successful integration of the loxP sites without unintended alterations. Founders were crossed to B6 to confirm ability to successfully propagate the *Ptprm-flox* allele; progeny from one founder, #679, were

used to subsequently propagate the line and further cross it back onto the B6 genetic background.

To generate the *Ptprm-KO* allele, I crossed a *Ptprm f/+* male to a *Sox2-Cre* female; progeny of these females exhibit embryonic Cre activity regardless of genotype (Hayashi et al, 2002), yielding global recombination of any floxed alleles present (Figure 11B). Approximately half of the progeny of this cross (5/8) had a recombined *Ptprm* allele to yield the *Ptprm-KO* allele, as predicted by the genotypes of the parents; recombination was verified by PCR and sequencing of the resulting bands. This also provided confirmation that the *Ptprm-flox* allele was designed correctly and could be recombined by Cre. Homozygous *Ptprm-KO* mice are viable and fertile, produced progeny in Mendelian ratios, and showed no obvious gross developmental impairments.

Global Ptprm *loss leads to a selective deficit in the optokinetic reflex*

Ptprm -/- mice were assessed for deficits in the optokinetic reflex (OKR), an image-stabilizing reflex that is mediated by ON-DSGCs (Simpson et al, 1984). This assay places head-fixed mice in a chamber surrounded by screens displaying checkerboard stimuli, traveling either continuously in one of four cardinal directions or sinusoidally along the horizontal or vertical axis, and tracking their left eye using recordings from an infrared camera. Stimuli travel at speeds slow enough to be detected enough by ON DSGCs (5 degrees of visual space per second for continuous stimuli, 0.1-0.2 Hz for sinusoidal stimuli). For continuous stimuli, the reflex is scored by

counting the number of “eye-tracking movements” (ETMs), defined as a slow eye movement tracking the moving stimulus followed by a rapid saccade to reset the eye position; for sinusoidal stimuli, it is quantified by measuring the gain of the sinusoidal eye movement (the velocity of the eye divided by the velocity of the stimulus; Yonehara et al, 2016).

Along the horizontal axis, no significant differences were observed in the responses of *Ptprm -/-* mice to nasotemporal motion (Figure 12A; control: 9.49 +/- 2.57 ETM/min; KO: 7.88 +/- 1.40 ETM/min; p=0.09, Mann-Whitney U Test). These results affirm that loss of *Ptprm* does not lead to a global disruption of retinal DS. Somewhat unexpectedly, *Ptprm -/-* mice showed a significantly impaired response to temperonasal motion (Figure 12B; control: 9.83 +/- 2.57 ETM/min; KO: 7.88 +/- 1.40 ETM/min; p=0.0038, Mann-Whitney U Test). Along the vertical axis, *Ptprm -/-* mice showed impaired responses to ventrodorsal (i.e. upward) motion (Figure 12C; control: 5.41 +/- 1.71 ETM/min, n=10; KO: 2.90 +/- 0.92 ETM/min, n=9; p=0.0015, Mann-Whitney U-Test), but not dorsoventral (i.e. downward) motion (Figure 12D; control: 1.77 +/- 1.24 ETM/min; KO: 0.94 +/- 0.54 ETM/min; p=0.13, Mann-Whitney U Test). The lack of a dorsoventral phenotype may be partially due to the documented weakness (Yonehara et al, 2016) of the OKR in this direction in WT mice. No significant differences were detected in response to sinusoidal stimuli in the vertical or horizontal axes (Figure 13). Intact overall visual function was further confirmed by normal responses of *Ptprm -/-* mice in the looming assay (Yilmaz & Meister, 2013), which tests a mouse’s ability to freeze and seek shelter in response to a simulated descending predator. Taken

together, these results indicate that *Ptprm -/-* mice show selective deficits in their response to upward and temperonasal stimuli.

Conditional deletion of Ptprm *using* Fibcd1^{Cre} *leads to a selective vertical deficit in the optokinetic reflex*

Although global loss of *Ptprm* induced the hypothesized deficits in the vertical OKR response, the possible expression of *Ptprm* in ON-BCs (Kay et al, 2011b) that provide excitatory input onto ON-Down DSGCs, as well as in non-SAC ACs (Yan et al, 2020), leaves open the possibility that the role for *Ptprm* in the DS circuitry detecting vertical motion lies outside of the DSGC. Furthermore, the defect in responses to temperonasal motion indicates that the role for *Ptprm* in DS extends beyond the circuit containing ON-Down DSGCs. While this is not fully surprising, given that *Ptprm* is expressed in many classes of RGCs (Rheaume et al, 2018), it underscores the need to perform experiments in mice in which *Ptprm* has been conditionally deleted in ON-Down DSGCs.

To address this, I generated *Fibcd1^{Cre};Ptprm f/-* CKOs. Although *Fibcd1^{Cre}* induces recombination in numerous classes of non-SAC ACs as well as ON-Down DSGCs, the overlap of *Fibcd1* and *Ptprm* expression in AC classes is quite minimal (Yan et al, 2020), suggesting that ON-Down DSGCs will be the overwhelming majority of cells whose endogenous expression of *Ptprm* is disrupted in this condition.

Similar to global *Ptprm* mutants, *Fibcd1^{Cre};Ptprm f/-* CKOs exhibited weaker responses to ventrodorsal motion than *Fibcd1^{Cre};Ptprm f/+* control littermates (Figure 14A; control: 4.16 +/- 0.72 ETM/min; CKO: 3.21 +/- 0.98 ETM/min; p=0.046, Mann-Whitney U-Test). These results argue that the deficit in this reflex observed in global *Ptprm* KOs is due to the loss of *Ptprm* in ON-Down DSGCs. Responses to dorsoventral motion were unaffected (Figure 14B; control: 1.79 +/- 1.35 ETM/min; CKO: 1.05 +/- 0.84 ETM/min; p=0.39, Mann-Whitney U Test), as they were in the global *Ptprm* null mutant. Importantly, restricting loss of *Ptprm* to *Fibcd1*+ cells leads to normal responses along the horizontal axis to tempronasal motion (Figure 14C; control: 11.22 +/- 2.20 ETM/min; CKO: 10.85 +/- 1.56 ETM/min; p=0.54, Mann-Whitney U Test), and also to nasotemporal motion, with no evidence of a significant impairment (Figure 14D; control: 10.27 +/- 2.77 ETM/min; CKO: 7.79 +/- 2.25 ETM/min; p=0.11, Mann-Whitney U Test). No significant differences were detected in response to either vertical or horizontal sinusoidal stimuli (Figure 15). Intact overall visual function was further confirmed by normal responses of *Fibcd1^{Cre};Ptprm* CKOs on the looming assay. These results suggest that *Ptprm* is specifically required in ON-Down DSGCs for the proper formation of the retinal DS circuitry detecting vertical motion.

MTN innervation is grossly normal in Ptprm -/- mice

A reduction in the ability to respond to vertical OKR stimuli could be the result of abnormal innervation of the MTN, preventing vertical directional information from being

transmitted to the brain region meant to receive it. This possibility is particularly plausible for *Ptprm*, given its hypothesized role as a retinotopic cue in the chick visual system (Burden-Gulley et al, 2002).

As a preliminary method for investigating this question, I labeled all retinofugal axons using intraocular injections of CTβ-555 in *Ptprm -/-* mice. In all mice (n=4), MTN innervation appeared grossly normal (Figure 16A). The fiber bundle innervating the vMTN, comprised mainly of ON-Down DSGCs, is also present (Figure 16B), suggesting that the appearance of normal MTN innervation is not the product of normal ON-Up DSGC innervation obscuring the absence of ON-Down DSGCs. These results are in line with the hypothesis that OKR impairments following loss of *Ptprm* is not due to ON-Down DSGC axons no longer reaching their targets in the MTN.

Discussion

These results demonstrate that *Ptprm* is required for the proper function of the DS circuitry containing ON-Down DSGCs. They provide further validation for the exploration of genes identified in the Kolodkin laboratory's scRNA-Seq experiment (Al-Khindi et al., 2022) to search for their involvement in the wiring of retinal DS circuitry. Additionally, they expand the role for members of the R2B family of RTPs in the development of ON DSGCs, further suggesting that *Ptprt* is critical for ON-Forward DSGCs. To date, work using an existing *Ptprt-KO* allele has not shown an impairment in the OKR (NH, unpublished data). However, it is important to note that this allele deletes

the phosphatase domains of *Ptprt* while leaving the extracellular, transmembrane, and some of the intracellular domains intact (Zhao et al, 2010). In experiments using Sf9 insect cells *in vitro,* the extracellular and juxtamembrane portions of PTPRM are capable of mediating cell-cell adhesion in the absence of the catalytic phosphatase domains (Gebbink et al, 1993); thus, if PTPRT mediates ON-Forward DSGC circuit development through cell-cell adhesion, its phosphatase domains may be dispensable, and this allele would therefore not produce an OKR phenotype. To further the study of R2B PTPs within the Kolodkin Lab, I generated a *Ptprt-flox* allele with a design analogous to *Ptprm-flox* (data not shown); we will cross this line to *Sox2-Cre* to generate a new *Ptprt-KO* allele that generates a true null. Aside from possibly providing further evidence for the importance of this family of PTPs in ON DSGCs, an OKR phenotype using this new *Ptprt-KO* allele would indicate that the phosphatase domain of PTPRT is not required for mediating ON-Forward DSGC circuit development. This would greatly narrow the range of potential molecular mechanisms for PTPRT and suggest that the phosphatase domains of PTPRK and PTPRM are also not required for their roles in their respective ON DSGCs.

The fact that the ventrodorsal phenotype observed in global *Ptprm -/-* mice is also observed in *Fibcd1*^{Cre} *Ptprm* CKOs strongly suggests that *Ptprm* is specifically required in ON-Down DSGCs for circuit integrity. However, although very few ACs express both *Fibcd1* and *Ptprm*, with SACs expressing neither, the presence of *Fibcd1*+ ACs prevents the completely definitive conclusion that the phenotype observed in these CKOs is purely due to loss of *Ptprm* in ON-Down DSGCs. To address this, we are

generating *Ptprm* CKOs using *VGlut2-Cre*, removing *Ptprm* from all RGCs and no other retinal cells (Wang et al, 2020), and *Ptf1a-Cre*, removing *Ptprm* from all ACs (Nakhai et al, 2007). If ON-Down DSGCs are the cells mediating the OKR phenotype in *Fibcd1*^{Cre} CKOs, the *VGlut2-Cre* CKOs should have the ventrodorsal phenotype and the *Ptf1a-Cre* CKOs should not. Moreover, if the *VGlut2-Cre* CKOs exhibit the temperonasal phenotype observed in global KOs, this would indicate that the ON DSGCs controlling that reflex require *Ptprm* for normal development.

Models for the role for *Ptprm* in the development of the DS circuitry containing ON-Down DSGCs must be informed by the recent finding that *Ptprk -/-* ON-Up DSGCs show no apparent reduction in their direction selectivity index (DSI) or change in tuning preference, but do exhibit increased firing rates in response to all directions (including the ND). However, these mutant ON-Up DSGCs also show increased firing in response to flashes of a static stimulus (T. Al-Khindi, in collaboration with the Lab of M. Feller, UC Berkeley, unpublished data). These data would suggest that loss of *Ptprk* increases excitation of ON-Up DSGCs, weakens inhibition onto them (without impairing the directionality of inhibition), or both. It is important to note that these recordings were done using stimuli different from those used in our OKR recordings; these experiments were done using bars, as opposed to the checkerboards in the OKR experiments, and these stimuli traveled across the visual field at a higher speed. While *Ptprk* does have a role in the normal development and function of ON-Up DSGCs, it is not required for these cells to acquire their directional preference. Similar electrophysiological

recordings must be done in *Ptprm*-KO ON-Down DSGCs to determine whether this firing rate phenotype is also present.

How might *Ptprk* exert these effects – and by extension, how might *Ptprm* be functioning? Preliminary data from the use of a gephyrin intrabody approach to label inhibitory postsynaptic densities suggest that loss of *Ptprk* does not alter inhibitory synapse number or distribution in ON-Up DSGCs (T. Al-Khindi, unpublished data). Inhibition could still be weakened, however, by a reduction in the efficacy of these inhibitory synapses. A study of mouse hippocampus and cortex found that phosphorylation of the a2 subunit of ionotropic $GABA_AR$s at Ser-359 reduces their ability to associate with gephyrin (Nakamura et al, 2020). This raises the possibility that PTPRK dephosphorylates a2 subunits to promote $GABA_AR$ binding to gephyrin; in its absence, inhibitory synapses are uniformly less effective across the dendritic arbor, yet the structural asymmetry of the circuit preserves the directional tuning of the DSGC's responses. One approach to test this hypothesis in ON-Up DSGCs might be to combine intrabody labeling of gephyrin with crosses to a mouse line that harbors a tagged a2 subunit to investigate whether colocalization of $GABA_AR$s with the inhibitory scaffold is altered following loss of *Ptprk*.

A recent study of cortical layer 2/3 excitatory neurons (Landau et al, 2022) provides a possible model for how altered dendritic geometry in *Ptprk -/-* ON-Up DSGCs could increase excitatory efficacy. This study investigated differences in calcium influx across segments of layer 2/3 excitatory neuron dendritic arbors in response to back-propagating action potentials (bAPs). While variation of bAP-induced calcium influx had

long been observed along the proximal-distal axis (Waters et al, 2003), these new recordings revealed that the factor that best explained influx strength was the complexity of the surrounding dendritic arbor. The authors posit that this is due to the fact that increased amount of dendritic arbor in a given area will reduce input resistance. Since loss of PTPRK reduces the amount of dendritic length per unit area of the ON-Up DSGC arbor, input resistance may be attenuated in these cells as well. This shift in input resistance may weaken the compartmentalization of excitation found in DSGC dendrites due to inhibitory control (Jain et al, 2020) and/or render excitatory inputs more effective in driving postsynaptic depolarization and thereby DSGC firing. This model provides a link between all observed *Ptprk -/-* phenotypes, which is not the case for the above $GABA_AR$ dephosphorylation model. This model could be tested using glutamate uncaging experiments in labeled *Pcdh9-Cre; Ptprk -/-* retinas, measuring whether a given amount of excitatory neurotransmitter leads to greater excitatory influx, followed by 2-photon calcium imaging in response to directional stimuli, to determine whether excitation is more widespread and/or of greater intensity.

Although *Ptprk* appears at present not required for ON-Up DSGCs to gain their directional preference, this possibility has not been ruled out for *Ptprm*. Our collaborators in the Lab of M. Feller at UC Berkeley were temporarily unable to perform patch-clamp recordings or calcium imaging experiments following the discovery of the *Ptprm* phenotype. Once these recordings become available again, it will be of the utmost importance to determine whether the DS of *Ptprm* CKO ON-Down DSGCs is impaired and/or whether firing rates globally increase, as is observed in *Ptprk -/-* retinas.

Future studies are needed to determine which components of the DS circuit containing ON-Down DSGCs are impaired following loss of *Ptprm*. For analysis of whether loss of *Ptprm* changes inhibitory synapse number and/or distribution, we will package the gephyrin intrabody into a rAAV2 capsid to allow for labeling via stereotaxic MTN injections; pilot experiments using intraocular injections of the intrabody construct packaged in AAV2 gave too much labeling of *Fibcd1*+ ACs to assign puncta to DSGCs, so it is necessary to avoid them via injections of rAAV2-packaged virus into the MTN (J. Kiraly, data not shown). Cloning the gephyrin intrabody construct into the pAAV-fNPY backbone is not viable due to AAV packaging size limitations. To examine connected SACs, we will inject P3 *Fibcd1*^{Cre}*;Ptprm* CKOs with Rabies-ΔG-mCherry and HSV-DIO-G-GFP. In this experimental paradigm, developed by T. Al-Khindi (unpublished observations), ON-Down DSGC starter cells are labeled with GFP and mCherry; these cells also express the G glycoprotein required for rabies to be transmitted presynaptically. These newly-infected presynaptic cells do not express G, preventing rabies from being transmitted to cells more than one synapse away from the starter cells. Connected SACs will distinguished from other presynaptic cells by staining for ChAT. We will collect retinas at P6, prior to the onset of DS, and at P10, following DS onset, to count connected SACs, measure the symmetry of their distribution, and examine whether these factors change with the onset of DS. Preliminary data show that in WT mice, this approach reveals an asymmetric distribution of connected SACs after P7 (Al-Khindi et al., unpublished observations). Additionally, we will label the dendritic arbors of *Fibcd1*^{Cre}*;Ptprm* CKO ON-Down DSGCs using AAV9-fNPY-FLEX-GFP to test

for changes in dendritic length, area, symmetry, and branch point number. The apparent normal innervation of the MTN in *Ptprm-KO* mice suggests that ON-Down DSGCs correctly route their axons to their intended target. To definitively test this, as well as check for the rerouting of axons to other targets, we will label *Fibcd1^{Cre};Ptprm* CKO ON-Down DSGCs using AAV2-FLEX-GFP and examine the trajectories of these axons into the brain stem and their retinorecipient targeting. Even if ON-Down DSGCs innervate the MTN in the absence of *Ptprm*, it would be possible that the axon terminals fail to form synapses. To address this, we will label cells in the MTN postsynaptic to ON-Down DSGCs using AAV2-CAG-DIO-WGA-mCherry, a novel Cre-dependent construct that fuses mCherry to a codon-optimized WGA in order to fluorescently label postsynaptic cells (Tsai et al, 2022). Finally, for testing whether these ON-Down DSGC synapses are driving activity in their postsynaptic targets, we will expose headfixed *Fibcd1^{Cre};Ptprm* CKO mice to directional stimuli, then immediately collect brain sections to stain for cFos, following the approach described in Yonehara et al, 2009. These experiments will establish how *Ptprm* is required for proper circuit formation, which will in turn inform subsequent mechanistic studies by providing a narrower domain of investigation.

Until all of the above studies have been performed to isolate which DS circuit component *Ptprm* regulates, the list of potential mechanisms for *Ptprm* involvement in DS tuning remains vast. In the following section, I will lay some of these out.

The potential mechanisms by which PTPRM could be acting homophilically are few, but still worth consideration. The only cells within the established DS circuit known to express *Ptprm* are ON-Down DSGCs and, possibly, the ON-BCs that provide them

with excitatory input (Kay et al, 2011b), which comprise types 5i, 5o, 5t, and 7 (Matsumoto et al, 2019). An atlas for BC subtypes (Shekhar et al, 2016) only probes gene expression at P19, past the second postnatal week in which DS appears and two weeks later than the data collected in Kay et al, 2011b; in this atlas, no BC subtypes express *Ptprm*, preventing a definitive assessment of whether the specific subtypes that connect with ON DSGCs express it during DS circuit development. One way to determine whether connected ON-BCs express *Ptprm* could be to perform the transsynaptic tracing experiment using with Rabies-ΔG-mCherry and HSV-DIO-G-GFP described above, collect retinas at P10, then probe retinal cross-sections for *Ptprm* expression using RNAScope, examining mCherry+ BC somas. Although this would not provide subtype-specific information about which ON-BC subtypes express *Ptprm,* the transsynaptic labeling would provide evidence as to whether any of the *Ptprm*+ ON-BCs are connected with ON-Down DSGCs. Should they express *Ptprm*, homophilic PTPRM interactions might be required for forming the arrangement of BC subtypes along the PD-ND axis based on their respective response kinetics (Matsumoto et al, 2019). If *Ptprm*-KO ON-Down DSGCs show dendritic phenotypes similar to *Ptprk*-KO ON-Up DSGCs, perhaps self-self interactions between PTPRM molecules on distinct dendritic branches of a single DSGC narrow the extent of their spread; a constraint on this model, however, is that a *trans* PTPRM-PTPRM dimer spans only 33 nm (Aricescu et al, 2007), providing a very limited window in which dendritic branches would be close enough for such an interaction.

Studies of associations between PTPRM and classical cadherins have been largely focused on type I classical cadherins; associations have been shown with Cdh1 (E-Cadherin; Hellburg et al, 2002), Cdh2 (N-Cadherin; Burden-Gulley and Brady-Kalnay, 1999), Cdh4 (Brady-Kalnay et al, 1995), and Cdh5 (VE-Cadherin; Sui et al, 2005). Cdh1 and Cdh5 are not expressed in neurons (Nollet et al, 2000; Brasch et al, 2011); Cdh2 is expressed at high levels in numerous retinal cell types, arguing against a DS circuit-specific mechanism (Kay et al, 2011b); and Cdh4 is not expressed in SACs, though it is in certain other GABAergic ACs (Kay et al, 2011b). Though associations of PTPRM with type I cadherins may not have direct implications for its function in the retina, they do suggest that interactions with type II cadherins are also possible. Given that the type II cadherin *Cdh6* is required for ON-OFF DSGCs preferring vertical, but not horizontal, directions to form proper connections with SACs (Duan et al, 2018), these molecules are promising targets. This promise is heightened by the fact that select expression of *Cdh6* in ON-OFF DSGCs with vertical, but not horizontal, tuning preferences is conserved in ON-DSGCs. Furthermore, in RGCs derived from chick embryos, catalytically-active PTPRM is required for neurite outgrowth on an N-cadherin substrate (Burden-Gulley and Brady-Kalnay, 1999). Thus, R2B RTPs may control the outgrowth of vertically-tuned ON DSGCs on the permissive Cdh6-containing SAC dendritic substrate. At adherens junctions containing type I cadherins, RTPs like PTPRM dephosphorylate the cadherins themselves as well as the catenins with which they associate, including $p120^{Ctn}$ and β-catenin; promoting the dephosphorylation of both classes of molecules is important for maintaining junction stability (Sallee et al,

2006). Not all RTP interactions at adherens junctions are phosphatase-dependent, however; in prostate carcinoma cells, PTPRM binding to E-cadherin and RACK1, a protein that serves as a scaffold for a variety of signaling pathways, does not require the catalytic phosphatase domains (Hellburg et al, 2002). Beyond the cadherins and their associated proteins, the numerous extracellular domains of *Ptprm* involved in cell adhesion provide the theoretical ability to associate with a wide array of proteins. The R2A subfamily of RTPs, including PTPRS, acts as presynaptic organizers capable of binding postsynaptic proteins such as NGL-3, TrkC, and members of the Slitrk family (Fukai and Yoshida, 2021). Though the arrangement of extracellular domains with putative adhesive properties is different in R2B RTPs, PTPRM might act in a similar fashion and molecular orientation for forming functional synapses with postsynaptic targets in the MTN, or it could bind presynaptic proteins with adhesive domains such as neurexins (Südhof, 2017).

These results thus represent an entry point into a complex set of biological questions regarding how *Ptprm* affects ON-Down DSGCs. While it is clear that the circuitry containing these DSGCs cannot properly function without *Ptprm*, much work is needed to identify which components of the circuit fail in its absence and what molecular events take place in its presence to promote proper wiring. These future studies will provide insight both into the specific mechanisms needed for assembly of the DS circuit and will inform our understanding of more general mechanisms used throughout the vertebrate nervous system to regulate sensory tuning responses.

Figure 11

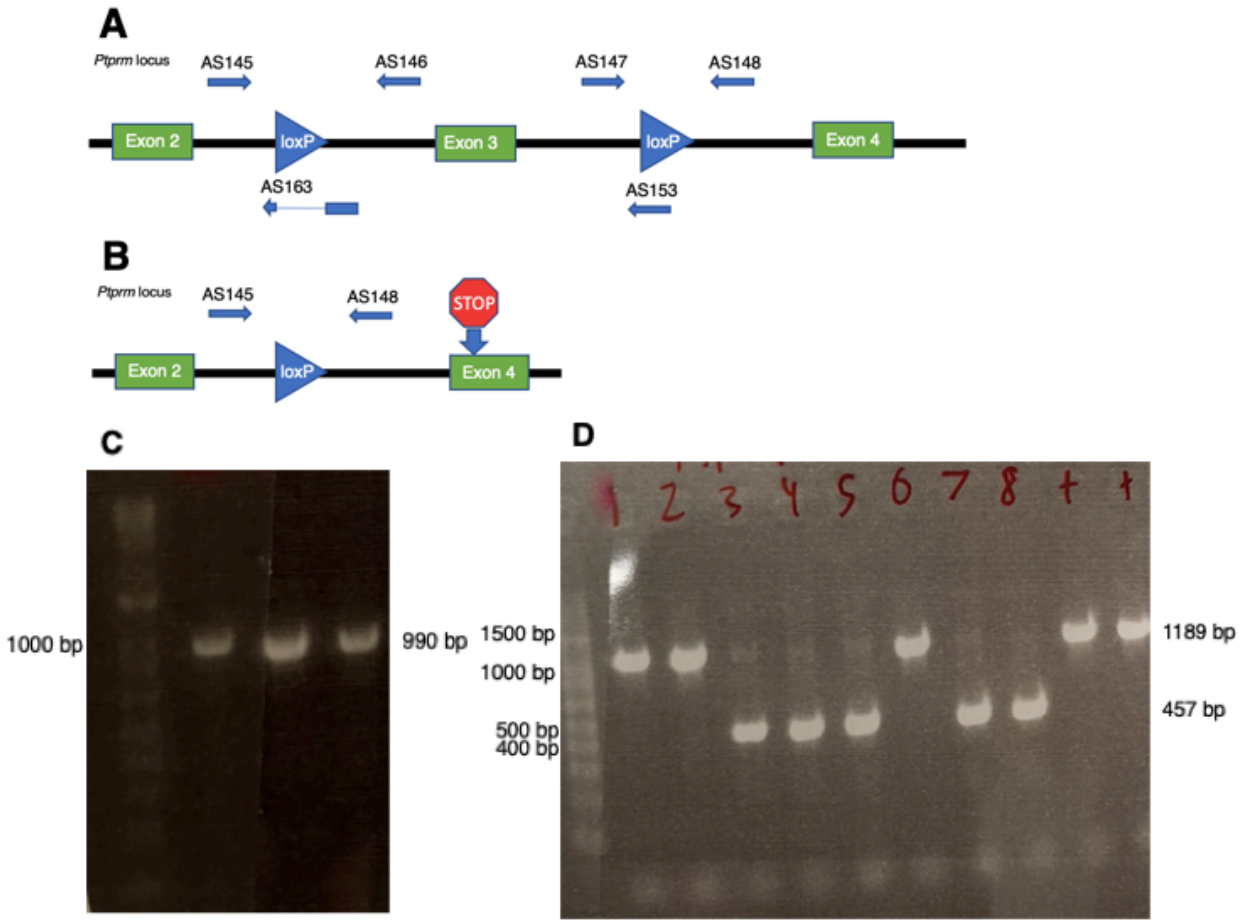
A
Ptprm locus
AS145
AS146
AS147
AS148
Exon 2
loxP
Exon 3
loxP
Exon 4
AS163
AS153
B
Ptprm locus
AS145
AS148
STOP
Exon 2
loxP
Exon 4
C
1000 bp
990 bp
D
1 2 3 4 5 6 7 8 + +
1500 bp
1000 bp
500 bp
400 bp
1189 bp
457 bp

Figure 11. Design of *Ptprm-flox* and *Ptprm-KO* alleles. (A) Schematic for *Ptprm-flox*. loxP sites were inserted flanking exon 3. Verification of correct insertion was performed with PCR reactions using AS145 & AS146 (5' loxP site) and AS147 & AS148 (3' loxP site). The 5' reaction gives a WT band of 286 bp and a KI band of 320 bp; the 3' reaction gives a WT band of 285 bp and a KI band of 319 bp. Subsequent genotyping reactions to detect *Ptprm-flox* used AS145 & AS153, which binds the genomic DNA of intron 3 & the 3' loxP site and yields a band of 990 bp when the allele is present. Genotyping reactions for *Ptprm-WT* used AS145 & AS163, whose target region in the genome is disrupted by the loxP site present in both *Ptprm-flox* and *Ptprm-KO*; the reaction yields a band of 258 bp when the allele is present. (B) Schematic for *Ptprm-KO*. A *Ptprm f/+* male was crossed to the germline Cre deleter line *Sox2-Cre*, removing exon 3 and leaving behind a loxP site between exons 2 and 4; this introduces a frameshift yielding a premature stop codon in exon 4. Genotyping for *Ptprm-KO* used AS145 & AS148. The KO allele gives a band of 456 bp, whereas the WT allele gives a band of 1121 bp and the flox allele gives a band of 1189 bp. Diagrams are not drawn to scale. (C) Genotyping of the 3 successful founder mice using AS145 & AS153 confirmed the presence of the 3' loxP site; sequencing of these bands affirms the presence of the 5' loxP site. (D) Genotyping of progeny from crossing a *Ptprm f/+* male to a *Sox2-Cre* female using AS145 & AS148 revealed 5/8 pups had a recombined floxed allele (i.e. Ptprm-KO); "+" denotes a WT control.

Figure 12

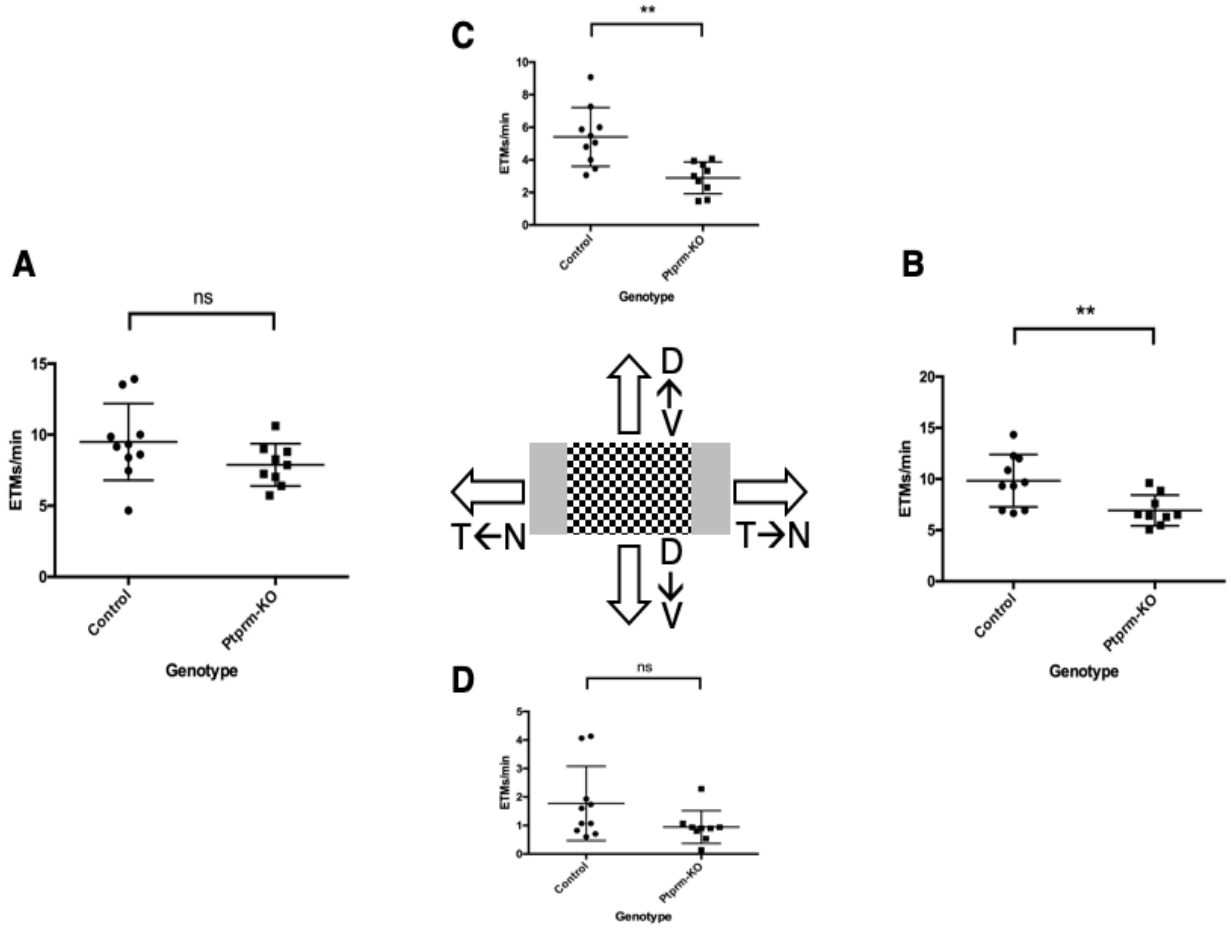

E	WT	*Ptprm -/-*
Freezing response	10/10 (100%)	9/9 (100%)
Escape response	10/10 (100%)	9/9 (100%)

Figure 12. *Ptprm -/-* mice show selective deficits in the optokinetic reflex.

Optokinetic reflex results from *Ptprm -/-* (n=9 mice) and littermate controls (n=10 mice) in response to (A) nasotemporal**,** (B) tempronasal, (C) ventrodorsal, and (D) dorsoventral motion. *Ptprm -/-* mice show selective deficits in their response to tempronasal and ventrodorsal motion. (E) *Ptprm -/-* mice show normal escape responses in the looming assay. ** denotes $p < 0.01$.

Figure 13

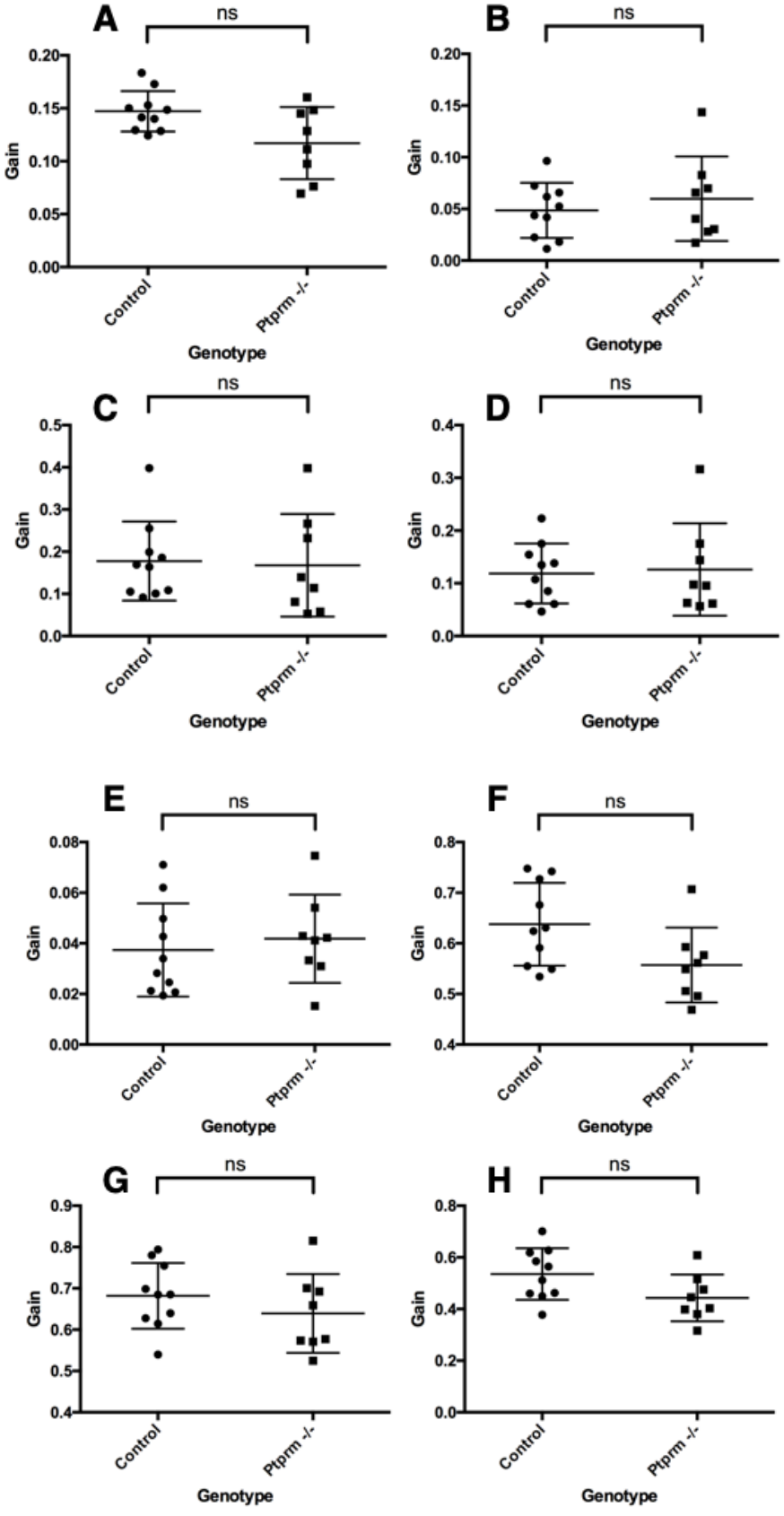
A
ns
Gain
0.20
0.15
0.10
0.05
0.00
Control
Ptprm -/-
Genotype
B
ns
Gain
0.20
0.15
0.10
0.05
0.00
Control
Ptprm -/-
Genotype
C
ns
Gain
0.5
0.4
0.3
0.2
0.1
0.0
Control
Ptprm -/-
Genotype
D
ns
Gain
0.4
0.3
0.2
0.1
0.0
Control
Ptprm -/-
Genotype
E
ns
Gain
0.08
0.06
0.04
0.02
0.00
Control
Ptprm -/-
Genotype
F
ns
Gain
0.8
0.7
0.6
0.5
0.4
Control
Ptprm -/-
Genotype
G
ns
Gain
0.9
0.8
0.7
0.6
0.5
0.4
Control
Ptprm -/-
Genotype
H
ns
Gain
0.8
0.6
0.4
0.2
0.0
Control
Ptprm -/-
Genotype

Figure 13. *Ptprm -/-* mice show no significant impairment in responses to sinusoidal stimuli. (A-D) Responses to 0.2 Hz vertical stimuli. (A) vertical gain; (B) horizontal gain; (C) tempronasal gain; (D) nasotemporal gain. (E-H) Responses to 0.2 Hz horizonal stimuli. (E) vertical gain; (F) horizontal gain; (G) tempronasal gain; (H) nasotemporal gain.

Figure 14

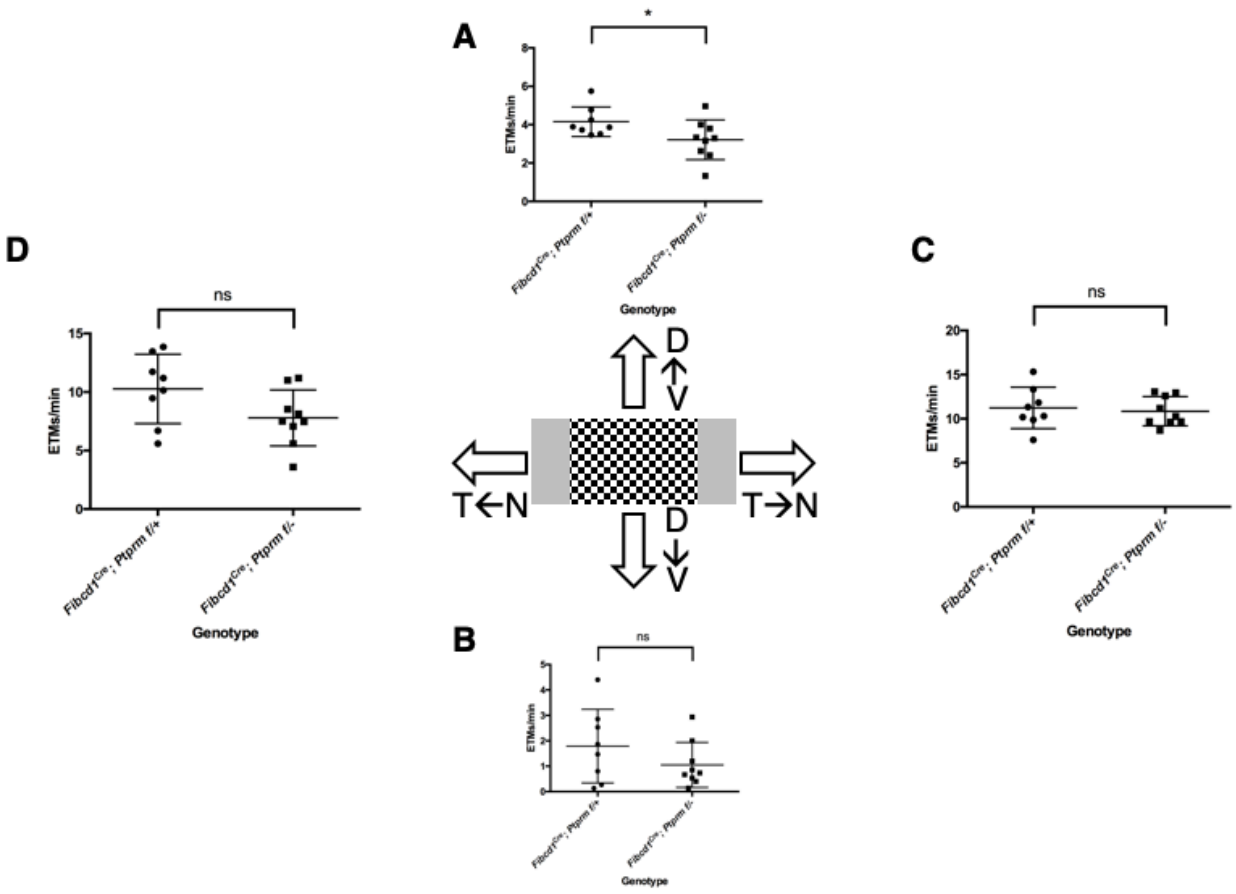

E	*Fibcd1^{Cre};Ptprm f/+*	*Fibcd1^{Cre};Ptprm f/-*
Freezing response	8/8 (100%)	8/9 (89%)
Escape response	8/8 (100%)	9/9 (100%)

Figure 14. *Fibcd1^{Cre};Ptprm* CKO mice show selective deficits in the detection of upward motion. Optokinetic reflex results from *Fibcd1^{Cre};Ptprm* CKOs (n=9 mice) and *Fibcd1^{Cre};Ptprm f/+* littermate controls (n=8 mice) in response to (A) ventrodorsal, (B) dorsoventral, (C) tempronasal, and (D) nasotemporal motion. *Fibcd1^{Cre};Ptprm* CKOs show a selective deficit in their responses to ventrodorsal motion. (E) *Fibcd1^{Cre};Ptprm* CKOs show normal escape responses in the looming assay. * denotes $p < 0.05$.

Figure 15

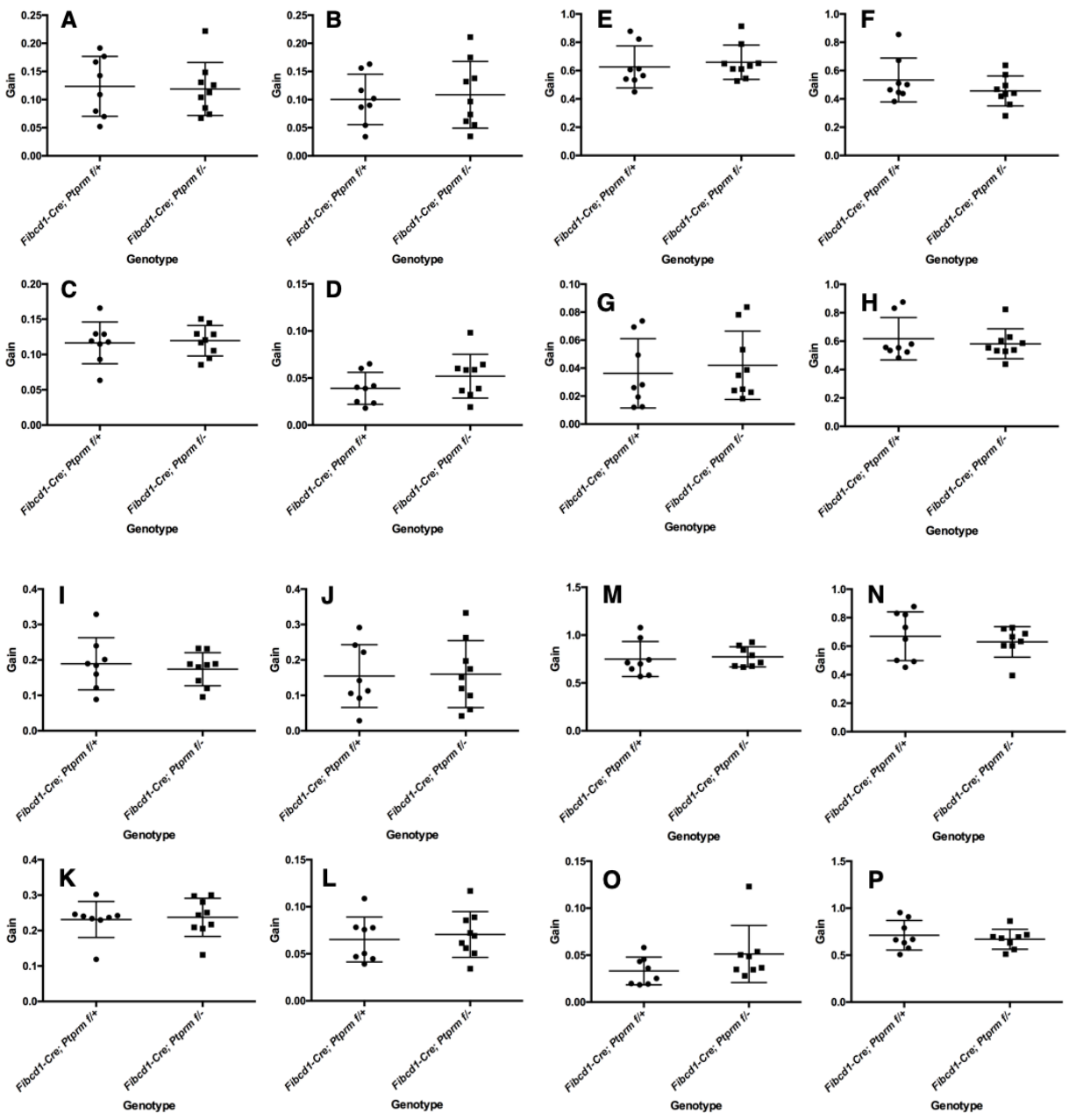
A
B
E
F
C
D
G
H
I
J
M
N
K
L
O
P
Gain
Genotype
Fibcd1-Cre; Ptprm f/+
Fibcd1-Cre; Ptprm f/-

Figure 15. *Fibcd1*^{Cre}*;Ptprm* CKO mice show no impairment in responses to sinusoidal stimuli. (A-D) Responses to 0.2 Hz vertical stimuli. (A) Tempronasal gain; (B) Nasotemporal gain; (C) Vertical gain; (D) Horizontal gain. (E-H) Responses to 0.2 Hz horizontal stimuli. (E) Tempronasal gain; (F) Nasotemporal gain; (G) Vertical gain; (H) Horizontal gain. (I-L) Responses to 0.1 Hz vertical stimuli. (I) Tempronasal gain; (J) Nasotemporal gain; (K) Vertical gain; (L) Horizontal gain. (M-P) Responses to 0.1 Hz vertical stimuli. (M) Tempronasal gain; (N) Nasotemporal gain; (O) Vertical gain; (P) Horizontal gain. All comparisons are non-significant ($p > 0.05$) by Mann-Whitney U Test.

Figure 16

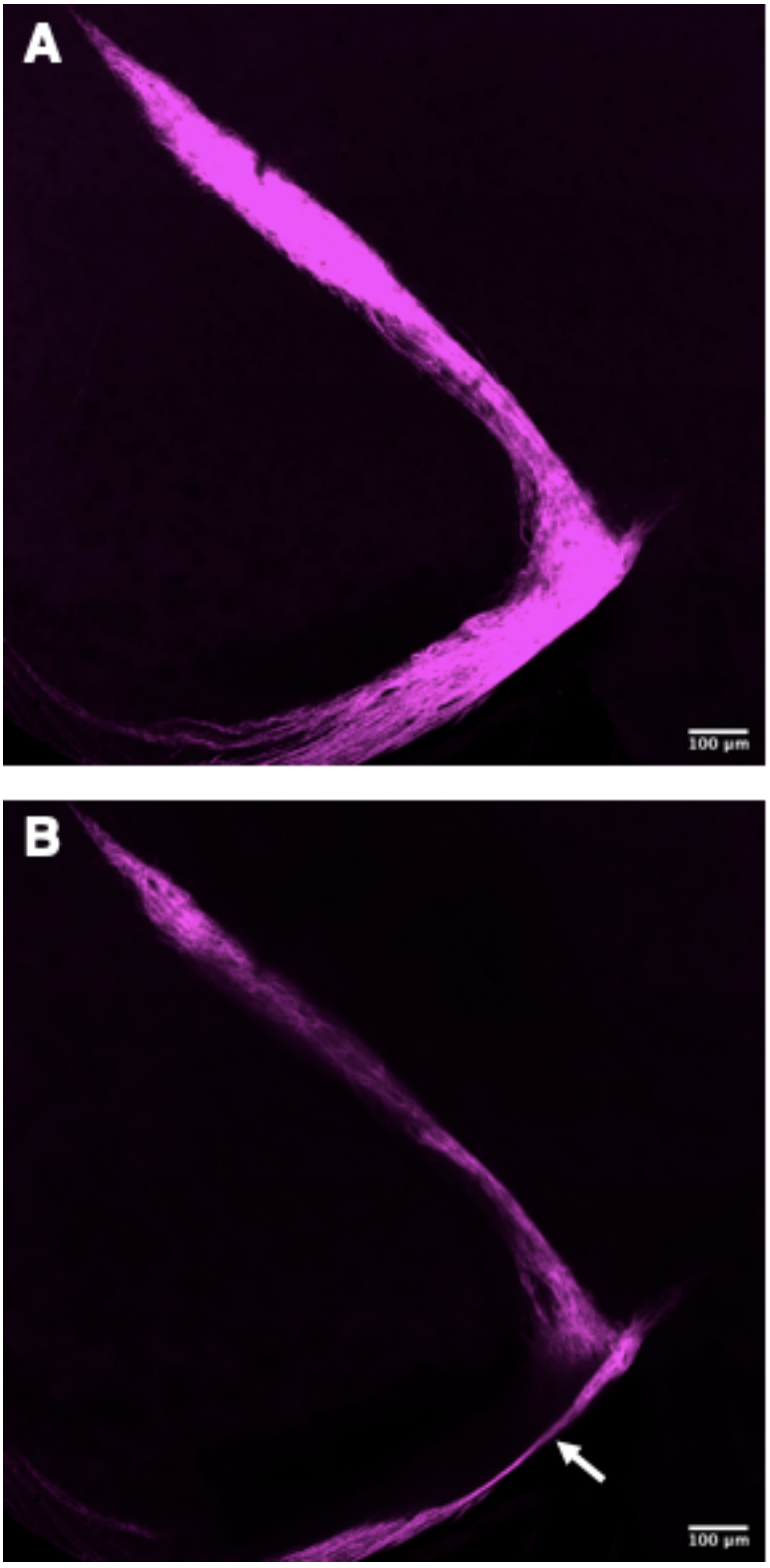

Figure 16. *Ptprm -/-* show no gross loss of MTN innervation. P22 *Ptprm -/-* mice were injected intraocularly with CTβ-555; brains were collected 2 days post-injection. (A) MTN innervation appears normal in *Ptprm -/-* brains. (B) Portion of the Z-stack in (A) highlighting the presence of the fiber bundle in the vMTN (arrow).

Chapter 4: Investigating a role for *Fibcd1* in ON-Down DSGC development

Introduction

In our scRNA-Seq experiment, the gene most significantly enriched in the ON-Down DSGC population is *Fibcd1*. This gene encodes the type II transmembrane protein Fibrinogen C Domain Containing 1. This protein consists of a small intracellular region, a single-pass transmembrane domain, and an extracellular region containing a coiled-coil domain, polycationic site, and a fibrinogen-related domain (FReD; Thomsen et al, 2010). The FReD domain is required for binding of Fibcd1 to acetylated molecules, most notably chitin (Schlosser et al, 2009). Chitin is the primary component of fungal cell walls, positioning Fibcd1, which is expressed within the epithelial cells lining the intestines and lungs, as a potential recognition factor for detecting fungal pathogens (Moeller et al, 2019; Jepsen et al, 2018).

The only work to date establishing a role for *Fibcd1* in the nervous system is a recent preprint finding that Fibcd1 recognizes chondroitin sulfate proteoglycans (CSPGs) containing a specific sulfate modification and mediates the responses of cultured hippocampal neurons to CSPGs (Fell et al, 2021). Fibcd1 binds to CSPGs with GAG side chains sulfated at carbon 4, but not those sulfated at carbon 6. While cultured hippocampal neurons show reduced ability to adhere to surfaces coated with CSPGs, and those that do adhere clump together by DIV14, these effects are not observed in *Fibcd1-KO* neurons. Loss of *Fibcd1* prevents cultured hippocampal neurons from

undergoing certain transcriptional changes in response to CSPG binding, such as reducing expression of the integrin subunits *Itga1* and *Itgam*. *Fibcd1-KO* mice also show deficits in hippocampal-dependent inhibitory avoidance learning tasks, suggesting impaired hippocampal function. Nevertheless, the fact that *Fibcd1* is the gene most significantly enriched in ON-Down DSGCs in our scRNA-Seq data and that it appears to be expressed exclusively, with respect to RGCs, in these DSGCs motivated the study of its potential role in wiring the DS circuitry containing these cells.

Results

Loss of Fibcd1 *does not impair responses to vertical stimuli*

Fibcd1 -/- mice were obtained from the MMRRC, which were generated by knocking a LacZ/neomycin cassette into exon 1 by homologous recombination (Tang et al, 2010). RT-PCR of *Fibcd1 -/-* hippocampus indicates that this allele eliminates expression of *Fibcd1* mRNA (Fell et al, 2021). Overall retinal architecture is normal in *Fibcd1 -/-* adult retinas as measured by staining for DAPI, ChAT, and calbindin (Figure 17). Adult *Fibcd1 -/-* mice and littermate controls were head-fixed and tested for responses to slowly-moving checkerboard stimuli in either direction along the horizontal and vertical axes. As expected, *Fibcd1 -/-* (n=7) showed no difference in responses to stimuli in either horizontal direction compared to controls (n=11; CCW: control: 7.67 +/- 3.51 ETM/min, KO: 6.64 +/- 4.13 ETM/min, Figure 18A; CW: control: 7.19 +/- 3.87

ETM/min, KO: 6.68 +/- 5.73 ETM/min Figure 18B). However, there were also no significant differences in responses to upward (control: 6.71 +/- 2.01 ETM/min, KO: 6.13 +/- 1.74 ETM/min, Figure 18C) or downward (control: 3.17 +/- 1.56 ETM/min, KO: 2.49 +/- 1.69 ETM/min, Figure 18D) stimuli. These results indicate that *Fibcd1 -/-* are able to respond normally to vertical stimuli, suggesting that the DS circuitry is not impaired in these mutants.

Dendritic area of ON-Down DSGCs may be expanded following loss of Fibcd1

Although *Fibcd1 -/-* mice do not show an OKR phenotype, this does not necessarily rule out a perturbation of the DS circuitry. Out of the 4 directional stimuli, downward stimuli trigger the weakest responses, as is documented in the literature (Yonehara et al, 2016); it is possible that while loss of *Fibcd1* induces a subtle deficit in the ability of ON-Down DSGCs to transmit directional information, the baseline response rate makes this deficit difficult to detect at the behavioral level. With this in mind, I sought to examine *Fibcd1-KO* ON-Down DSGCs for evidence of ON-Down DSGC morphological perturbation.

In order to assess dendritic morphology of ON-Down DSGCs following loss of *Fibcd1*, I performed stereotaxic injections of rAAV2-FLEX-GFP into the MTN of *Fibcd1 Cre/-* mice and *Cre/+* littermates; as the *Fibcd1-Cre* allele is a null allele, *Fibcd1 Cre/-* mice are homozygous null for *Fibcd1* and *Fibcd1 Cre/+* mice are heterozygous. MTN injections were chosen in order to avoid labeling the numerous *Fibcd1*+ ACs that would

be labeled with existing tools delivered by intraocular injection, which would render finding well-isolated DSGCs for tracing difficult. Tracings were performed in Single Neurite Tracer in collaboration with Maame Amoah-Dankwah, a research technician in the Kolodkin Lab, using only cells that were isolated enough to allow for unambiguous assignment of dendritic segments to the cells in question. Analysis revealed a modest but significant increase in dendritic area following loss of *Fibcd1* (Figure 19C, Control: 51,557.2 +/- 2,028.3 μm^2, n=5 neurons from 2 retinas; KO: 58,354.4 +/- 10,175.5 μm^2, n=17 neurons from 6 retinas; p=0.048, Mann-Whitney U Test). No significant changes were observed in dendritic length (Figure 19D, Control: 5,704.4 +/- 670.5 μm; KO: 6,166.1 +/- 882.2 μm; p=0.32, Mann-Whitney U Test) or branch point number (Figure 19E, Control: 82.6 +/- 14.8 branch points; KO: 74.9 +/- 17.3 branch points; p=0.43, Mann-Whitney U Test). These results raise the possibility that *Fibcd1* is required for normal ON-Down DSGC dendritic development.

Discussion

Fibcd1 is the gene most significantly enriched in ON-Down DSGCs in our scRNA-Seq dataset, making it a promising candidate for study in the context of ON-Down DSGC development and function. These results provide preliminary insight into the role of *Fibcd1* in the development of the DS circuit containing ON-Down DSGCs. Though it appears dispensable for DS circuit function, at least at the level of the OKR, they do suggest that *Fibcd1* is involved in regulating ON-Down DSGC dendritic arbors.

It is somewhat surprising that loss of the gene most significantly enriched in ON-Down DSGCs did not lead to a significant deficit in the OKR. This does not match what was observed in the ON-Up DSGCs with *Ptprk*, the second-most significantly enriched gene in that subtype. As the *Fibcd1-KO* allele was generated through targeting exon 1 via homologous recombination (Tang et al, 2010), it is unlikely that this is due to the mutant allele being a hypomorph since the disruptive cassette is placed immediately following the endogenous start codon. Given that the OKR response is a less refined readout of DS circuitry functionality compared to electrophysiological recordings, it is possible that there is a subtle impairment in ON-Down DSGC responses that would only be apparent by measuring spiking rates and/or synaptic currents. If *Fibcd1* were required for restricting the ON-Down DSGC dendritic arbor to the ON SAC sublamina, with mutants extending their dendrites into the OFF SAC sublamina, it could be important for controlling the components of the overall DS circuitry with which these DSGCs form connections, while still not being essential for the DS responses responsible for the OKR. Alternatively, *Fibcd1* may simply function in a manner wholly unrelated to DS responses, with its presence in ON-Down DSGCs and absence in ON-Ups a coincidence; while our success rate in identifying critical genes through probing scRNA-Seq-derived candidates demonstrates the value of exploring those that show significantly differential expression, this is no guarantee that every gene found this way will prove important.

Although the analysis of ON-Down DSGC dendritic arbors following loss of *Fibcd1* needs repetition, due to the small sample size of mice used (n=1 for *Fibcd1*

Cre/+; n=3 for *Fibcd1 Cre/-*), it provides room for speculation for which aspects of dendritic arbor morphology are required for normal DSGC function. As in *Ptprk -/-* ON-Up DSGC arbors, *Fibcd1 -/-* ON-Down DSGC arbors are expanded in area and not in dendritic length. Unlike with *Ptprk*, however, loss of *Fibcd1* does not lead to a reduction in branch point number. Additional geometric measures are needed to identify precisely how the *Fibcd1 -/-* arbor achieves a wider area without changing dendritic length or branch point number. For example, Sholl analysis and assessment of where branch points are located within the arbor might reveal that *Fibcd1 -/-* arbors bias placement of terminal dendrites towards distal portions of the arbor, allowing them to contribute to the dendritic area in ways that terminal dendrites in proximal portions of the arbor do not. Nevertheless, these results raise the possibility that the reduction in branch point number is the key factor for how loss of *Ptprk* impairs DS functionality, as opposed to dendritic arbor size. In rabbit ON DSGCs, branch points at which terminal dendritic segments join parent dendritic segments serve as crucial inhibitory veto checkpoints, preventing the initiation of dendritic spikes from the excitation of terminal dendrites (Sivyer and Williams, 2013). While dendritic spiking has not been identified in mouse DSGCs, excitation does undergo nonlinear amplification via NMDA receptors as it travels through the dendritic arbor (Poleg-Polsky and Diamond, 2016); perhaps branch points provide opportunities for preventing this form of excitatory amplification as well.

How might *Fibcd1* regulate dendritic arbor size? In contrast to the vast literature exploring interactions between RTPs and other molecules present in neurons & other tissues, information for Fibcd1 is less abundant. This is in part due to the focus on its

recognition of fungal cell walls, reducing emphasis on finding binding partners present in vertebrates, and the discovery of roles with potential implications for neurodevelopment – or, indeed, development in general – only being very recent (Fells et al, 2021). However, this previous work does still provide some potential avenues for exploration. CSPGs have been long established as components of the extracellular matrix (ECM) essential for regulating neuronal development and function (Carulli et al, 2005). Perhaps the recognition of CSPGs whose GAG side chains are sulfated at carbon 4 by Fibcd1 (Fells et al, 2021) provides ON-Down DSGCs with molecular information needed for constraining arbor size. A preliminary experiment to test this could examine *Fibcd1 Cre/-* and *Cre/+* retinal sections with labeled ON-Down DSGCs by staining with an antibody that specifically recognizes CSPGs sulfated at carbon 4 (Yi et al, 2012), seeing whether DSGCs show altered colocalization with these CSPGs following loss of *Fibcd1*. Additionally, the domain responsible for known Fibcd1 function is the FReD domain, named for its similarities to fibrinogen. During blood clotting, fibrinogen is proteolytically converted to fibrin and forms a polymer (Mosesson, 1992); perhaps the FReD domain of Fibcd1 in ON-Down DSGCs forms a homophilic interaction with Fibcd1 expressed in non-SAC ACs to regulate arbor size. Fibrin and fibrinogen are also capable of binding integrins and VE-cadherin (Bach et al, 1998), providing additional classes of molecules important for neuronal circuit development that could serve as binding partners for Fibcd1. Given the vast number of integrins and cadherins, it may be worthwhile to perform an *in vitro* binding assay screen to identify all members of these families

capable of binding Fibcd1, followed by loss-of-function experiments to test if loss of those proteins affects the dendritic morphology of ON-Down DSGCs.

The lack of an OKR phenotype in *Fibcd1 -/-* mice renders the study of this gene less of a priority for future work compared to genes associated with a phenotype, such as *Ptprm*. Nonetheless, its presence in a number of AC subtypes and robust expression in the hippocampus render it an intriguing molecule for the broader neuroscience community.

Figure 17

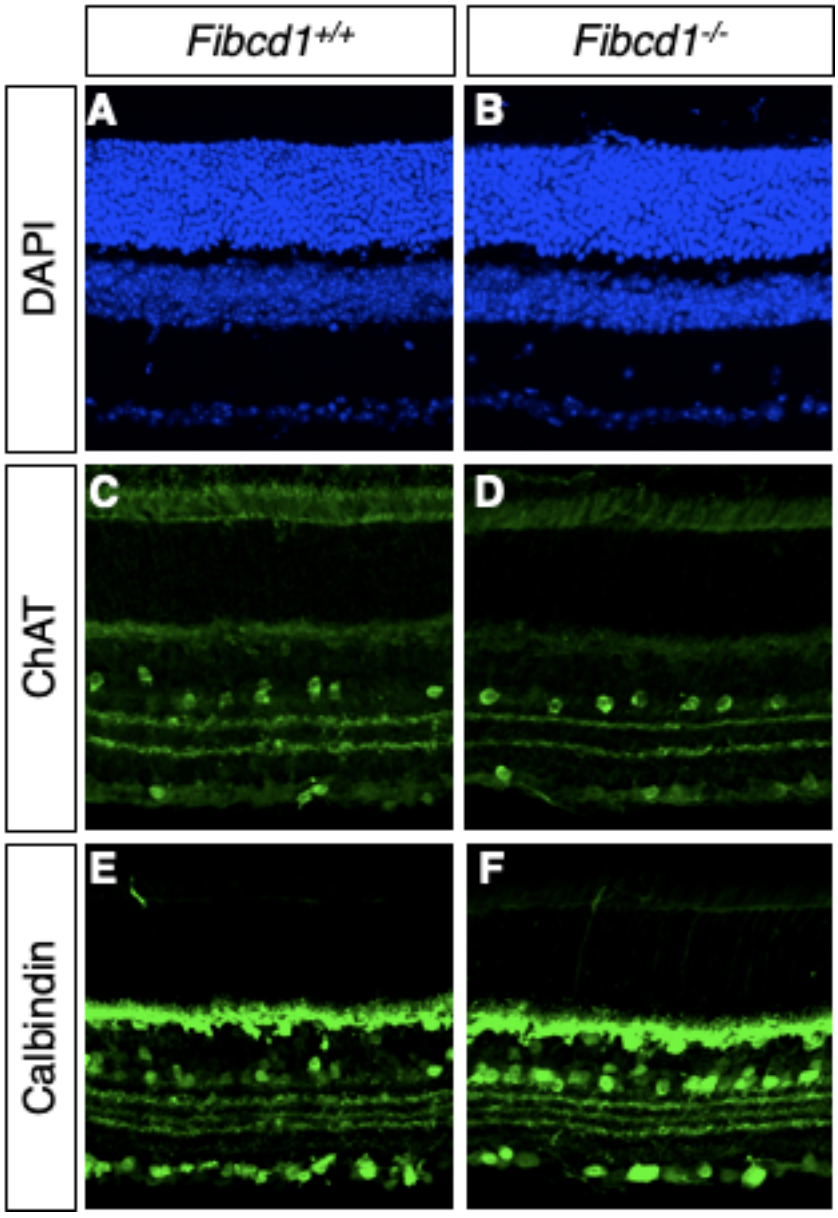

Figure 17. Retinal architecture is normal in *Fibcd1 -/-* retinas. Retinas *from Fibcd1 +/+* (A, C, E) and *Fibcd1 -/-* (B, D, F) were stained for DAPI (A-B), ChAT (C-D), and calbindin (E-F). No gross changes to retinal architecture are present. Data courtesy of Timour Al-Khindi, Kolodkin Lab, unpublished work.

Figure 18

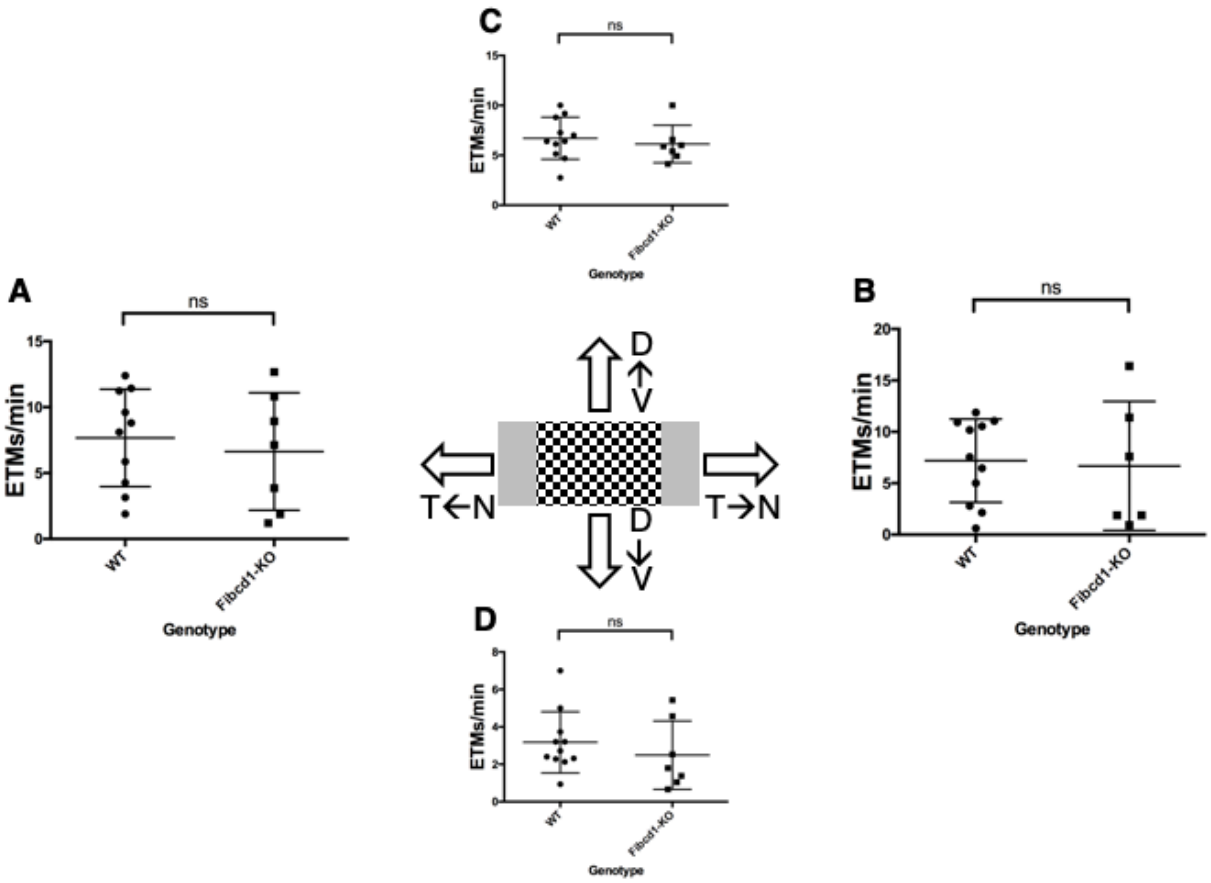
A
ns
ETMs/min
15
10
5
0
WT
Fibcd1-KO
Genotype
C
ns
ETMs/min
15
10
5
0
WT
Fibcd1-KO
Genotype
B
ns
ETMs/min
20
15
10
5
0
WT
Fibcd1-KO
Genotype
D
T←N
T→N
D
D
ns
ETMs/min
8
6
4
2
0
WT
Fibcd1-KO
Genotype

Figure 18. *Fibcd1 -/-* mice show no impairments in response to slowly-moving directional stimuli. Optokinetic reflex results from *Fibcd1 -/-* (n=7 mice) and littermate controls (n=11 mice) in response to (A) nasotemporal**,** (B) tempronasal, (C) ventrodorsal, and (D) dorsoventral motion. *Fibcd1 -/-* mice show no differences in their responses to any direction that are significant by Mann-Whitney U Test.

Figure 19

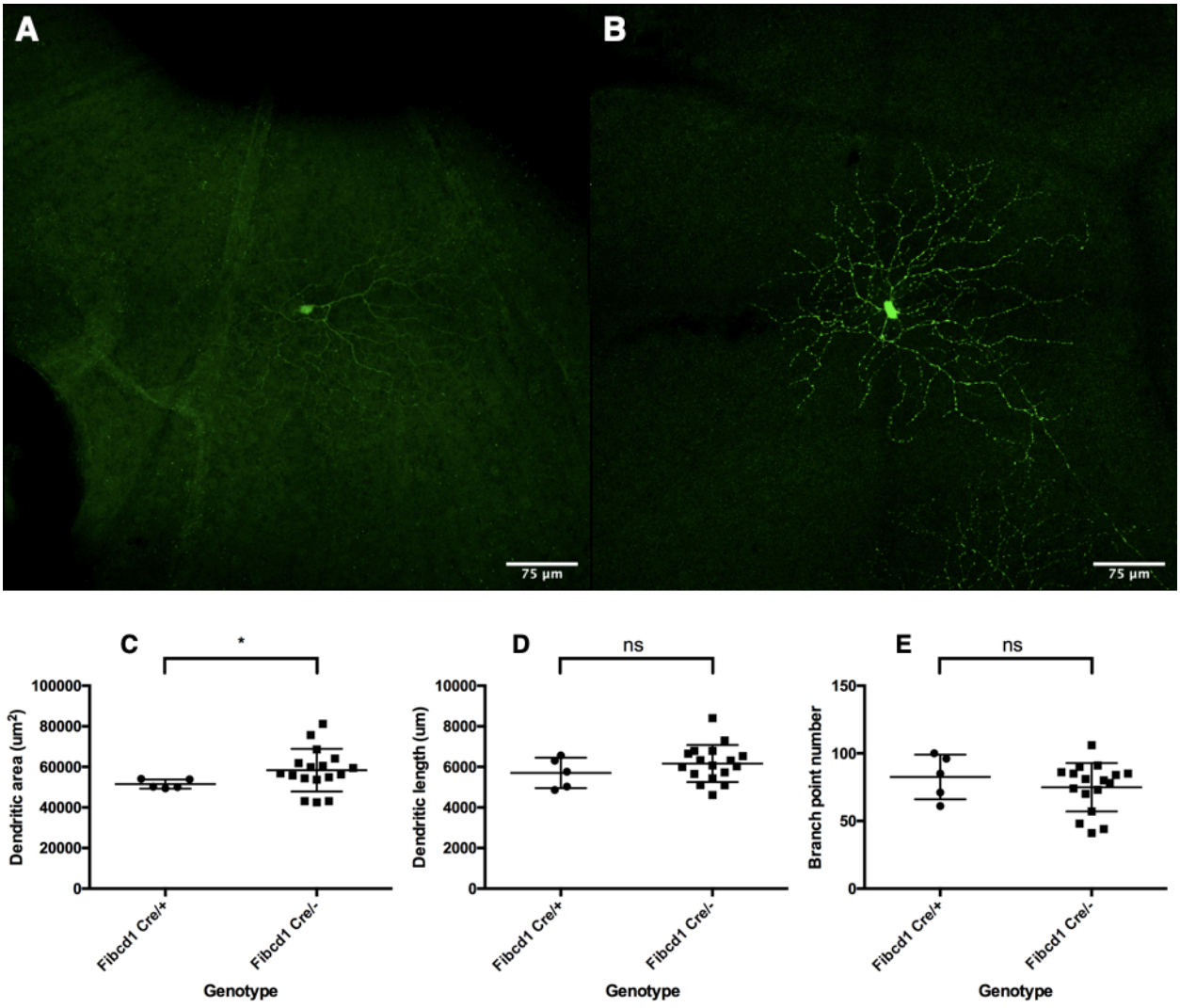
A
B
75 µm
75 µm
C
*
Dendritic area (um²)
100000
80000
60000
40000
20000
0
Fibcd1 Cre/+
Fibcd1 Cre/-
Genotype
D
ns
Dendritic length (um)
10000
8000
6000
4000
2000
0
Fibcd1 Cre/+
Fibcd1 Cre/-
Genotype
E
ns
Branch point number
150
100
50
0
Fibcd1 Cre/+
Fibcd1 Cre/-
Genotype

Figure 19. *Fibcd1 -/-* dendritic arbors show modestly expanded area. (A-B) Representative images of *Fibcd1 Cre/+* (*Fibcd1 +/-*, A) and *Fibcd1 Cre/-* (*Fibcd1 -/-*, B). (C-E) Analysis of dendritic arbors for (C) area, (D) dendritic length, and (E) branch point number. * denotes $p < 0.05$, Mann-Whitney U Test.

Chapter 5: Conclusions

Among the numerous classes of RGCs tuned to respond to particular features of the visual scene, DSGCs provide a uniquely rich model for studying wiring mechanisms in the CNS due to our detailed knowledge of the presynaptic partners and arrangement of synaptic connections required to perform DS computations (Vaney et al, 2012). Uncovering these mechanisms for ON DSGCs has been greatly aided by a scRNA-Seq experiment in our group comparing the transcriptome of ON-Up and ON-Down DSGCs (Al-Khindi et al., *in press*). While this database has already provided insight into ON-Up DSGC development, with analyses of mutants for *Ptprk* and *Tbx5* revealing roles for each, little progress has been made in the study of genes associated with ON-Down DSGCs. In part, this is due to a lack of mouse lines that would allow for their specific labeling, preventing the attribution of any behavioral phenotypes caused by the loss of a gene to changes in the DSGCs themselves.

My thesis sought to begin this analysis by generating a mouse line that would enable the labeling of ON-Down DSGCs and testing two promising genes from our scRNA-Seq screen, *Ptprm* and *Fibcd1*, enriched in these cells. The first goal was achieved by knocking Cre into the locus of *Fibcd1* itself, as it was the gene most significantly enriched in ON-Down DSGCs and a previous P5 RGC atlas suggested it is expressed in few to no other RGC subtypes (Rheaume et al, 2018). *Fibcd1*^{Cre}+ RGCs are rare, MTN-projecting RGCs that are comparable in number to, and do not overlap with, ON-Up DSGCs. Though we are awaiting electrophysiological recordings in

collaboration with Prof. Marla Feller at UC Berkeley to truly confirm their identity, the evidence I have collected thus far strongly argues that *Fibcd1*^{Cre}+ RGCs are ON-Down DSGCs. The results of examining the two candidate genes were more mixed; *Ptprm* did show an OKR phenotype, but *Fibcd1* did not.

The greatest impact from this work is from gaining molecular access to ON-Down DSGCs. Although the indirect methods used in previous studies did allow for their visualization, direct targeted access to these cells is essential for understanding the molecular mechanisms associated with their development and function. Being able to use *Fibcd1* as a marker gene for ON-Down DSGCs and *Fibcd1*^{Cre} to gain genetic access to them will allow for our knowledge of these cells to become comparable to that of other DSGC subtypes. This is especially important for being able to demonstrate selective effects of a given gene on a specific DSGC subtype; for example, we are now able to test whether the dendritic morphology phenotype observed in *Ptprk -/-* ON-Up DSGCs is particularly limited to them or present in multiple DSGC subtypes. Our ability to study these DSGCs will be further aided by the AAV9-fNPY-FLEX-GFP viral construct, enabling the visualization of well-isolated DSGCs without the confounding issues associated with MTN injections. Given the immense work needed for understanding the molecular mechanisms driving neuronal subtype specification & development throughout the nervous system, future studies may be well-served to adopt a similar approach of gathering transcriptomic data to identify marker genes and generating knock-in mice to access cells expressing those markers, especially if done in a combinatorial approach to further refine labeled cells to the desired subtype.

A recent study found that a *Flrt3-CreERT2* mouse line labels a class of DSGC which responds to downward motion and projects to the MTN; while it responds solely to light increments (i.e. is functionally an ON DSGC), its dendrites stratify with both ON & OFF SACs and it expresses the ON-OFF DSGC marker CART (Ruff et al, 2021). This stratification pattern is perplexing, as the characterization of all MTN-projecting RGCs at P12 found them to be uniformly monostratified (Yonehara et al, 2009), and while previous characterizations of ON DSGCs in the adult found them to have a portion of their dendrites in the OFF sublamina (Lilley et al, 2019), this OFF arborization is much smaller than that observed in the *Flrt3-CreERT2* DSGCs. It would appear, then, that either these *Flrt3+* RGCs form their projections into the MTN later than P10 (the age at which the injections in Yonehara et al, 2009 were performed); they extensively arborize within the OFF sublamina later than P12; the sample size of 11 non-ON-Up DSGCs projecting to the MTN in Yonehara et al, 2009 was not sufficient to capture the bistratified *Flrt3+* RGCs; or that the *Flrt3-CreERT2* allele itself is disrupting normal development and causing another cell type to take on this fate. The stratification pattern and CART expression suggest that these are distinct from ON-Down DSGCs, and *Flrt3* does not appear in our scRNA-Seq study as a differentially expressed gene. It is important to note, however, that our transcriptomic analysis went no later than P12, while Cre-mediated recombination & labeling was induced for the study of *Flrt3*+ RGCs in mice no younger than P60. Regardless, all evidence suggests that *Flrt3-CreERT2* labels a class of DSGC distinct from those labeled by *Fibcd1*^{Cre}. Furthermore, at least 3 other RGC subtypes are also labeled by *Flrt3-CreERT2* – 2 ON-RGCs and 1 OFF-RGC

– whereas only ON-Down DSGCs are labeled by *Fibcd1*^{Cre}, providing an additional advantage of the *Fibcd1*^{Cre} line even if future work were to find that they label the same DSGCs.

The results observed in *Ptprm* loss-of-function mice affirm our hypothesis that the R2B RTPs expressed in each class of vertical-preferring ON DSGC are critical for proper DS circuit function. This affirmation renders even more exciting the work our lab is performing to investigate *Ptprt* in ON-Forward DSGCs with the new *Ptprt-null* allele currently in production. That preliminary results show DS is unaltered in *Ptprk -/-* ON-Up DSGCs does suggest that these RTPs do not serve as a master "molecular code" dictating the directional preference of each ON DSGC subtype; nevertheless, their differential expression, OKR phenotypes, and the electrophysiological phenotype observed in various mutants highlight their potential importance for development of DSGC tuning properties. All evidence thus far suggests that *Ptprm* represents the first gene found to be required for proper ON-Down DSGC development and function; however, until these mutant DSGCs are subjected to recording during exposure to stimuli and are fully characterized, the strongest statement that can be made is that *Ptprm* is generally required for proper circuit function, even if the behavioral phenotype in *Fibcd1*^{Cre}*;Ptprm* CKOs argues that this requirement lies in the ON-Down DSGCs themselves. This hypothesis will be further tested with *Ptprm* CKOs using *VGlut2-Cre* (RGCs) and *Ptf1a-Cre* (ACs), providing a more definitive answer as to whether or not *Fibcd1+* ACs contribute to the *Fibcd1*^{Cre} CKO phenotype.

Up to this point, the examination of how RTPs affect specific ON DSGC subtypes has been limited to the study of *Ptprk -/-* ON-Up DSGCs using *Pcdh9-Cre*. The dendritic morphology phenotype observed in these cells provides clear evidence for *Ptprk* being required for normal ON-Up DSGC development. While this is highly informative, much more work is needed to further our understanding of these RTPs in ON DSGCs. We will subject *Fibcd1^{Cre};Ptprm* CKOs to the full range of assays described in Chapter 3 for identifying which components of ON-Down DSGC circuitry are impaired. Additionally, though our transcriptomic data strongly argue against appreciable expression of *Ptprk* in ON-Down DSGCs, we have not yet tested for effects from loss of *Ptprk* in these DSGCs. To address this, we will generate *Fibcd1^{Cre};Ptprk -/-* mice and examine their ON-Down DSGCs for defects, with a primary focus on dendritic morphology. Reciprocally, we will generate *Pcdh9-Cre;Ptprm -/-* to test for phenotypes in ON-Up DSGCs, with the expectation that these cells will show no deficits.

While the goal of this thesis was to better understand the mechanisms driving ON-Down DSGC development, an overarching aim of a project such as this is to allow research into whether these mechanisms are used similarly in other contexts. To this end, the presence of the temperonasal OKR phenotype in global *Ptprm* mutants that is absent in *Fibcd1^{Cre}* CKOs presents the possibility that *Ptprm* is also required for development of the circuit responsible for detecting and responding to this direction of motion. This hypothesis will be tested further with the *VGlut2-Cre* CKO experiments; if the temperonasal phenotype is retained, suggesting that the DSGCs detecting temperonasal motion require *Ptprm*, it could be additionally tested with CKOs using

Piezo2-Cre, which according to preliminary work from our group may label at least some horizontally-tuned ON DSGCs (Natalie Hamilton, unpublished work). Though a P5 RGC atlas suggests that ON-Up DSGCs may be the only RGCs expressing *Ptprk*, it suggests that many RGC subtypes beyond ON-Down DSGCs express *Ptprm*, including at least a subset of intrinsically photosensitive RGCs based on *Opn4* expression (Rheaume et al, 2018). This positions *Ptprm* as a molecule with potentially broad relevance to RGC development.

The lack of a behavioral phenotype in *Fibcd1-KO* mice was somewhat unexpected, given that *Fibcd1* is the most significantly-enriched gene for ON-Down DSGCs in our transcriptomic dataset. *Cdh6* marks vertical ON-OFF DSGCs (Kay et al, 2011a) and is involved in their connecting with the SAC dendritic scaffold (Duan et al, 2018). However, despite the longstanding knowledge that *Spig1* (Yonehara et al, 2009) and *Mmp17* (Kay et al, 2011a) serve as markers for particular DSGC subtypes, no phenotypes have yet been reported in mutants for these genes; thus, it is possible that these genes are dispensable for the DSGC subtypes which they mark, which would place *Fibcd1* in line with certain other DSGC marker genes for not having a phenotype. The preliminary analysis of *Fibcd1-KO* dendritic arbors also suggests that ON-Down DSGCs do require *Fibcd1* for normal development, but that it is not required for the developmental events critical for DS functionality. Furthermore, it remains possible that these mutants show a defect in DS circuit function that is too subtle to detect at the level of the OKR; electrophysiological recordings from *Fibcd1-KO* ON-Down DSGCs and

examination of connectivity with the MTN will provide more conclusive evidence in this matter.

Should the electrophysiology of *Ptprm -/-* ON-Down DSGCs resemble that of *Ptprk -/-* ON-Up DSGCs, it would appear that *Ptprm* is not one of the long-sought molecules dictating the asymmetric inhibitory connections from SACs onto DSGCs to generate their DS responses. Nevertheless, this work provides evidence that meaningful ON DSGC-related phenotypes can be found through studying genes identified in our scRNA-Seq experiment as enriched in ON-Down DSGCs, just as *Ptprk* and *Tbx5* provided such support for analyzing genes enriched in ON-Up DSGCs. We have only begun to investigate the candidate genes from our transcriptomic analysis; further study may yet yield the molecules that program connectivity between SACs and specific DSGC subtypes. The reagents generated in this study will prove invaluable in the search for the molecular determinants of SAC-DSGC wiring, with the phenotypes observed following loss of *Ptprm* underscoring the utility of delving further into the candidates from our scRNA-Seq screen and the use of such screens more generally for identifying wiring cues throughout the myriad circuits of the CNS that give rise to its computational power.

Methods

Animals

The date of birth was designated as postnatal day 0 (P0). Mice of either sex were used. *Fibcd1-KO* mice were obtained from the MMRRC. *Spig1-GFP* mice were a gift from the lab of Dr. M. Noda and were previously described in Yonehara et al, 2008. *Sox2-Cre* (ID #008454) and *Ai14* (ID #007914) mice were obtained from the Jackson Laboratory (Bar Harbor, ME). *Fibcd1-Cre*, *Ptprm-flox*, and *Ptprm-KO* were generated in-house and described below. Animals were housed in a 12-hour light-dark cycle and provided food & water *ad libitum*. All experiments were approved by the Animal Care and Use Committee of the Johns Hopkins University.

Generating Fibcd1-Cre *mouse line*

To generate the *Fibcd1-Cre* mouse line, CRISPR-Cas9 was used to induce a double-stranded break 22 bp following the *Fibcd1* start codon, using a gRNA with the sequence 5' ccacgagcgguggaagaccgugg 3'. The double-stranded insert used for this experiment provided a full-length Cre cassette immediately following the endogenous start codon and a rabbit globulin polyA tail, flanked by a 5' homology arm 210 bp in length (ending with the start codon) and 3' homology arm 206 bp in length (starting 9 bp following the start codon). The insert and gRNA were provided to the Johns Hopkins

Murine Mutagenesis Core for performing CRISPR-mediated mutagenesis. Verification of integration at the 5' end used the FOR primer TAK666 5' gaagacgcggagactgagcc 3' and REV primer TAK700 5' catgatgtccccataatttttggcagaggg 3'; verification at the 3' end used TAK673 5' gttagcaccgcaggtgtag 3' and TAK671 5' ggagcccagagttcaagactcc 3'. Subsequent genotyping for *Fibcd1-Cre* used TAK666 and TAK700.

Generating Ptprm-flox *and* Ptprm-null *mouse lines*

To generate the *Ptprm-flox* mouse, CRISPR-Cas9 was used to induce a pair of double-stranded breaks in the introns flanking exon 3 of *Ptprm*, using gRNAs with the sequences 5' UAAGAUUAUACACCGAAAAGAGG 3' (5' intron) and 5' UCAGAAGAGCAUACCUACUGUGG 3' (3' intron). The single-stranded insert (Integrated DNA Technologies) provided loxP sites in the same orientation at the double-stranded breaks and had homology arms of 105 bp and 36 bp at the 5' and 3' ends, respectively, with the endogenous PAM sites mutated such that the integrated sequence would not be recognized by Cas9. The insert and gRNAs were provided to the Johns Hopkins Murine Mutagenesis Core for performing CRISPR-mediated mutagenesis. 5' loxP site integration was verified using the FOR primer AS145 5' GGACACATGAAATGGCTCCAGTG 3' and REV primer AS146 5' ATGCCACCACAGTTGGCTTG 3'; 3' loxP site integration was verified using the FOR primer AS147 5' GGACATTTCATGGTTTTAAGTCATC 3' and the REV primer AS148 5'

CATGTGGTTGCTGGAACCAGG 3'. Mice indicating successful integration were backcrossed to B6.

To generate the *Ptprm-KO* mouse, a *Ptprm f/+* male was crossed to a *Sox2-Cre* female (JAX ID 008454). Progeny were genotyped for *Ptprm-KO* using AS145 and AS148, with a WT band at 1189 bp and a KO band at 456 bp. In subsequent genotyping, mice were genotyped for the WT allele using AS145 and the reverse primer AS163 5' TTCAGTCTCTTTTGGCTCTTTTCGG 3'; mice were genotyped for the floxed allele using AS145 and the reverse primer AS153 5' GTATGCTATACGAAGTTATCTGTGCC 3'. The binding sequence for AS163 is interrupted by the 5' loxP site of the floxed allele and partially deleted in the KO allele, thus only giving a band in the presence of the WT allele; the binding sequence for AS153 spans the border of the floxed region and the 3' loxP site, which can only recognize its full target sequence in the floxed allele.

Immunohistochemistry

Whole-mount retinal staining was performed as described in Sun et al, 2015 with minor modifications. Mice were perfused intracardially with phospho-buffered saline (PBS), then 4% (v/v) Paraformaldehyde (PFA; Electron Microscopy Services, Hatfield, PA). Eyes were enucleated and post-fixed for 1 hour at 4°C in 4% PFA. Retinas were dissected in PBS, blocked for 1 hour in Blocking Solution (0.5% Triton X-100, 0.05% sodium azide, and either 5% goat serum or 3% donkey serum, in PBS and sterile-

filtered), then incubated for 3 days at 4°C in Blocking Solution with desired primary antibodies added. Primary antibody solutions were removed, for reuse up to two additional times, and retinas were washed 4 times for 1 hour in PBS-T (0.5% Triton-X 100 in PBS) before being incubated overnight at 4°C in Blocking Solution with desired secondary antibodies added. Retinas were washed 4 times for 1 hour in PBS-T, flattened, mounted with FluoroGel, and imaged using a Zeiss LSM 700 confocal microscope.

Staining of floating brain sections was performed as described in Riccomagno et al, 2012 with minor modifications. Mice were perfused intracardially with PBS, then 4% PFA. Brains were removed and post-fixed for 1 hour at 4°C in 4% PFA. Brains were embedded in 4% low-melting-point agarose (w/v, in PBS) and sectioned coronally to the desired thickness via Vibratome. Sections were blocked overnight at 4°C in BSA Blocking Buffer (3% bovine serum albumin, 0.3% Triton-X 100, 0.1% sodium azide, in PBS and sterile filtered), then incubated overnight at 4°C in BSA Blocking Buffer with desired primary antibodies added. Primary antibody solutions were removed, for reuse up to two additional times, and sections were washed 3 times for 1 hour in PBS. Sections were incubated overnight with BSA Blocking Buffer with 5% goat serum (or donkey serum) and the desired secondary antibodies. Sections were washed 2 times for 1 hour in PBS, then washed overnight at 4°C in PBS, mounted in FluoroGel, and imaged using a Zeiss LSM 700 confocal microscope.

Primary antibodies used in this study include: chicken anti-GFP (Aves, 1:1000), rabbit anti-dsRed (Living Colors, 1:500), goat anti-ChAT (Millipore, 1:250), guinea pig anti-RBPMS (PhosphoSolutions, 1:500).

Headposting surgery

Headposting surgery was performed as described in Al-Khindi et al, *submitted*. Adult mice (P42 and older) were anesthetized with isoflurane; skull was secured in a stereotaxic apparatus. Four holes were drilled into the skull, with one pair flanking the junction between the sagittal & coronal sutures and one pair flanking the junction between the sagittal & lambdoidal sutures; one 1.00UNM x 0.120" stainless steel screw was placed into each hole. The screws were used as the foundation of a pedestal formed by enrobing the screws in dental cement (Ortho-Jet, Lang Dental; Wheeling, IL) and placing upon them a headpost (made in-house) composed of two M1.4 hex nuts encased in dental cement. Mice were provided at least 7 days to recover from implantation prior to behavioral analysis.

Optokinetic reflex recording and analysis

Headposted mice were held in place with a custom mouse holder (fabricated in-house) and were surrounded by 4 computer monitors (12" in length, 20" in width) inside a darkened box. Eye position was recorded by a fixed infrared camera; mice were

oriented such that the pupil was in the center of the camera's recording field. Stimuli consisted of black-and-white checkboards (stripe width = 5° of the visual field) at approximately 10 lux. Sinusoidal stimuli consisted of 10 cycles at either 0.1 Hz or 0.2 Hz; continuous stimuli consisted of 5 trial blocks consisting of 30 sec of checkerboards moving at 5°/sec followed by 30 sec of a grey screen. All stimuli were preceded and proceeded by 3 sec of a grey screen. Horizontal and vertical stimuli were used for all experiments. The conversion of the linear 2D displacement of the pupil recorded by the infrared camera to rotational movement of the eye was per Stahl et al, 2000.

All optokinetic reflex recording data were analyzed using Igor Pro v6 and v9 (WaveMetrics; Portland, OR). For analysis of data from sinusoidal stimuli, saccadic eye movements were manually removed from analysis, then gain (defined as the ratio of the eye velocity to the stimulus velocity) was calculated using code from Kodama & du Lac, 2016. Analysis of data from continuous stimuli consisted of quantifying the number of eye-tracking movements (ETMs), consisting of 1 slow phase and 1 saccadic eye movement, and converting to an average ETM/minute rate per Yonehara et al, 2016. Recording data were neither collected nor scored blinded.

Looming assay

The looming assay (Yilmaz & Meister, 2013) apparatus consists of a clear plexiglass box (10" width x 20" length x 15" height) with a computer monitor on top, with the screen facing the floor of the box. A cardboard shelter (triangular prism, 4.5" per

side x 6.25” length) was placed in one corner of the box and a 4.5 in^2 box was marked in the center of the floor. Behavior was recorded using a camera with night vision in a darkened room where the only light source is the monitor. Mice were dark-adapted for at least 1 hour prior to analysis.

The looming stimulus consists of an expanding black circle against a white background, with 15 cycles of expansion over 10 seconds; stimulus was controlled using Microsoft PowerPoint and manually activated when mice entered the box at the center of the floor. Mice were placed in the plexiglass box and given 10 minutes to acclimate prior to triggering the stimulus. A response was considered successful if the mouse froze and/or escaped to the shelter in response to the stimulus. Mice were tested in 2 trials separated by at least 3 minutes.

Stereotaxic injections

Stereotaxic injections were performed as described in Lilley et al, 2019. Mice were anesthetized with isoflurane and placed in a stereotaxic apparatus. Injections were performed with a Hamilton Neuros syringe controlled by a computerized microsyringe pump controller (World Precision Instruments; Sarasota, FL). After the desired injection was performed, needle was left in place for 5 minutes to allow injected material to diffuse through the injection site prior to needle removal. For injections of rAAV2-FLEX-GFP (Addgene, stock #51502-AAVrg), 200 nL of virus was injected into the MTN at 10 nL/sec. The stereotaxic coordinates are as follows: AP -0.34mm, ML $\pm$ 0.94mm, DV -

5.528 mm (relative to bregma) with needle angled 30° posteriorly (coordinates from Al-Khindi et al, *submitted*).

Intraocular CTB and AAV injections

Intraocular injections were performed as described in Lilley et al, 2019. Adult mice were anesthetized using isoflurane and secured in a stereotaxic apparatus. A hole was bored at the corneal limbus using a 30 gauge needle. A Hamilton Neuros syringe was manually loaded and inserted into the bored hole; injection volume was injected under manual control. Needle was left in place for 30 sec to allow the injection volume to diffuse through the vitreous humor prior to removal of the needle.

For intraocular injections of CTB, 1 μL of cholera toxin B conjugated to Alexa-555 (1 mg/mL, ThermoFisher Scientific) was injected into each eye. The following virus was used: AAV9-BbChT (Addgene, stock #45186-AAV9).

Generating AAV9-fNPY-FLEX-GFP virus

To generate pAAV-fNPY-FLEX-GFP, we synthesized the GFP coding sequence and bGH polyA signal of pAAV-fNPY-GFP (gift of Dr. E. Callaway, Addgene, stock #22912) with loxP/lox2272 sites flanking this sequence in a flip-excision (FLEX) configuration, as well as a 5' NotI site and 3' PstI site (Integrated DNA Technologies). We then removed the original GFP coding sequence and bGH polyA signal from pAAV-

fNPY-GFP using NotI/PstI sites and inserted the FLEX-GFP-polyA at these sites; this reverses the orientation of the GFP-polyA sequence relative to the original plasmid such that it only enters the correct configuration upon Cre recombination. AAV9-fNPY-FLEX-GFP and AAV9-fNPY-GFP virions were produced and titered by the University of North Carolina BRAIN Initiative NeuroTools Vector Core.

Statistical analyses

DSGC dendrites were traced using the Simple Neurite Tracer (SNT) package in ImageJ software (National Institutes of Health; Bethesda, MD). Dendritic length and branch point number were automatically calculated by SNT; dendritic area was computed by skeletonizing the trace, drawing a polygon surrounding the dendritic arbor in ImageJ, and calculating the area of the polygon. Images were collected and scored blinded to genotype.

Graphs were generated using Prism v 6.0h (Graphpad; San Diego, CA). Mann-Whitney U Tests for assessing differences in OKR responses were performed in Prism. Significance was defined as $p < 0.05$.

References

Aricescu, A.R., Hon, W.C., Siebold, C., Lu, W., van der Merwe, P.A., and Jones, E.Y. (2006). Molecular analysis of receptor protein tyrosine phosphatase mu-mediated cell adhesion. EMBO J *25*, 701-712. 10.1038/sj.emboj.7600974.

Aricescu, A.R., Siebold, C., Choudhuri, K., Chang, V.T., Lu, W., Davis, S.J., van der Merwe, P.A., and Jones, E.Y. (2007). Structure of a tyrosine phosphatase adhesive interaction reveals a spacer-clamp mechanism. Science *317*, 1217-1220. 10.1126/science.1144646.

Auferkorte, O.N., Baden, T., Kaushalya, S.K., Zabouri, N., Rudolph, U., Haverkamp, S., and Euler, T. (2012). GABA(A) receptors containing the α2 subunit are critical for direction-selective inhibition in the retina. PLoS One *7*, e35109. 10.1371/journal.pone.0035109.

Bach, T.L., Barsigian, C., Yaen, C.H., and Martinez, J. (1998). Endothelial cell VE-cadherin functions as a receptor for the beta15-42 sequence of fibrin. J Biol Chem *273*, 30719-30728. 10.1074/jbc.273.46.30719.

Barbieri, A.M., Broccoli, V., Bovolenta, P., Alfano, G., Marchitiello, A., Mocchetti, C., Crippa, L., Bulfone, A., Marigo, V., Ballabio, A., and Banfi, S. (2002). Vax2 inactivation in mouse determines alteration of the eye dorsal-ventral axis, misrouting of the optic fibres and eye coloboma. Development *129*, 805-813. 10.1242/dev.129.3.805.

Barlow, H.B., and Hill, R.M. (1963). Selective sensitivity to direction of movement in ganglion cells of the rabbit retina. Science *139*, 412-414. 10.1126/science.139.3553.412.

Behrens, J., Vakaet, L., Friis, R., Winterhager, E., Van Roy, F., Mareel, M.M., and Birchmeier, W. (1993). Loss of epithelial differentiation and gain of invasiveness correlates with tyrosine phosphorylation of the E-cadherin/beta-catenin complex in cells transformed with a temperature-sensitive v-SRC gene. J Cell Biol *120*, 757-766. 10.1083/jcb.120.3.757.

Borst, A., and Euler, T. (2011). Seeing things in motion: models, circuits, and mechanisms. Neuron *71*, 974-994. 10.1016/j.neuron.2011.08.031.

Brady-Kalnay, S.M., Rimm, D.L., and Tonks, N.K. (1995). Receptor protein tyrosine phosphatase PTPmu associates with cadherins and catenins in vivo. J Cell Biol *130*, 977-986. 10.1083/jcb.130.4.977.

Brasch, J., Harrison, O.J., Ahlsen, G., Carnally, S.M., Henderson, R.M., Honig, B., and Shapiro, L. (2011). Structure and binding mechanism of vascular endothelial cadherin: a divergent classical cadherin. J Mol Biol *408*, 57-73. 10.1016/j.jmb.2011.01.031.

Briggman, K.L., Helmstaedter, M., and Denk, W. (2011). Wiring specificity in the direction-selectivity circuit of the retina. Nature *471*, 183-188. 10.1038/nature09818.

Burden-Gulley, S.M., and Brady-Kalnay, S.M. (1999). PTPmu regulates N-cadherin-dependent neurite outgrowth. J Cell Biol *144*, 1323-1336. 10.1083/jcb.144.6.1323.

Burden-Gulley, S.M., Ensslen, S.E., and Brady-Kalnay, S.M. (2002). Protein tyrosine phosphatase-mu differentially regulates neurite outgrowth of nasal and temporal neurons in the retina. J Neurosci *22*, 3615-3627. 20026276.

Carulli, D., Laabs, T., Geller, H.M., and Fawcett, J.W. (2005). Chondroitin sulfate proteoglycans in neural development and regeneration. Curr Opin Neurobiol *15*, 116-120. 10.1016/j.conb.2005.01.014.

Crossland, W.J., Cowan, W.M., and Rogers, L.A. (1975). Studies on the development of the chick optic tectum. IV. An autoradiographic study of the development of retino-tectal connections. Brain Res *91*, 1-23. 10.1016/0006-8993(75)90463-1.

Dhande, O.S., Estevez, M.E., Quattrochi, L.E., El-Danaf, R.N., Nguyen, P.L., Berson, D.M., and Huberman, A.D. (2013). Genetic dissection of retinal inputs to brainstem nuclei controlling image stabilization. J Neurosci *33*, 17797-17813. 10.1523/JNEUROSCI.2778-13.2013.

Dhande, O.S., and Huberman, A.D. (2014). Retinal ganglion cell maps in the brain: implications for visual processing. Curr Opin Neurobiol *24*, 133-142. 10.1016/j.conb.2013.08.006.

Dhande, O.S., Stafford, B.K., Lim, J.A., and Huberman, A.D. (2015). Contributions of Retinal Ganglion Cells to Subcortical Visual Processing and Behaviors. Annu Rev Vis Sci *1*, 291-328. 10.1146/annurev-vision-082114-035502.

Duan, X., Krishnaswamy, A., Laboulaye, M.A., Liu, J., Peng, Y.R., Yamagata, M., Toma, K., and Sanes, J.R. (2018). Cadherin Combinations Recruit Dendrites of Distinct Retinal Neurons to a Shared Interneuronal Scaffold. Neuron *99*, 1145-1154.e1146. 10.1016/j.neuron.2018.08.019.

Fell, C.W., Hagelkruys, A., Cicvaric, A., Horrer, M., Liu, L., Li, J.S.S., Stadlmann, J., Polyansky, A.A., Mereiter, S., Tejada, M.A., et al. (2021). FIBCD1 is a Conserved Receptor for Chondroitin Sulphate Proteoglycans of the Brain Extracellular Matrix and a Candidate Gene for a Complex Neurodevelopmental Disorder. bioRxiv, 2021.2009.2009.459581. 10.1101/2021.09.09.459581.

Fredericks, C.A., Giolli, R.A., Blanks, R.H., and Sadun, A.A. (1988). The human accessory optic system. Brain Res *454*, 116-122. 10.1016/0006-8993(88)90809-8.

Fried, S.I., Münch, T.A., and Werblin, F.S. (2002). Mechanisms and circuitry underlying directional selectivity in the retina. Nature *420*, 411-414. 10.1038/nature01179.

Fukai, S., and Yoshida, T. (2021). Roles of type IIa receptor protein tyrosine phosphatases as synaptic organizers. FEBS J *288*, 6913-6926. 10.1111/febs.15666.

Gebbink, M.F., Zondag, G.C., Wubbolts, R.W., Beijersbergen, R.L., van Etten, I., and Moolenaar, W.H. (1993). Cell-cell adhesion mediated by a receptor-like protein tyrosine phosphatase. J Biol Chem *268*, 16101-16104.

Giolli, R.A., Blanks, R.H., and Lui, F. (2006). The accessory optic system: basic organization with an update on connectivity, neurochemistry, and function. Prog Brain Res *151*, 407-440. 10.1016/S0079-6123(05)51013-6.

Hayashi, S., Lewis, P., Pevny, L., and McMahon, A.P. (2002). Efficient gene modulation in mouse epiblast using a Sox2Cre transgenic mouse strain. Gene Expr Patterns *2*, 93-97. 10.1016/s0925-4773(02)00292-7.

Hellberg, C.B., Burden-Gulley, S.M., Pietz, G.E., and Brady-Kalnay, S.M. (2002). Expression of the receptor protein-tyrosine phosphatase, PTPmu, restores E-cadherin-dependent adhesion in human prostate carcinoma cells. J Biol Chem *277*, 11165-11173. 10.1074/jbc.M112157200.

Jain, V., Murphy-Baum, B.L., deRosenroll, G., Sethuramanujam, S., Delsey, M., Delaney, K.R., and Awatramani, G.B. (2020). The functional organization of excitation and inhibition in the dendrites of mouse direction-selective ganglion cells. Elife *9*. 10.7554/eLife.52949.

Jepsen, C.S., Dubey, L.K., Colmorten, K.B., Moeller, J.B., Hammond, M.A., Nielsen, O., Schlosser, A., Templeton, S.P., Sorensen, G.L., and Holmskov, U. (2018). FIBCD1 Binds. Front Immunol *9*, 1967. 10.3389/fimmu.2018.01967.

Jiang, L., Li, Y., Yang, K., Wang, Y., Wang, J., Cui, X., Mao, J., Gao, Y., Yi, P., Wang, L., and Liu, J.Y. (2020). FRMD7 Mutations Disrupt the Interaction with GABRA2 and May Result in Infantile Nystagmus Syndrome. Invest Ophthalmol Vis Sci *61*, 41. 10.1167/iovs.61.5.41.

Kay, J.N., De la Huerta, I., Kim, I.J., Zhang, Y., Yamagata, M., Chu, M.W., Meister, M., and Sanes, J.R. (2011a). Retinal ganglion cells with distinct directional preferences differ in molecular identity, structure, and central projections. J Neurosci *31*, 7753-7762. 10.1523/JNEUROSCI.0907-11.2011.

Kay, J.N., Voinescu, P.E., Chu, M.W., and Sanes, J.R. (2011b). Neurod6 expression defines new retinal amacrine cell subtypes and regulates their fate. Nat Neurosci *14*, 965-972. 10.1038/nn.2859.

Kodama, T., and du Lac, S. (2016). Adaptive Acceleration of Visually Evoked Smooth Eye Movements in Mice. J Neurosci *36*, 6836-6849. 10.1523/JNEUROSCI.0067-16.2016.

Koop, E.A., Lopes, S.M., Feiken, E., Bluyssen, H.A., van der Valk, M., Voest, E.E., Mummery, C.L., Moolenaar, W.H., and Gebbink, M.F. (2003). Receptor protein tyrosine phosphatase mu expression as a marker for endothelial cell heterogeneity; analysis of RPTPmu gene expression using LacZ knock-in mice. Int J Dev Biol *47*, 345-354.

Laboulaye, M.A., Duan, X., Qiao, M., Whitney, I.E., and Sanes, J.R. (2018). Mapping Transgene Insertion Sites Reveals Complex Interactions Between Mouse Transgenes and Neighboring Endogenous Genes. Front Mol Neurosci *11*, 385. 10.3389/fnmol.2018.00385.

Landau, A.T., Park, P., Wong-Campos, J.D., Tian, H., Cohen, A.E., and Sabatini, B.L. (2022). Dendritic branch structure compartmentalizes voltage-dependent calcium influx in cortical layer 2/3 pyramidal cells. Elife *11*. 10.7554/eLife.76993.

Lilley, B.N., Sabbah, S., Hunyara, J.L., Gribble, K.D., Al-Khindi, T., Xiong, J., Wu, Z., Berson, D.M., and Kolodkin, A.L. (2019). Genetic access to neurons in the accessory optic system reveals a role for Sema6A in midbrain circuitry mediating motion perception. J Comp Neurol *527*, 282-296. 10.1002/cne.24507.

Macosko, E.Z., Basu, A., Satija, R., Nemesh, J., Shekhar, K., Goldman, M., Tirosh, I., Bialas, A.R., Kamitaki, N., Martersteck, E.M., et al. (2015). Highly Parallel Genome-wide Expression Profiling of Individual Cells Using Nanoliter Droplets. Cell *161*, 1202-1214. 10.1016/j.cell.2015.05.002.

Martersteck, E.M., Hirokawa, K.E., Evarts, M., Bernard, A., Duan, X., Li, Y., Ng, L., Oh, S.W., Ouellette, B., Royall, J.J., et al. (2017). Diverse Central Projection Patterns of Retinal Ganglion Cells. Cell Rep *18*, 2058-2072. 10.1016/j.celrep.2017.01.075.

Masland, R.H. (2012). The neuronal organization of the retina. Neuron *76*, 266-280. 10.1016/j.neuron.2012.10.002.

Masseck, O.A., and Hoffmann, K.P. (2009). Comparative neurobiology of the optokinetic reflex. Ann N Y Acad Sci *1164*, 430-439. 10.1111/j.1749-6632.2009.03854.x.

Matsumoto, A., Briggman, K.L., and Yonehara, K. (2019). Spatiotemporally Asymmetric Excitation Supports Mammalian Retinal Motion Sensitivity. Curr Biol *29*, 3277-3288.e3275. 10.1016/j.cub.2019.08.048.

Matsuoka, R.L., Chivatakarn, O., Badea, T.C., Samuels, I.S., Cahill, H., Katayama, K., Kumar, S.R., Suto, F., Chédotal, A., Peachey, N.S., et al. (2011). Class 5 transmembrane

semaphorins control selective Mammalian retinal lamination and function. Neuron *71*, 460-473. 10.1016/j.neuron.2011.06.009.

Matsuoka, R.L., Jiang, Z., Samuels, I.S., Nguyen-Ba-Charvet, K.T., Sun, L.O., Peachey, N.S., Chédotal, A., Yau, K.W., and Kolodkin, A.L. (2012). Guidance-cue control of horizontal cell morphology, lamination, and synapse formation in the mammalian outer retina. J Neurosci *32*, 6859-6868. 10.1523/JNEUROSCI.0267-12.2012.

Moeller, J.B., Leonardi, I., Schlosser, A., Flamar, A.L., Bessman, N.J., Putzel, G.G., Thomsen, T., Hammond, M., Jepsen, C.S., Skjødt, K., et al. (2019). Modulation of the fungal mycobiome is regulated by the chitin-binding receptor FIBCD1. J Exp Med *216*, 2689-2700. 10.1084/jem.20182244.

Morrie, R.D., and Feller, M.B. (2015). An Asymmetric Increase in Inhibitory Synapse Number Underlies the Development of a Direction Selective Circuit in the Retina. J Neurosci *35*, 9281-9286. 10.1523/JNEUROSCI.0670-15.2015.

Morrie, R.D., and Feller, M.B. (2016). Development of synaptic connectivity in the retinal direction selective circuit. Curr Opin Neurobiol *40*, 45-52. 10.1016/j.conb.2016.06.009.

Morrie, R.D., and Feller, M.B. (2018). A Dense Starburst Plexus Is Critical for Generating Direction Selectivity. Curr Biol *28*, 1204-1212.e1205. 10.1016/j.cub.2018.03.001.

Mosesson, M.W. (1992). The roles of fibrinogen and fibrin in hemostasis and thrombosis. Semin Hematol *29*, 177-188.

Nakamura, Y., Morrow, D.H., Nathanson, A.J., Henley, J.M., Wilkinson, K.A., and Moss, S.J. (2020). Phosphorylation on Ser-359 of the α2 subunit in GABA type A receptors down-regulates their density at inhibitory synapses. J Biol Chem *295*, 12330-12342. 10.1074/jbc.RA120.014303.

Nakhai, H., Sel, S., Favor, J., Mendoza-Torres, L., Paulsen, F., Duncker, G.I., and Schmid, R.M. (2007). Ptf1a is essential for the differentiation of GABAergic and glycinergic amacrine cells and horizontal cells in the mouse retina. Development *134*, 1151-1160. 10.1242/dev.02781.

Nathanson, J.L., Jappelli, R., Scheeff, E.D., Manning, G., Obata, K., Brenner, S., and Callaway, E.M. (2009). Short Promoters in Viral Vectors Drive Selective Expression in Mammalian Inhibitory Neurons, but do not Restrict Activity to Specific Inhibitory Cell-Types. Front Neural Circuits *3*, 19. 10.3389/neuro.04.019.2009.

Nollet, F., Kools, P., and van Roy, F. (2000). Phylogenetic analysis of the cadherin superfamily allows identification of six major subfamilies besides several solitary members. J Mol Biol *299*, 551-572. 10.1006/jmbi.2000.3777.

Osterhout, J.A., Stafford, B.K., Nguyen, P.L., Yoshihara, Y., and Huberman, A.D. (2015). Contactin-4 mediates axon-target specificity and functional development of the accessory optic system. Neuron *86*, 985-999. 10.1016/j.neuron.2015.04.005.

Peng, Y.R., James, R.E., Yan, W., Kay, J.N., Kolodkin, A.L., and Sanes, J.R. (2020). Binary Fate Choice between Closely Related Interneuronal Types Is Determined by a Fezf1-Dependent Postmitotic Transcriptional Switch. Neuron *105*, 464-474.e466. 10.1016/j.neuron.2019.11.002.

Peng, Y.R., Tran, N.M., Krishnaswamy, A., Kostadinov, D., Martersteck, E.M., and Sanes, J.R. (2017). Satb1 Regulates Contactin 5 to Pattern Dendrites of a Mammalian Retinal Ganglion Cell. Neuron *95*, 869-883.e866. 10.1016/j.neuron.2017.07.019.

Picelli, S., Faridani, O.R., Björklund, A.K., Winberg, G., Sagasser, S., and Sandberg, R. (2014). Full-length RNA-seq from single cells using Smart-seq2. Nat Protoc *9*, 171-181. 10.1038/nprot.2014.006.

Poleg-Polsky, A., and Diamond, J.S. (2011). Imperfect space clamp permits electrotonic interactions between inhibitory and excitatory synaptic conductances, distorting voltage clamp recordings. PLoS One *6*, e19463. 10.1371/journal.pone.0019463.

Pu, J., Mao, Y., Lei, X., Yan, Y., Lu, X., Tian, J., Yin, X., Zhao, G., and Zhang, B. (2013). FERM domain containing protein 7 interacts with the Rho GDP dissociation inhibitor and specifically activates Rac1 signaling. PLoS One *8*, e73108. 10.1371/journal.pone.0073108.

Rasmussen, R., Matsumoto, A., Dahlstrup Sietam, M., and Yonehara, K. (2020). A segregated cortical stream for retinal direction selectivity. Nat Commun *11*, 831. 10.1038/s41467-020-14643-z.

Rheaume, B.A., Jereen, A., Bolisetty, M., Sajid, M.S., Yang, Y., Renna, K., Sun, L., Robson, P., and Trakhtenberg, E.F. (2018). Single cell transcriptome profiling of retinal ganglion cells identifies cellular subtypes. Nat Commun *9*, 2759. 10.1038/s41467-018-05134-3.

Riccomagno, M.M., Hurtado, A., Wang, H., Macopson, J.G., Griner, E.M., Betz, A., Brose, N., Kazanietz, M.G., and Kolodkin, A.L. (2012). The RacGAP β2-Chimaerin selectively mediates axonal pruning in the hippocampus. Cell *149*, 1594-1606. 10.1016/j.cell.2012.05.018.

Rivlin-Etzion, M., Zhou, K., Wei, W., Elstrott, J., Nguyen, P.L., Barres, B.A., Huberman, A.D., and Feller, M.B. (2011). Transgenic mice reveal unexpected diversity of on-off direction-selective retinal ganglion cell subtypes and brain structures involved in motion processing. J Neurosci *31*, 8760-8769. 10.1523/JNEUROSCI.0564-11.2011.

Ruff, T., Peters, C., Matsumoto, A., Ihle, S.J., Morales, P.A., Gaitanos, L., Yonehara, K., Del Toro, D., and Klein, R. (2021). FLRT3 Marks Direction-Selective Retinal Ganglion Cells That

Project to the Medial Terminal Nucleus. Front Mol Neurosci *14*, 790466. 10.3389/fnmol.2021.790466.

Sabbah, S., Gemmer, J.A., Bhatia-Lin, A., Manoff, G., Castro, G., Siegel, J.K., Jeffery, N., and Berson, D.M. (2017). A retinal code for motion along the gravitational and body axes. Nature *546*, 492-497. 10.1038/nature22818.

Sallee, J.L., Wittchen, E.S., and Burridge, K. (2006). Regulation of cell adhesion by protein-tyrosine phosphatases: II. Cell-cell adhesion. J Biol Chem *281*, 16189-16192. 10.1074/jbc.R600003200.

Sanes, J.R., and Masland, R.H. (2015). The types of retinal ganglion cells: current status and implications for neuronal classification. Annu Rev Neurosci *38*, 221-246. 10.1146/annurev-neuro-071714-034120.

Schlosser, A., Thomsen, T., Moeller, J.B., Nielsen, O., Tornøe, I., Mollenhauer, J., Moestrup, S.K., and Holmskov, U. (2009). Characterization of FIBCD1 as an acetyl group-binding receptor that binds chitin. J Immunol *183*, 3800-3809. 10.4049/jimmunol.0901526.

Shekhar, K., Lapan, S.W., Whitney, I.E., Tran, N.M., Macosko, E.Z., Kowalczyk, M., Adiconis, X., Levin, J.Z., Nemesh, J., Goldman, M., et al. (2016). Comprehensive Classification of

Retinal Bipolar Neurons by Single-Cell Transcriptomics. Cell *166*, 1308-1323.e1330. 10.1016/j.cell.2016.07.054.

Simpson, J.I. (1984). The accessory optic system. Annu Rev Neurosci *7*, 13-41. 10.1146/annurev.ne.07.030184.000305.

Sivyer, B., and Williams, S.R. (2013). Direction selectivity is computed by active dendritic integration in retinal ganglion cells. Nat Neurosci *16*, 1848-1856. 10.1038/nn.3565.

Stahl, J.S., van Alphen, A.M., and De Zeeuw, C.I. (2000). A comparison of video and magnetic search coil recordings of mouse eye movements. J Neurosci Methods *99*, 101-110. 10.1016/s0165-0270(00)00218-1.

Sui, X.F., Kiser, T.D., Hyun, S.W., Angelini, D.J., Del Vecchio, R.L., Young, B.A., Hasday, J.D., Romer, L.H., Passaniti, A., Tonks, N.K., and Goldblum, S.E. (2005). Receptor protein tyrosine phosphatase micro regulates the paracellular pathway in human lung microvascular endothelia. Am J Pathol *166*, 1247-1258. 10.1016/s0002-9440(10)62343-7.

Sun, L.O., Brady, C.M., Cahill, H., Al-Khindi, T., Sakuta, H., Dhande, O.S., Noda, M., Huberman, A.D., Nathans, J., and Kolodkin, A.L. (2015). Functional assembly of accessory optic system circuitry critical for compensatory eye movements. Neuron *86*, 971-984. 10.1016/j.neuron.2015.03.064.

Südhof, T.C. (2017). Synaptic Neurexin Complexes: A Molecular Code for the Logic of Neural Circuits. Cell *171*, 745-769. 10.1016/j.cell.2017.10.024.

Tang, T., Li, L., Tang, J., Li, Y., Lin, W.Y., Martin, F., Grant, D., Solloway, M., Parker, L., Ye, W., et al. (2010). A mouse knockout library for secreted and transmembrane proteins. Nat Biotechnol *28*, 749-755. 10.1038/nbt.1644.

Tarpey, P., Thomas, S., Sarvananthan, N., Mallya, U., Lisgo, S., Talbot, C.J., Roberts, E.O., Awan, M., Surendran, M., McLean, R.J., et al. (2006). Mutations in FRMD7, a newly identified member of the FERM family, cause X-linked idiopathic congenital nystagmus. Nat Genet *38*, 1242-1244. 10.1038/ng1893.

Thomas, S., Proudlock, F.A., Sarvananthan, N., Roberts, E.O., Awan, M., McLean, R., Surendran, M., Kumar, A.S., Farooq, S.J., Degg, C., et al. (2008). Phenotypical characteristics of idiopathic infantile nystagmus with and without mutations in FRMD7. Brain *131*, 1259-1267. 10.1093/brain/awn046.

Thomsen, T., Moeller, J.B., Schlosser, A., Sorensen, G.L., Moestrup, S.K., Palaniyar, N., Wallis, R., Mollenhauer, J., and Holmskov, U. (2010). The recognition unit of FIBCD1 organizes into a noncovalently linked tetrameric structure and uses a hydrophobic funnel (S1) for acetyl group recognition. J Biol Chem *285*, 1229-1238. 10.1074/jbc.M109.061523.

Tonks, N.K. (2006). Protein tyrosine phosphatases: from genes, to function, to disease. Nat Rev Mol Cell Biol *7*, 833-846. 10.1038/nrm2039.

Tran, N.M., Shekhar, K., Whitney, I.E., Jacobi, A., Benhar, I., Hong, G., Yan, W., Adiconis, X., Arnold, M.E., Lee, J.M., et al. (2019). Single-Cell Profiles of Retinal Ganglion Cells Differing in Resilience to Injury Reveal Neuroprotective Genes. Neuron *104*, 1039-1055.e1012. 10.1016/j.neuron.2019.11.006.

Trenholm, S., Johnson, K., Li, X., Smith, R.G., and Awatramani, G.B. (2011). Parallel mechanisms encode direction in the retina. Neuron *71*, 683-694. 10.1016/j.neuron.2011.06.020.

Tsai, N.Y., Wang, F., Toma, K., Yin, C., Takatoh, J., Pai, E.L., Wu, K., Matcham, A.C., Yin, L., Dang, E.J., et al. (2022). Trans-Seq maps a selective mammalian retinotectal synapse instructed by Nephronectin. Nat Neurosci *25*, 659-674. 10.1038/s41593-022-01068-8.

Vaney, D.I., Sivyer, B., and Taylor, W.R. (2012). Direction selectivity in the retina: symmetry and asymmetry in structure and function. Nat Rev Neurosci *13*, 194-208. 10.1038/nrn3165.

Waldron, L., Steimle, J.D., Greco, T.M., Gomez, N.C., Dorr, K.M., Kweon, J., Temple, B., Yang, X.H., Wilczewski, C.M., Davis, I.J., et al. (2016). The Cardiac TBX5 Interactome

Reveals a Chromatin Remodeling Network Essential for Cardiac Septation. Dev Cell *36*, 262-275. 10.1016/j.devcel.2016.01.009.

Wang, L., Klingeborn, M., Travis, A.M., Hao, Y., Arshavsky, V.Y., and Gospe, S.M. (2020). Progressive optic atrophy in a retinal ganglion cell-specific mouse model of complex I deficiency. Sci Rep *10*, 16326. 10.1038/s41598-020-73353-0.

Waters, J., Larkum, M., Sakmann, B., and Helmchen, F. (2003). Supralinear Ca2+ influx into dendritic tufts of layer 2/3 neocortical pyramidal neurons in vitro and in vivo. J Neurosci *23*, 8558-8567.

Watkins, R.J., Patil, R., Goult, B.T., Thomas, M.G., Gottlob, I., and Shackleton, S. (2013). A novel interaction between FRMD7 and CASK: evidence for a causal role in idiopathic infantile nystagmus. Hum Mol Genet *22*, 2105-2118. 10.1093/hmg/ddt060.

Wei, W., and Feller, M.B. (2011). Organization and development of direction-selective circuits in the retina. Trends Neurosci *34*, 638-645. 10.1016/j.tins.2011.08.002.

Wei, W., Hamby, A.M., Zhou, K., and Feller, M.B. (2011). Development of asymmetric inhibition underlying direction selectivity in the retina. Nature *469*, 402-406. 10.1038/nature09600.

Wong, K., Bumpstead, S., Van Der Weyden, L., Reinholdt, L.G., Wilming, L.G., Adams, D.J., and Keane, T.M. (2012). Sequencing and characterization of the FVB/NJ mouse genome. Genome Biol *13*, R72. 10.1186/gb-2012-13-8-r72.

Xie, Q., Li, J., Li, H., Udeshi, N.D., Svinkina, T., Orlin, D., Kohani, S., Guajardo, R., Mani, D.R., Xu, C., et al. (2022). Transcription factor Acj6 controls dendrite targeting via a combinatorial cell-surface code. Neuron *110*, 2299-2314.e2298. 10.1016/j.neuron.2022.04.026.

Yan, W., Laboulaye, M.A., Tran, N.M., Whitney, I.E., Benhar, I., and Sanes, J.R. (2020). Mouse Retinal Cell Atlas: Molecular Identification of over Sixty Amacrine Cell Types. J Neurosci *40*, 5177-5195. 10.1523/JNEUROSCI.0471-20.2020.

Yilmaz, M., and Meister, M. (2013). Rapid innate defensive responses of mice to looming visual stimuli. Curr Biol *23*, 2011-2015. 10.1016/j.cub.2013.08.015.

Yonehara, K., Balint, K., Noda, M., Nagel, G., Bamberg, E., and Roska, B. (2011). Spatially asymmetric reorganization of inhibition establishes a motion-sensitive circuit. Nature *469*, 407-410. 10.1038/nature09711.

Yonehara, K., Farrow, K., Ghanem, A., Hillier, D., Balint, K., Teixeira, M., Jüttner, J., Noda, M., Neve, R.L., Conzelmann, K.K., and Roska, B. (2013). The first stage of cardinal direction

selectivity is localized to the dendrites of retinal ganglion cells. Neuron *79*, 1078-1085. 10.1016/j.neuron.2013.08.005.

Yonehara, K., Fiscella, M., Drinnenberg, A., Esposti, F., Trenholm, S., Krol, J., Franke, F., Scherf, B.G., Kusnyerik, A., Müller, J., et al. (2016). Congenital Nystagmus Gene FRMD7 Is Necessary for Establishing a Neuronal Circuit Asymmetry for Direction Selectivity. Neuron *89*, 177-193. 10.1016/j.neuron.2015.11.032.

Yonehara, K., Ishikane, H., Sakuta, H., Shintani, T., Nakamura-Yonehara, K., Kamiji, N.L., Usui, S., and Noda, M. (2009). Identification of retinal ganglion cells and their projections involved in central transmission of information about upward and downward image motion. PLoS One *4*, e4320. 10.1371/journal.pone.0004320.

Yonehara, K., Shintani, T., Suzuki, R., Sakuta, H., Takeuchi, Y., Nakamura-Yonehara, K., and Noda, M. (2008). Expression of SPIG1 reveals development of a retinal ganglion cell subtype projecting to the medial terminal nucleus in the mouse. PLoS One *3*, e1533. 10.1371/journal.pone.0001533.

Yoshida, K., Watanabe, D., Ishikane, H., Tachibana, M., Pastan, I., and Nakanishi, S. (2001). A key role of starburst amacrine cells in originating retinal directional selectivity and optokinetic eye movement. Neuron *30*, 771-780. 10.1016/s0896-6273(01)00316-6.

Zhang, C., Kolodkin, A.L., Wong, R.O., and James, R.E. (2017). Establishing Wiring Specificity in Visual System Circuits: From the Retina to the Brain. Annu Rev Neurosci *40*, 395-424. 10.1146/annurev-neuro-072116-031607.

Zhao, Y., Zhang, X., Guda, K., Lawrence, E., Sun, Q., Watanabe, T., Iwakura, Y., Asano, M., Wei, L., Yang, Z., et al. (2010). Identification and functional characterization of paxillin as a target of protein tyrosine phosphatase receptor T. Proc Natl Acad Sci U S A *107*, 2592-2597. 10.1073/pnas.0914884107.

Zondag, G.C., Koningstein, G.M., Jiang, Y.P., Sap, J., Moolenaar, W.H., and Gebbink, M.F. (1995). Homophilic interactions mediated by receptor tyrosine phosphatases mu and kappa. A critical role for the novel extracellular MAM domain. J Biol Chem *270*, 14247-14250. 10.1074/jbc.270.24.14247.

Zondag, G.C., Reynolds, A.B., and Moolenaar, W.H. (2000). Receptor protein-tyrosine phosphatase RPTPmu binds to and dephosphorylates the catenin p120(ctn). J Biol Chem *275*, 11264-11269. 10.1074/jbc.275.15.11264.

CURRICULUM VITAE FOR Ph.D. CANDIDATES

The Johns Hopkins University School of Medicine

Andrew Scasny — Name

August 5, 2022 — Date of this version

Educational History:

Ph.D. expected	2022	Program in Neuroscience	Johns Hopkins School of Medicine
B.S.	2016	Biology	University of Chicago

Publications:

- Hamilton NR, **Scasny AJ**, Kolodkin AL. (2021) Development of the Vertebrate Retinal Direction-selective Circuit. Developmental Biology. 477: 273-283.
- Onishi KG, Maneval AC, Cable EC, Touhy MC, **Scasny AJ**, Sterina E, Love JA, Riggle JP, Mukerji A, Novo JS, Appah-Sampong A, Gary JB, Prendergast BJ. (2020) Circadian and Circannual Timescales Interact to Generate Seasonal Changes in Immune Function. Brain Behavior and Immunity. 83: 33-43.

Service and leadership:

August 2017 – December 2017	Teaching Assistant, Neuroscience and Cognition I, Johns Hopkins School of Medicine